Optimal Model Coordination for Integrated Transmission and Distribution Systems

Final Project Report

T-61

Power Systems Engineering Research Center
Empowering Minds to Engineer
the Future Electric Energy System

Optimal Model Coordination for Integrated Transmission and Distribution Systems

Final Project Report

Project Team

Visvakumar Aravinthan, Project Leader
Ward Jewell
Wichita State University

Lindsay Anderson
Cornell University

Judy Cardell
Smith College

Graduate Students

Suvagata Chakraborty
Arun-Kaarthick Manoharan
Sandhya Nadipalli
Mojtaba Sepehry
Wichita State University

Jialin Liu
Luckny Zéphyr
Cornell University

PSERC Publication 21-13

November 2021

For information about this project, contact:

Visvakumar Aravinthan
Wichita State University
1845 N Fairmount St
Wichita, KS 67260
Office: JB 222
Phone: (316) 978-6324
Email: visvakumar.aravinthan@wichita.edu

Power Systems Engineering Research Center

The Power Systems Engineering Research Center (PSERC) is a multi-university Center conducting research on challenges facing the electric power industry and educating the next generation of power engineers. More information about PSERC can be found at the Center's website: http://www.pserc.org.

For additional information, contact:

Power Systems Engineering Research Center
Arizona State University
527 Engineering Research Center
Tempe, Arizona 85287-5706
Phone: 480-965-1643
Fax: 480-727-2052

Notice Concerning Copyright Material

Acknowledgements

We wish to thank our current and former industry advisory board members for their time commitment and feedback.

- Jim Price, CAISO
- Miaolei Shao, GE
- Devin Vanzandt, GE
- Evangelos Farantatos, EPRI
- Jay Caspary, SPP
- Mirrasoul Mousavi, ABB
- Mike Swider, NYISO
- Tongxin Zheng, ISO New England

Executive Summary

The integrated analysis and coordination of transmission and distribution systems is considered as one of the key requirements for efficient operation of the future grid with high penetration of renewable energy resources. The primary focus of the existing literature on integration studies can be categorized into, (i) developing generic co-simulation platforms and (ii) application specific integrated analysis. The literature survey conducted for this work found that a research gap existed in the optimal models for coordinating transmission and distribution (T and D) system and analysis. This work presents the initial attempt to identify the limitations and opportunities of data and load aggregation for integrated T and D analysis, and the exploration of potential impacts of optimal coordination of T and D systems.

The main contributions of this work can be delineated as follows (i) Error correction model for distribution system data aggregation (ii) framework for distribution system load aggregation and management, (iii) new technique to provide estimates of unmonitored distributed solar photovoltaic (PV) generation on a distribution system, (iv) development of a co-optimization framework to coordinate T and D operational decisions. All of these aspects were developed with the focus on future data-centric system solutions for integrated T and D operations. The numerical analysis performed show the significance and the improvements provided by the proposed methods.

Part #1: Distribution System Data Aggregation for Coordinated Operation of Transmission and Distribution System: Impacts and Modeling

- The reliance on real-time distribution system data and load management is high in case of performing system operations using integrated analysis of T and D. In such cases the need for accurate representation of distribution system becomes paramount. A detailed study was done to realize the significance of data aggregation and granularity on distribution system analysis.
- Based on the study it was found that error correction models developed in this work are significant for improving the accuracy of distribution system representation, which is a key factor in integrated T and D analysis.
- Secondly, a two-part framework to aggregate and manage responsive distribution system load and resources is developed in this work. The novelty of this work is the development of a heterogeneous clustering technique that can be used for aggregating loads/energy resources considering the customer behavior and system requirements.
- The proposed framework/models for distribution system load and data aggregation can be incorporated as a part of any integrated T and D analysis. And including them would result in optimal coordination.

Part #2: Modeling Distributed Rooftop Solar Generation

- A new technique is presented to provide estimates of unmonitored distributed solar photovoltaic (PV) generation on a distribution system for transmission planning and operations estimates that can be made in real time.
- The data required are the total capacity of distributed PV generation on the distribution system and historical data of the output of those systems. Distribution operators collect capacity data for all interconnected systems. Smart meters can provide the historical data on actual energy generated. Once the model is developed for a feeder or substation, it should be updated annually. To provide generation estimates, the model uses real-time or historical solar radiation data as its only input.
- In practice, the model parameters would be developed by the distribution operator and provided to the transmission operator for use. The limited data needed for the model is all aggregate data for a service area, and the actual model provided to the transmission operator should pose no privacy concerns for customers.

Part #3: Co-optimization of Transmission & Distribution Operations

In Part 3, a co-optimization formulation is developed to analyze the potential for coordinated decisions in T and D systems, with highlights as follows:

- The proposed co-optimization framework can be implemented for a single transmission system in coordination with multiple distribution systems, showing that operational decisions leverage differences between system capabilities.
- A bi-level formulation of the co-optimization problem incorporates the network model and power flow for the distribution systems in the transmission optimization problem.
- Co-optimization enables competition between distribution systems to provide flexibility to the transmission system, which is not possible in the single level optimization approach commonly used.

Project Publications:

[1] S. Chakraborty, A. K. Manoharan, A. Hettiarachchige-Don, T. Balachandran, and V. Aravinthan. "Modeling and Evaluating the Effect of Data Aggregation Inteval on Cyber-Enabled Power Distribution System." *IEEE Transactions on Power Systems* (To be Submitted).

[2] J. Liu, L. Zephyr, and C. Lindsay Anderson. "Optimal Operation of Microgrids with Load-Differentiated Demand Response and Renewable Resources." Journal of Energy Engineering 146.4 (2020):04020027.

[3] J. Liu, L. Zephyr, and J. Cardell. (2020). "Co-optimizing High and Low Voltage Systems: Bi-Level vs. Single-Level Approach."

[4] J. Liu, L. Zephyr, J. Cardell, and C. L. Anderson. Co-optimization of Transmission and Microgrid Operations: Leveraging Renewable Generation and Demand Response, International Journal of Electric Power Systems (under revision).

[5] A. K. Manoharan, S. Gampa, Md. Rahman and V. Aravinthan. "Context-Aware Heterogeneous Clustering Algorithm for Load Management: A Case Study with Electric Vehicle Charge Scheduling." IEEE Transactions on Power Systems (Under Review).

[6] M. Sepehry, M. H. Kapourchali, V. Aravinthan and W. Jewell, "Robust Day-Ahead Operation Planning of Unbalanced Microgrids," in IEEE Transactions on Industrial Informatics, vol. 15, no. 8, pp. 4545-4557, Aug. 2019, doi:10.1109/TII.22019.2895080.

[7] C. Shek, A. K. Manoharan, and V. Aravinthan. "Optimization of Electric Vehicle Charging Schedule Using Distributed Network Computing." in Proc. 2020 North American Power Symposium (NAPS). Oct. 2020.

[8] C. Shek, A. K. Manoharan, S. Gampa, T. Chandrappa and V. Aravinthan. "A Diversity-Based Clustering Technique For Implementing Decentralized Node Level Charge Scheduling of Electric Vehicles." in Proc. 2019 North American Power Symposium (NAPS). IEEE, 2019.

[9] Z. Wang, C. L. Anderson. "A Progressive Period Optimal Power Flow for Systems with High Penetration of Variable Renewable Energy Sources." Energies 2021, 14, 2815. https://doi.org/10.3390/en14102815.

Student Theses:

[1] Suvagata Chakraborty, "*Bound Based Optimal Decision for Cyber-Enabled Distribution System*". Doctoral dissertation, Wichita State University, December 2021.

[2] Jialin Liu (2019) A Bi-Level Approach To Future Power System Co-Optimization With High Penetration Of Renewable Energy And Responsive Demand. Ph.D. Thesis, Cornell University.

[3] Arun Kaarthick Manoharan, "*Optimal model of Distribution System and Transmission & Distribution Interface for Integrated Analysis*". Doctoral dissertation, Wichita State University, May 2022.

[4] Sandhya Nadipalli, "*Modeling of Distributed Rooftop Solar Generation for Transmission Operation and Planning*," Doctoral dissertation, Wichita State University, expected May 2022.

[5] Mojtaba Sepehry, "*Microgrid Operation and Planning Under Uncertainty*". Doctoral dissertation, Wichita State University, May 2019.

Part I

Distribution System Models for Integrated Analysis

Visvakumar Aravinthan
Suvagata Chakraborty, Graduate Student
Arun-Kaarthick Manoharan, Graduate Student
Mojtaba Sepehry, Graduate Student

Wichita State University

For information about this project, contact

Visvakumar Aravinthan
Wichita State University
1845 N Fairmount St
Wichita, KS 67260
Office: JB 222
Phone: (316) 978-6324
Email: visvakumar.aravinthan@wichita.edu

Power Systems Engineering Research Center

The Power Systems Engineering Research Center (PSERC) is a multi-university Center conducting research on challenges facing the electric power industry and educating the next generation of power engineers. More information about PSERC can be found at the Center's website: http://www.pserc.org.

For additional information, contact:

Power Systems Engineering Research Center
Arizona State University
527 Engineering Research Center
Tempe, Arizona 85287-5706
Phone: 480-965-1643
Fax: 480-727-2052

Notice Concerning Copyright Material

Table of Contents

List of Figures

List of Tables

1. Introduction

The increase in the Distributed Generation (DG) and its variable nature has introduced both challenges and opportunities to the systems planning and operation [1]. The DG resources such as solar photovoltaic (PV) have been existing in distribution system but with the increase in such sources and variable loads such as electric vehicle (EV) charging the rate of change in demand becomes significant as demonstrated in figure 1.1. In this figure, the daily load curve of a distribution system with peak demand of 30 MW is considered to demonstrate the impact of PV generation and EV charging. Despite the PV penetration and EV charging being less than 25% and 15% of the daily peak demand, it still contributes significantly to the steep change in the demand specifically around the sunset (peak demand period of the distribution system). It must be noted that the aggregate PV generation shown in figure 1.1 was for a day in summer with clear sky as the goal is to show the impact on operations at the scale of several minutes to hours. However, unaggregated generation (node level or end user level) at a granular level (seconds to few minutes) would have more stochasticity, the primary focus of this work is on system operations at the scale of several minutes to hours.

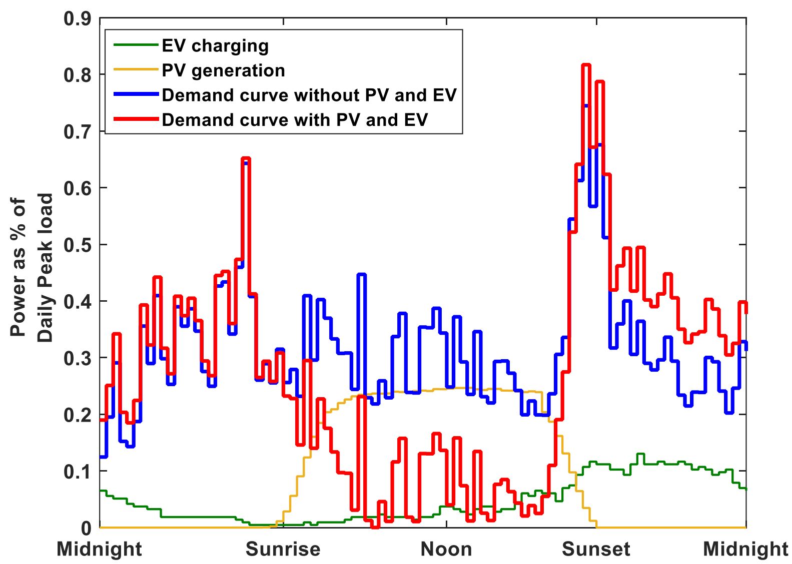

Figure 1.1 Impact of EV and DG

1.1 Motivation

Several solutions are proposed in the existing literature to encounter the impact of DG and loads such as EV. With the advancements in communication, computing and control technologies the integrated analysis of transmission and distribution systems is considered as one of the primary enhancements to systems operations and planning [2]. Effective coordinated operation of transmission and distribution systems is considered extremely necessary for the future electric power grid [3]. This is motived by the following: (i) large penetration of distributed generation [3], (ii) communication availability [4], and (iii) new trends in grid edge technologies [5]. Recent trends in the literature facilitate co-optimized operation of transmission and distribution systems [4]-[6]. This is feasible through data sharing between transmission and distribution systems at the common coupling points [5]. However, for effective coordination comprehensive models must be developed to represent responsive distribution demand (also energy resources) at the transmission level analysis. An overview of the integration and the associated modeling required, is presented in the block diagram in figure 1.2. In this figure, the integration is represented through the participation of demand response providers (DRP) at the transmission level. Although several existing works [7] – [16] have proposed solutions for this problem, the goal of this work is to, (i) develop models that aid in improving the data aggregation and (ii) include the customer behavior (in addition to system requirements and benefits) into the aggregation process for fair and effective load management through distribution demand/energy resource aggregators.

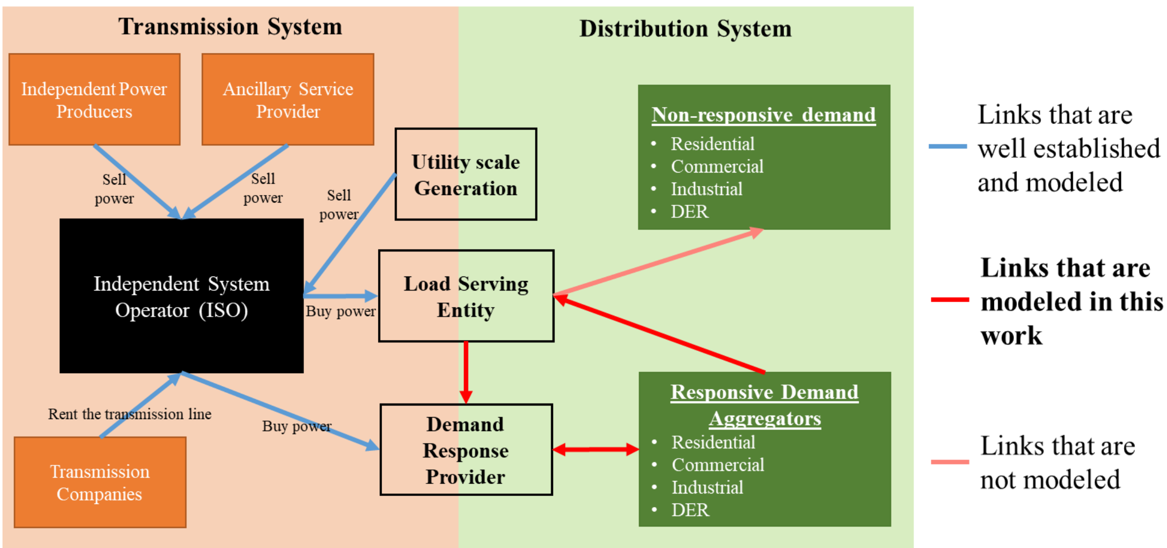

Figure 1.2 Overview of the Integration study from markets perspective

1.2 Organization of the Report

The rest of this report is organized as follows, Chapter 2 presents the preliminary study on existing literature in T and D integration, to understand the requirements for effective coordination and finding the research gap; Chapter 3 presents the detailed analysis on the development of error correction models to improve the accuracy of aggregated distribution system data; Chapter 4 presents the proposed framework for aggregation and management of responsive demand to aid the DRPs in effectively representing the distribution system resources at the transmission markets; and the final remarks and conclusion is presented in chapter 5.

2. Preliminary Integration Study

2.1 Background Study

The first step in developing an integrated analysis is to develop a procedure to combine transmission and distribution system i.e., how to couple the analysis of transmission and distribution system. There are different methods proposed in the existing literature on how to implement the T and D analysis [17]-[29]. Each method has its own advantage and in most cases is developed for a very specific application. In short, the existing methods can be put into following categories,

1. One single model for T and D: Combined T and D analysis
2. Separate model for T and D: Separate T and D analysis with data exchange at point of common coupling (PCC).
    a. Loosely coupled: Single data exchange per time step
    b. Tightly coupled: Iterative solution process for each time step

The summary of some of the methods proposed in the existing literature and their corresponding application/purpose are given in Table 2.1.

Table 2.1 Application/Purpose and The Corresponding Integration Methods Used

Reference	Application/Purpose	Integration Method
[17],[18]	T and D systems communication and market interaction using off the shelf tools	Hierarchical Engine for Large-scale Infrastructure Co-simulation (HELICS). HELICS facilitates interaction between different tools that are used for transmission, distribution, and communication.
[19], [20]	Setting up combined simulation using existing software platforms	Simultaneous simulation of T and D
[21]	General Framework for tightly or loosely coupled co-simulation	Interconnection at the boundary bus using phase-sequence
[22]	Fault Recovery	Mixed three phase/three sequence modelling
[23]	DER Integration	Quasi-static Mixed three phase/three sequence modelling
[24]	Stochasticity of Distribution Load in T and D decision making	Interconnection of separate Three phase T-model and Three phase D-model
[25]	Volt-Var control impact on Transmission system	Transmission and Distribution AC Optimal Power Flow (TDOPF). Two separate functions for TSO and DSO in Objective function
[26]	Load dynamics modelling	Interconnection through data exchange between T and D. Positive sequence to three sequence
[27]	Cost Minimization	Separate Convex optimization of T-OPF and D-OPF through iterative information exchange
[28], [29]	Battery Energy Storage Management	Iterative Data exchange through OPENADR

2.2 Loosely Coupled Test System

The main goal of developing integrated T and D test systems is to study the benefits of different integration techniques and levels of coupling. For the preliminary studies, the test system was developed using multiple platforms such as, (i) MATPOWER (Transmission Optimal Power Flow (T-OPF)), (ii) OpenDSS (Distribution system analysis) and (iii) MATLAB (interface between (i) and (ii)). The test system developed has a 6-bus transmission system with three generator and three load buses. This system modeled in MATPOWER to run T-OPF, is analyzed with the assumption that all three phases are balanced. But the load bus (node number 4 in the 6-bus transmission system) represented using IEEE 13 bus system is analyzed in OpenDSS as unbalanced. To address this mismatch an interfacing function is created in MATLAB to convert the three-phase unbalanced voltage and power to positive sequence equivalents, which in turn will be used as the value to represent distribution node in the T-OPF. But the three-phase power calculated for unbalanced system will be converted to balanced positive sequence equivalent and used in T-OPF.

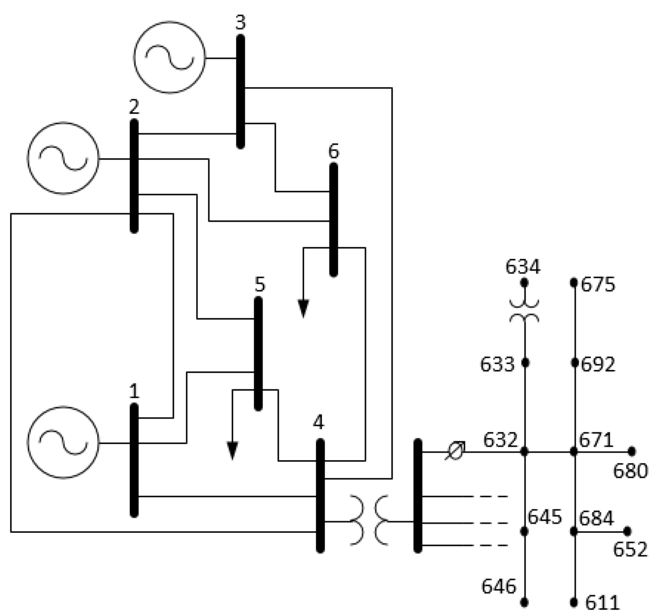

Figure 2.1 Integrated T and D test system

This test system has three modes of integration, ***Mode A: No coupling-*** T and D systems operate independently with no information transfer between each other. The distribution system will be statically represented using forecasted value of power in T-OPF. ***Mode B:*** **Coupling with magnitude data-** the power and voltage magnitude information from the distribution substation will be used by the interfacing function to get the positive sequence voltage and power that will be used to represent the distribution system in the T-OPF. ***Mode C: Coupling with magnitude and angle data-*** the power, voltage angle and voltage magnitude information will be used by the interfacing function. The test system given by figure 2.1 with 3 modes of integration (represented in figure 2.2), were tested with different load curves to observe the performance of each method of integration. The different load curves used, and the performance evaluation index developed are given below.

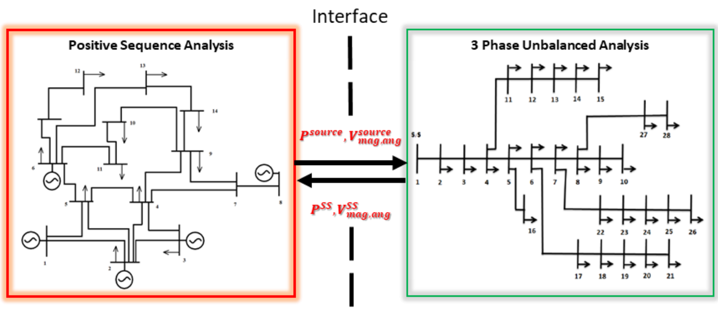

Figure 2.2 Data exchange between T & D systems

The above test system in the three different modes was tested using a forecasted load curve and 4 other variants of it. Each load during each time interval from base curve was varied by $\pm5\%$, $\pm10\%$, $\pm15\%$ and $\pm20\%$ to create the other load curves. The graph in figure 2.3 shows the hourly demand forecast for base case and the simulated actual demand with up to 20% variation. This was done for 8760 hours for all the nodes in the IEEE 13 bus system. The purpose of the test was to analyze the performance of each mode of integration under varying level of uncertainty in distribution system load/generation.

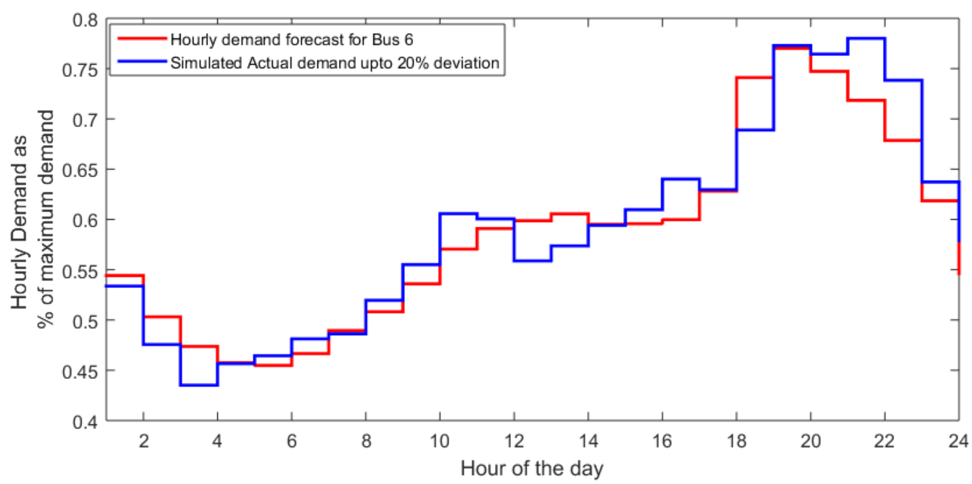

Figure 2.3 Forecasted and actual demand

The number of tap operations was used as a tool to gauge the performance. A performance index called Tap-index was developed. The tap index ϵ_{Tap}^{m} of a mode of integration m is given by,

$$\varepsilon_{Tap}^{m} = \sqrt{\sum \left(\frac{Tap_i^m - Tap_i^a}{Tap_i^m} \right)^2}$$

Where,

Tap_i^a- tap operations in mode a, for i^{th} load curve

Tap_i^m- tap operations in mode m: $m = \{b, c\}$, for i^{th} load curve

The results from the tests are given by figure 2.4 and the tap index scores are listed in table 2.2. From the graph in figure 2.4, it is evident that mode A with no coupling has more tap operations and having some integrated analysis is better. From the tap-index in table 2.2 mode B has a higher score than mode C which means the number of tap operations in mode B is lesser than that of mode C. Although more information in shared case of mode C it results in more tap operations than mode B. Further investigation must be done on the representation of unbalanced three phases using positive sequence with and without phasor angle of voltages in the boundary bus could be investigated. Also, the accuracy of results obtained in both the modes must be studied to understand this behavior better.

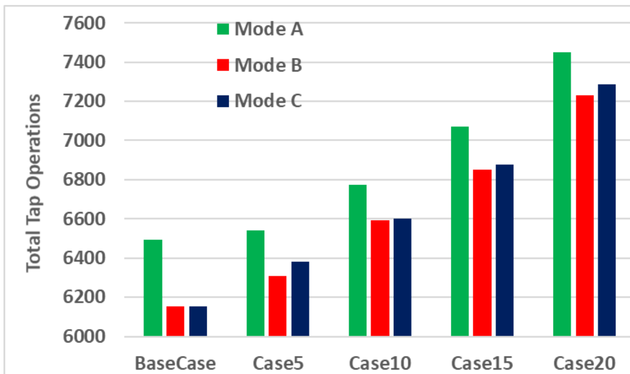

Figure 2.4 Performance of Modes A, B and C (vs) Load Variation

Table 2.2 Tap-Index Score

Mode of Integration	Tap-Index
Mode B	0.0812
Mode C	0.0725

2.3 Inference and Research Gap

The primary goal of this chapter was not to develop a coordination model but to understand the intricate details that make the coordination effective. As such it is important to mention that the works such as [23] have already shown the superiority of tight coupling as it results in more accurate coordination. But from the results in figure 2.4 and table 2.2 it can be seen that accurate representation may not guarantee better output. Therefore, the key takeaway is that the performance of the coordinated analysis also depends on the improved control coordination, along with accurate representation of each individual system. This research gap is addressed in this work by (i) error estimation models considering distribution data aggregation and desired applications' control interval (chapter 3) and (ii) two -part framework for aiding the demand response aggregator participating in the transmission market (chapter 4).

3. Impact of Distribution System Data Aggregation

3.1 Introduction

The advent of grid edge technologies has increased the scope of utilizing distributed generation facilities and responsive demands for better operation of distribution system [30]. However, one of the challenges in utilizing them in any real-time decision making is the regulations that govern the information exchange requirements of these resources. For example, CPUC Rule 21, provides the telemetry requirement for distributed generation resources based on the type and size and the CPUC Rule 24/32 and IEEE.2030.5 that regulates the data exchange between end user and demand response service provider [31] [32]. These rules and regulations that govern the different resources lead to each of them reporting information at different granularity and aggregation intervals. Thus, the distribution system level decision making must be equipped with models to handle this discrepancy.

Current advancements in the power system have focused on developing solutions and technical frameworks for the next-generation distribution system demand response as described by the authors in [30]. Installation of intelligent electronic devices (smart meters, micro-PMUs etc.) at distribution level provides better observability of the system and increases the potential benefits of end user participation. Granularity of end use residential and small-scale commercial consumption data thus becomes a key factor to enable more advanced profiling of consumers [31], [32]. The literature identifies several consumer-level demand response schemes: (a) managing demand based on consumer comfort (b) utilizing a market-based or price-based demand response [33], [34]; (c) employing home energy management and control [35] [36]; and (d) using demand response for grid control requirements [37], [38]. One of the limitations of the work presented in the literature is identifying an appropriate relationship between demand management and its benefits to the power grid using the information from end user. There is no study to quantify the effect of data granularity on those schemes.

It is necessary to determine the incremental benefits to a distribution system for incremental load management. The available literature in this area is minimal. Safdarian et al. [39] aimed to quantify the benefits of demand response at the residential level using an appliance-level load profile. Here the impacts of responsive loads on voltage drop, power loss, and service reliability indices at different levels of penetration of demand response were analyzed using field data. This is one of the initial quantitative efforts in this area, and the model has been instrumental in developing value-based demand response schemes [40], [41]. However, aggregated load-based grid impacts are not evaluated in the aforementioned work.

Granularity of data being used for operation and planning of the power grid much depends on which part of the system is being analyzed. Low granularity information is adequate for analyzing system with less uncertainty, whereas need of granularity becomes highly important for performing planning and operation of system with high uncertainty due to renewables or distributed generation. A low granular data may be sufficient for electric grid simulation, whereas analyzing data on the individual customer level, when looking at multiple households, much of the short-term fluctuations are balanced out due to aggregation of different profiles.

Distribution system real-time demand management requires increased feeder-level observation. The advanced metering infrastructure (AMI) (smart meters) and distributed intelligent devices allow better monitoring and control, but this requires a reliable and seamless communication infrastructure [42]. This is a major concern for electric utilities because they are either leasing such networks from third-party providers at a higher price, or they are building their own infrastructures and in turn leasing out bandwidth (especially at the backhaul) to recover investment costs. Also, the smart meter will produce high data transfer rates considering all future needs like heat, gas and water in addition to power consumption. Analysis of this big data in real time requires implementation of huge resources, which is time dependent and costly. Furthermore, reliability of communication between power distribution systems could be an issue by means of link failure [40], [43] due to jittering, packet loss, or packet delay. Therefore, lower data-transfer rates could result in higher probability of information loss.

These limitations lead to the use of different aggregation intervals (Ais) [44]. The method of obtaining useful data by integrating data containing granule information is known as data aggregation, and the time period over which the data is aggregated is referred to as the data aggregation interval [45]. From a power system point of view, aggregating demand data from the consumer end at a certain demand/aggregation interval is used to reduce the granularity of the data. For example, Elphick et al. investigated the impact of data AIs on the monitoring of power quality [46]. Based on their analysis, the authors concluded that a lower AI (high granularity) can provide more insight and hence be used for several power quality surveys. The IEC61000-4-30 standard suggests that ten-minute data AIs are appropriate for routine power quality monitoring [46].

The lack of comparability of aggregated data across spatial resolutions seriously limits the usefulness while multi-scale remotely sensed data are becoming increasingly available. Synchronizing these aggregated data from multiple resolution remote terminal devices is a big challenge for future cyber physical power system. The potential challenges due to multi-resolution data for effective aggregation is addressed through the framework developed in this work.

A long or high aggregation interval can result in less granular data and may lead to the loss of important details. Adding more accuracy by increasing granularity comes with the need to acknowledge the unpredictable nature of the short-term fluctuations. In addition, lower AI may result in copious amounts of data that are difficult to assess using highly complex models and/or may create storage concerns if the data is to be retained for a long period of time [45], [46]. Effect of AI and data granularity on accuracy of performance evaluation, estimation of power consumption using real voltage and current measurements from sensors of a utility substation is demonstrated in this section. From figure 3.1, it can be seen that lower AI such as one-minute estimation captures the sudden rises and dips in the consumption than the cases with higher AI (low granularity). This highlights the fact that estimation with higher AI is more prone to lose accuracy compared to low AI. This effect becomes significant when analyzing power distribution system as it tends to use low granularity data for planning and operation. Thus, choosing the effective aggregation interval will depend on threshold for estimation error and control interval, which are specific to an application.

This work focuses on the effect of aggregation on data collected from remote terminal units at distribution end (like smart meter, distribution PMU) to control unit, while control signals/commands directed from the control unit are not considered for aggregation as shown in figure 3.1. The control commands are not considered for aggregation as it works as trigger command for terminal units to execute necessary action.

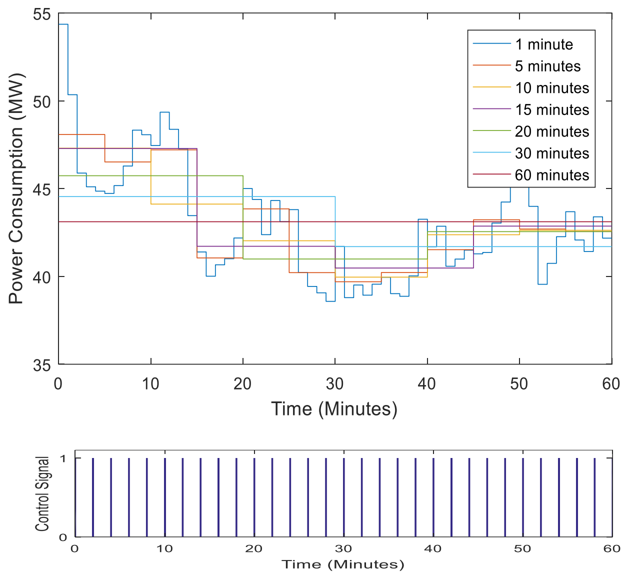

Figure 3.1 Effect of Aggregation Interval on data Granularity independent of control interval

In this work an application specific error model is being developed to account for data aggregation error. Prior works in [46] – [49] have introduced data aggregation for distribution system applications but does not quantify the impact of data granularity on the estimation of distribution system performance. Thus, the objective of this work is to analyze the tradeoff between data granularity and accuracy of the application data collected and evaluate data aggregation and its impact on distribution feeder-level applications. This work proposes a framework for effective data aggregation at the distribution level. The main contributions of this work are as follows:

- Integration of distribution system factors and data granularity into a single performance-evaluation framework.
- A statistical modeling approach for estimating the deviation of performance parameters from the actual values due to reduced data granularity.
- A framework to estimate the actual performance parameters using lower granular (high AI) data reported by the smart meters.

This framework or method requires less computational time and provides practicable accuracy; hence it is well suited for critical decision-making process where time is of essence. Two performance parameters—voltage regulation and power loss—are used in this work to illustrate the proposed framework models.

3.2 Performance Evaluation Framework Model

The three layers of the future power system are, (i) power network, (ii) communication framework to aggregate data at each node, and (iii) data aggregator to aggregate data while preserving the total demand information. After the data is aggregated and the demand is computed for a particular aggregation interval, the demand data is used for estimating system performance. Since the average demand is used, spikes and dips within that period are masked, as shown in figure 3.1. This masking will create an error in the performance evaluation.

3.2.1 Performance Parameter Selection

Voltage regulation in a distribution feeder is maintained by the tap-changing operation of the transformer. Frequent switching of the tap changer easily damages the equipment, lowering the reliability at the distribution-feeder level [47], [48]. Accurate predictions of tap-changing operations could reduce time [49]. One of the objectives of the smart grid is to reduce the cost of operations, which can be achieved by reducing distribution-level losses. The increase of photovoltaic (PV) integration in a distribution system could potentially cause problems in terms of system operation by introducing a reverse power flow, resulting in the rise of bus voltages and feeder losses [50]. Thus, tap changer operations to provide voltage regulation and line loss estimation were selected as the parameters to be analyzed with and without PV penetration in the system.

This approach could be used for any application in cyber power distribution system. Thus, the focus of the work is to analyze performance parameters which can affect the power system applications and create a guideline to use lower granularity data with more accuracy within communication limitation and protecting customer privacy.

3.2.2 Methodology for Ranking Contributing Factors

Conventional distribution system factors such as feeder type, dynamic loading, and month of the year, along with availability of distributed generation and aggregation interval are considered as the contributing factors which can affect the consumer data and distributed generation information to observe tap change operations and line loss. The objective is to only highlight the impact of the contribution factors, without changing the control settings of tap changer, hence feeder type is considered as a contributing factor to analyze cumulative effect of tap control settings and in turn observe the effect of data granularity on the estimation of system performance. The following steps were taken in this process:

Step 1: Determine or generate a one-minute demand for each consumer based on the consumer-demand pattern.

Step 2: Determine nodes or locations in the grid where consumer data would be aggregated, in order to reduce the total data received by the distribution system operator (DSO). Data aggregation is dependent on geographical location. Typically based on available bandwidth and packet size, effective number of consumers within one aggregation node need to be determined. Furthermore, based on the total number of consumers, the required levels of aggregation also must be determined. Since the focus of this work is limited to the aggregation data interval and power system performance estimation, one level of aggregation with different intervals is sufficient. However, if cyber network performance is included, then more layers of data aggregation should be utilized.

Step 3: Perform voltage drop analysis and power flow analysis for the given time interval.

Step 4: Repeat step 3 for different aggregation intervals.

Step 5: Determine the difference between the estimated values for number of tap changes and power loss for each time interval and the reference aggregation interval. The total estimation deviation is computed as

$$\delta_\tau = \frac{\kappa_\tau - \kappa_{ref}}{\kappa_{ref}}$$

Where κ_τ is the measurement of the performance parameter (which in this work is either the total number of tap changes in a given month or the total line loss in a given month) for the given aggregation interval τ and κ_{ref} is the same for the reference aggregation interval. For accuracy, the reference time interval will be the smallest time interval.

Step 6: Statistically determine the significance of different contributing factors for the model development, which in this work are considered to be the following: (a) size and type of distribution system; (b) season or month of the year; (c) aggregation interval; and (d) combination of these factors.

Step 7: Once the significant contributing factors are evaluated, determine the relationship between the contributing factors and the estimation error.

3.2.3 Performance Parameter Estimation Model

Active residential consumer participation using the advanced metering infrastructure will allow them to share their demand at a certain time interval. This information can be used to estimate the voltage drop across the feeder. Furthermore, the AMI can be used to better forecast consumers' future load, which could be shared with the utility to better plan distribution system operations. This work assumes that the load current can be better estimated at the load points using AMI data at a given data granularity. With this information, an approach is proposed to determine the following performance parameters at the distribution level: (*i*) tap changing operations in a day, and (*ii*) power loss in the entire feeder.

Figure 3.2 shows a one-line diagram for a radial feeder with n nodes, where A_i and B_i are ladder sweep matrices from the iterative power flow model [51], and I_i is the estimated load current at node i as in Appendix, Part A.

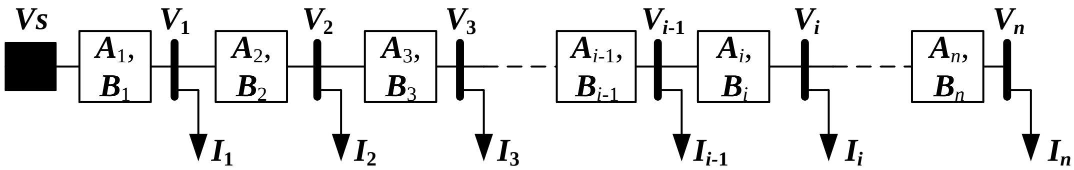

Figure 3.2 Voltage drop Calculation for distribution feeder

To determine the number of tap-changing operations the flowchart in figure 3.3 can be used. The proposed tap-change estimation model and line-loss estimation model given in Appendix Part B can be used in radial distribution systems to determine the estimated values for different data granularities.

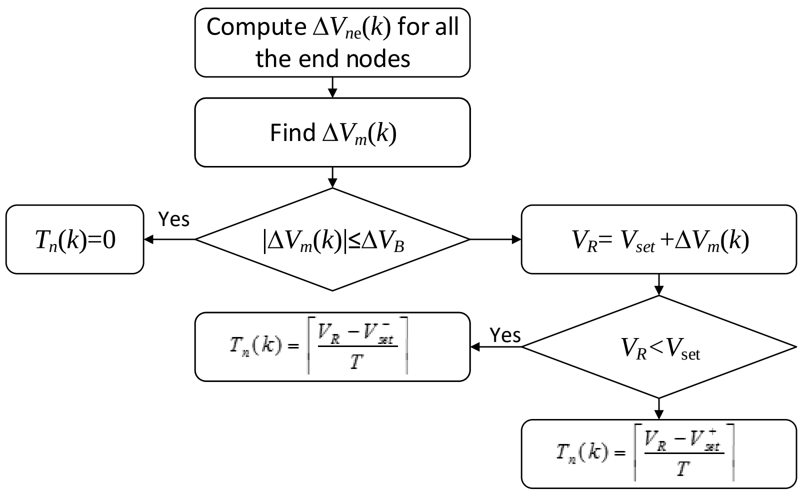

Figure 3.3 Flowchart used to compute number of tap changes

3.3 Generalized Models for Distribution Feeders

The previous section proposes two models to evaluate performance in the presence of aggregated feeder-level data. Since test feeders only provide the average load at each node, to perform a time sequential analysis, a residential load generator for each residential house was developed. Using the load profiles from available data [52], a log-normal distribution-based load generator was developed, and its statistical validity was verified. The number of houses for each node was calculated using a 0.55 coincidence factor [53].

One of the objectives here is to develop a generalized model. The least-dominant performance parameters can be neglected to develop the most practical model for performance evaluation. Therefore, a statistical approach is applied to determine the dominant parameters out of several, such as month of the year, data aggregation, type of feeder, and presence of renewable resources.

When more than one input/contributing parameter is suspected of influencing a relationship, then a statistical approach such as the design of experiments (DoE) can be used to determine and validate the significance of each factor and to develop a predictive equation [54]. DoE is used to analyze the design of this task that aims to describe or explain the variation of information under conditions that are hypothesized to reflect the variation. This work uses the DoE to determine the significance of each parameter on the accuracy of the performance parameter estimation. Based on step 6 in sub-section 3.2.2, the following are used in this work:

Size and type of distribution system: IEEE 13- and 34-node test feeders were used here to determine the significance of distribution feeder type. These two feeders were chosen because they are distinctly different in terms of length, loading, voltage regulation, voltage level, and load unbalance. Also tap control settings are kept constant, respective of the feeder system so that effect of data granularity can be highlighted on the performance parameter.

Season or month of the year: The effect of an operational time period on the estimation accuracy is incorporated by including data for one entire year. By analysing one whole year, the randomness in loading and seasonal effect on load can be included in the analysis.

Distributed generation availability: The effect of uncertainty in distributed renewable energy resources on estimation accuracy is incorporated by statistically comparing systems with and without DG. Solar photovoltaics are used, and the renewable output is determined based on solar irradiation at that moment using PV data from the National Renewable Energy Laboratory (NREL) [55]. This work assumes that the solar PVs are operated in the maximum power tracking mode with the unity power factor.

Aggregation interval: One of the key contributions of this work is to include data granularity into the power system performance quantification. Aggregated demand for 5, 15, 20, 30, 40, 45, and 60 minutes is used here. Due to the typical voltage regulator delay settings, a one-minute demand is considered as real-time demand. To minimize data storage and privacy concerns, it is assumed that each residential unit will aggregate the load by choosing these demand intervals.

The DoE was carried out with system data for both 13- and 34-node test systems. The half-normal plot is an effective tool to quantitatively determine important factors/parameters [54]. Figure 3.4 shows the half-normal plots for the system data. For simplicity, the following notations are used in these plots: A is the data granularity/aggregation interval, B is the month of the year, C is the type of the system, and D refers to PV availability. Cross terms such as AB are the combined effect of two parameters. Parameters close to the indicated fitted line are considered near-zone or unimportant factors. Their effect can be modeled using a normal distribution with zero mean and therefore can be eliminated [56].

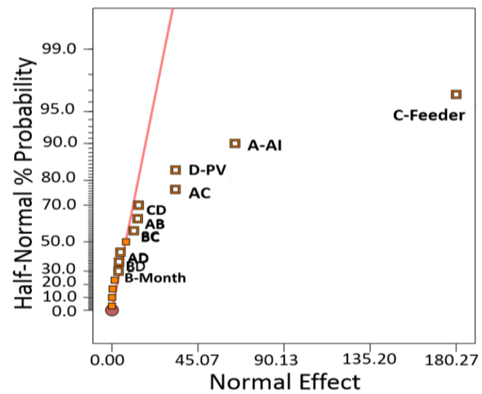

Figure 3.4 Half-normal plots considering all parameters for all busses.

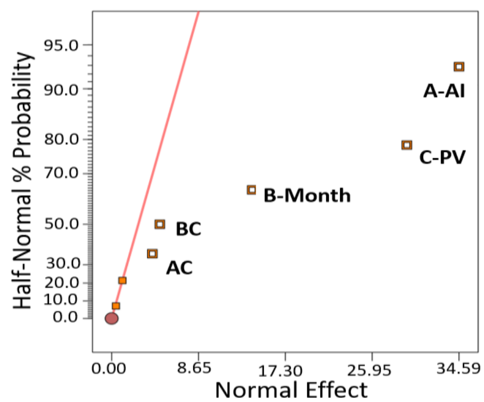

Figure 3.5 Half-normal plots considering all parameters for single bus.

Figure 3.4 shows that bus type significantly influences the voltage regulation and therefore is determined to be the most dominant parameter. The models are specific to each feeder type and based on the feeder configuration, must be developed a priori.

Figure 3.5 shows the significance of the parameters for a single network. Both the IEEE 13-node system and 34-node system were tested, and similar results were obtained. As shown in figure 3.5, both the aggregation interval and presence of distributed generation affect the accuracy of the models for single feeder system. Therefore, this work proposes that the performance evaluation model must separate the feeder type, data AI, and DG availability. Since the objective of this work is to incorporate the effect of data aggregation on a given feeder, the analysis is carried out for specific feeders. The following subsections explain the process to select the significant factors and develop the performance model. Both IEEE 13-node and 34-node systems are evaluated separately. The same procedure should be carried out for each specific feeder.

3.3.1 Tap-Changing Operations Modeling

Impact of the aggregation interval on the number of tap changes was separately analyzed with and without PV penetration. To better illustrate the effects of the data AI, both IEEE 13-node and 34-node feeders with and without distributed generation (solar PV) were considered, and a DoE with two factors and multiple levels was used to analyze the modeling significance and accuracy. Figure 3.6 and 3.7 show the half-normal probability plots for both feeders. From these figures, it can be inferred that the individual month of a year (factor B) has a negligible effect on the number of tap changes, compared to the data AI (factor A) for both small and large distribution network.

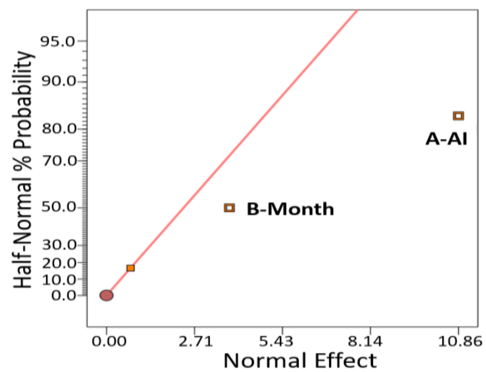

Figure 3.6 Half-normal plots of tap-change analysis: without PV penetration

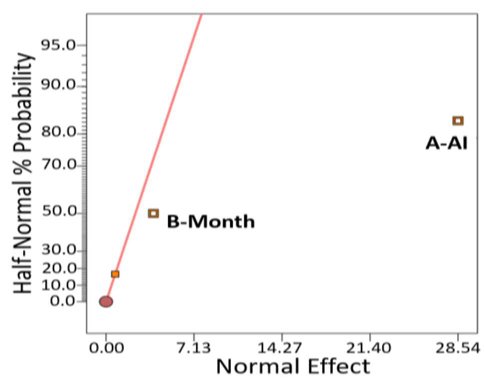

Figure 3.7 Half-normal plots of tap-change analysis: without PV penetration

Since any one season does not influence the performance model, by using load data from multiple residential units for the entire year, the number of tap-changing operations was computed, based on a one-minute demand from each residential unit, which was considered to be the benchmarking load. The demand data was aggregated in time intervals of 5, 10, 15, 20, 30, 40, 45, and 60 minutes, and the corresponding number of tap changes was recorded. The estimated deviation for τ-minute data aggregation interval was computed using the following:

$$\epsilon(\tau) = \frac{Total\ Tap\ Change(\tau) - Total\ Tap\ Change(1min)}{Total\ Tap\ Change(1min)}$$

Each of the four systems (13-node, 34-node, 13-node with DG, and 34-node with DG) was analyzed separately for the entire year. The number of tap changes in the online tap changer was computed using the model proposed in Appendix B for each data aggregation interval. For models with DG, 30% penetration of solar PV is considered here.

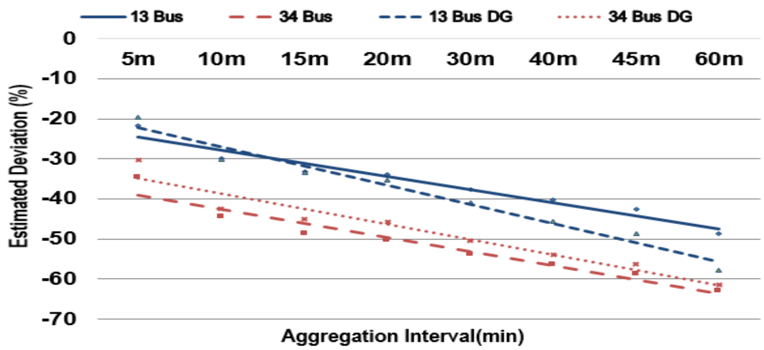

Figure 3.8 Estimated deviation in tap-changing operations.

Figure 3.8 shows the estimated deviation of tap-changing operations of load tap changers for 13- and 34-node systems with and without solar PV. These plots show that all four models have a linear relationship in terms of data AI and the estimated division in online load tap-changer operations. Goodness-of-fit tests of the developed linear and second-order polynomial models were developed, and the corresponding R^2 values were computed. Table 3.1 shows the estimated deviation in online tap-changer operations dependency on the data aggregation interval for each system with R^2 values. As can be seen, the estimated deviation model can be modelled as either a linear function or a second-order polynomial. Fitness of the model increases with the higher-order polynomial; however, based on the computational burden and the necessary precision, an appropriate model can be utilized.

Table 3.1 Estimated Deviation in Online Tap-Changer Estimation Models

System	**Estimated Deviation Model**	**R^2 Value (%)**
13-Node	$-3.2864\tau - 21.21$	95.23
	$0.0852\tau^2 - 4.0533\tau - 19.931$	95.49
13-Node with DG	$-4.777\tau - 17.44$	96.99
	$-0.0109\tau^2 - 4.6788\tau - 17.602$	97.00
34-Node	$-3.517\tau - 35.44$	93.99
	$0.2962\tau^2 - 6.1832\tau - 31$	96.66
34-Node with DG	$-3.795\tau - 31.13$	93.29
	$0.2233\tau^2 - 5.8053\tau - 27.78$	94.58

3.3.2 Line-Loss Modelling (without PV)

Similar to the voltage drop analysis, a DoE was used to determine the line-loss estimation error modelling. Fig. 7 shows the half-normal probability plots for IEEE 13- node feeders.

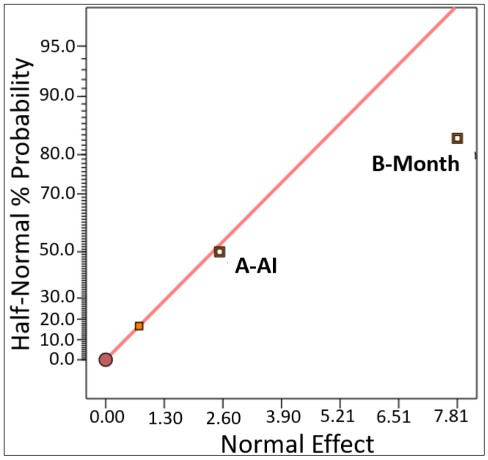

Figure 3.9 Half-normal plots of line-loss analysis of 13-node system without PV penetration

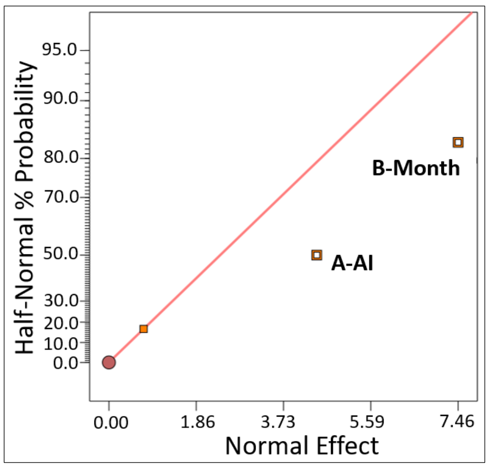

Figure 3.10 Half-normal plots of line-loss analysis of 34-node system without PV penetration

From figure 3.9 it can be inferred that the individual month of a year (factor B) significantly affects the feeder line loss, compared to the data aggregation interval (factor A). When the entire 12 months are considered together, the significance of the month is higher; however, when the year is divided into seasons, the effect of the month is much smaller, compared to the data-aggregation rate, as shown in figure 3.10. When each season is considered separately, the AI effect was significant. Therefore, line loss for each of the 16 systems (13-node-Winter, 13-node-Spring, 13-node-Summer, 13-node-Fall, 34-node-Winter, 34-node-Spring, 34-node-Summer, 34-node-Fall, 13-node with DG-Winter, 13-node with DG-Spring, 13-node with DG-Summer, 13-node with DG-Fall, 34-node with DG-Winter, 34-node with DG-Spring, 34-node with DG-Summer, and 34-node with DG-Fall) was analyzed separately for each season. The total line loss in the feeder was computed using the model proposed in Appendix B for each data AI. Similar to voltage-drop analysis, for models with DG, 30% penetration of solar PV is considered in this work. Table 3.2 and figure 3.11 shows the estimated deviation in power-loss computation models and results, respectively, for each case. Models were developed based on goodness-of-fit tests.

Table 3.2 Estimated Deviation in Power-Loss Computation Models

System	Estimated Deviation Model	R^2 Value (%)
13-N-Winter	$1.4579\tau^2 - 4.1440\tau + 39.8970$	98.22
13-N-Spring	$-0.6899\tau^2 + 15.6280\tau - 1.0090$	94.31
13-N-Summer	$-0.4257\tau^2 + 140248\tau - 11.9080$	96.00
13-N-Fall	$1.7466\tau^2 - 3.6285\tau + 17.9380$	96.87
13-N with DG-Winter	$1.7979\tau^2 - 6.9606\tau + 39.9420$	97.75
13-N with DG-Spring	$-0.7044\tau^2 + 16.2500\tau + 3.3921$	91.13
13-N with DG-Summer	$-0.4212\tau^2 + 14.4630\tau - 12.166$	96.46
13-N with DG-Fall	$2.1232\tau^2 - 4.8233\tau + 23.8770$	96.93
34-N-Winter	$0.5290\tau^2 - 1.6235\tau + 3.9660$	97.64
34-N-Spring	$0.2596\tau^2 + 4.147\tau + 2.1700$	97.06
34-N-Summer	$0.3867\tau^2 + 0.6907\tau - 1.3242$	98.49
34-N-Fall	$0.5560\tau^2 - 1.3226\tau + 2.8180$	97.15
34-N with DG-Winter	$2.1232\tau^2 - 4.8233\tau + 23.8770$	96.31
34-N with DG-Spring	$0.2457\tau^2 + 5.4347\tau + 1.7678$	96.21
34-N with DG-Summer	$0.4018\tau^2 + 1.0775\tau + 0.9381$	99.04
34-N with DG-Fall	$0.8359\tau^2 - 2.6944\tau + 7.6579$	97.99

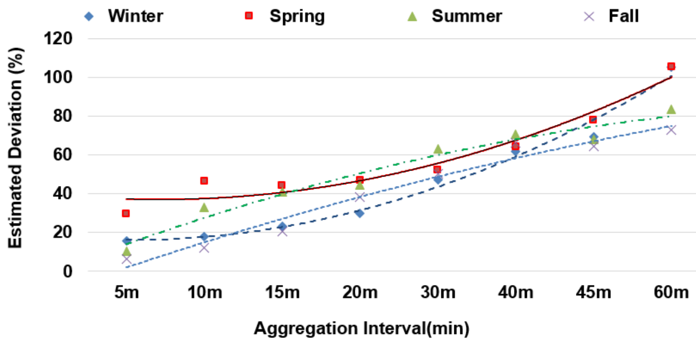

(a) 13-Node System with No Distributed Generation

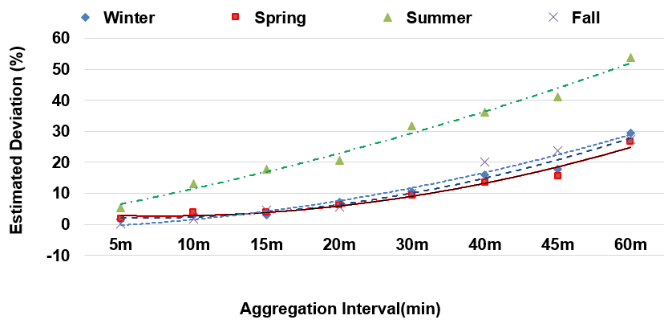

(b) 34-Node System with No Distributed Generation

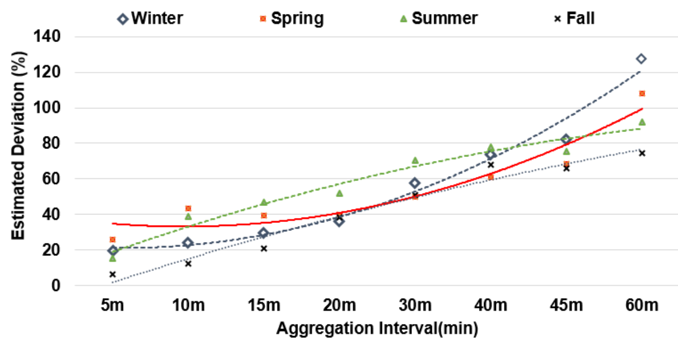

(c) 13-Node System with 30% Solar PV Penetration

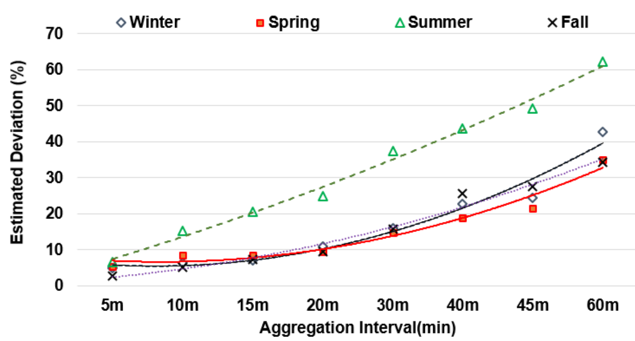

(d) 34-Node System with 30% Solar PV Penetration

Figure 3.11 Estimated deviation in power-loss computation.

Based on the two networks that were analysed with and without DG, the second-order polynomial is the lowest order polynomial that would provide a reasonable goodness of fit for the estimated deviation in power-loss computation. Higher-order models can be used to provide more accuracy.

3.4 Potential Application

Feeder-level data-driven distribution system operational planning can be considered one of the potential applications of the proposed model. For this purpose, the effective aggregation interval must be determined. This part focuses on determining the effective AI using the proposed models.

The above proposed deviation model $(\varepsilon_\tau(\alpha, s, \tau))$ can be used at every aggregation interval (τ) to determine the expected deviation (ε_τ) for both the number of tap-changing operations and the power-loss calculation. Using the calculated online tap-changing operations and power loss $(x_m(\tau))$ at a particular demand/aggregation interval, the likely calculated online tap changers and power loss were estimated $(x_{\tau,k})$. Then the system was simulated with the actual demand, the actual system parameters were evaluated and compared with the estimated system parameters, and the error $(e_{\tau,k})$ was calculated. This procedure was repeated for all samples, and then the mean error (e_m) was calculated. Figure 3.11 shows this process in a flowchart.

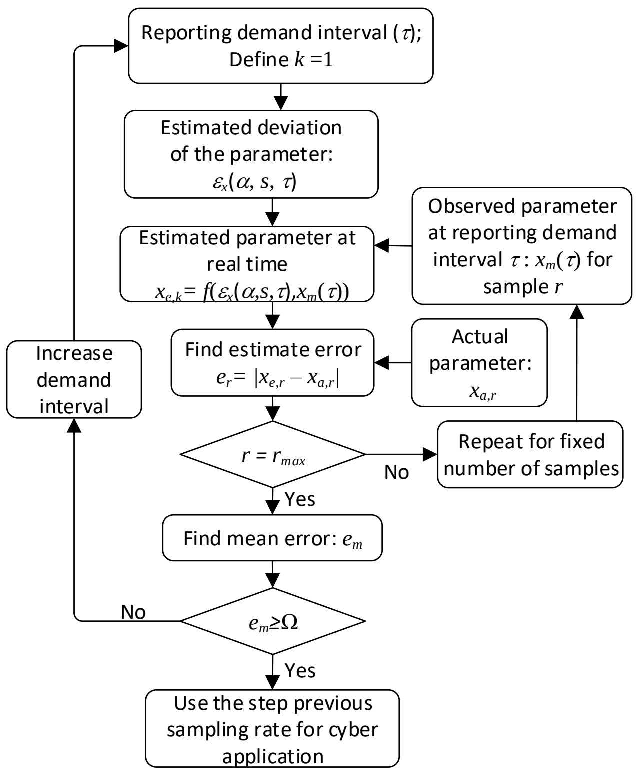

Figure 3.12 Flowchart comparing predicted and actual power loss in system.

3.4.1 Model Verification and Application

Both a model verification process and a procedure to incorporate the proposed model into the distribution system, based on the model verification process, are presented in the following subsections.

For the purpose of model verification, the estimated power loss and number of tap changes are compared with the actual system power loss and tap changes. The proposed estimated deviation models were verified using a new set of data for the same test feeders. In this work, results for the IEEE 13-node test system are presented. Test cases were generated for a different year than that for the modeling data. For the voltage-drop analysis, 40 days were randomly selected from the entire year, and for the power-loss model, 40 days were randomly selected from the winter months.

Both online tap-changing operations and power loss were computed using the models developed in Appendix A and B for aggregated demand at 5-, 10-, 15-, 20-, 30-, 40-, 45-, and 60-minute intervals. Then using the appropriate estimated deviation models from Tables 3.1 and 3.2, the predicted online tap-changing operations and power loss were computed. The predicted values were then compared with actual values and the percentage error computed using the following relationship:

$$e_r(\tau) = \frac{x(\tau) - x(t)}{x(t)}$$

Where $x(\tau)$ is the predicted value of the online tap-changing operation or power loss, and $x(t)$ is the actual value of these parameters. Figures 3.13 and 3.14 show the comparison of predicted error plots for actual line loss and actual number of tap changes, respectively.

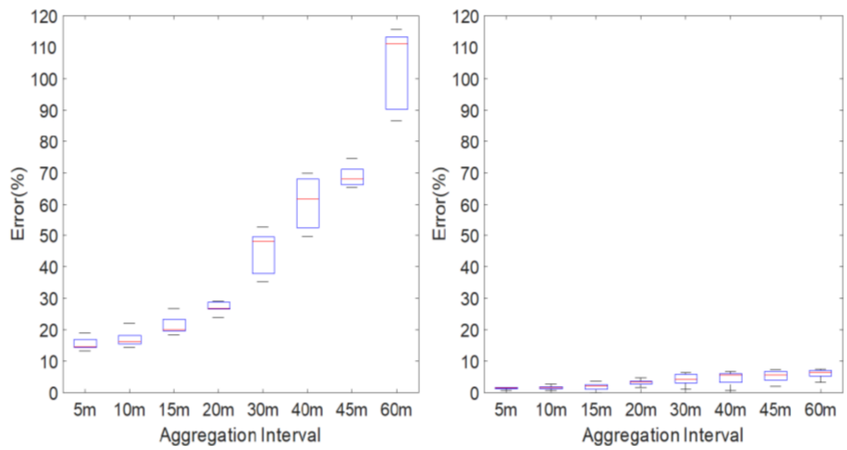

(a) Estimated deviation ***not*** considered (b) Estimated deviation considered

Figure 3.13 Comparison of estimated and actual line loss

Figure 3.13 provides a comparison of the percentage of error in power loss between the predicted and the actual loss in the system for different aggregation intervals with and without considering estimated deviation from the proposed model. It is evident that the error due to aggregating the load is significant and needs to be incorporated into data-driven decision models. Figure 3.13 (a) and (b) shows higher AI leads to high percentage of error, resulting in more deviation of the predicted value from the actual one. A comparison between figures 3.14 (a) and (b) shows percentage of error for predicting values with higher AI / (low granularity) data is attenuated due to use of the modelled estimated deviation. Thus, it can be stated that using the proposed model, higher AI data can be used to predict values with acceptable accuracy. Like the power-loss model error, the error in the likely number of online tap-changing operations is shown in figure 3.14.

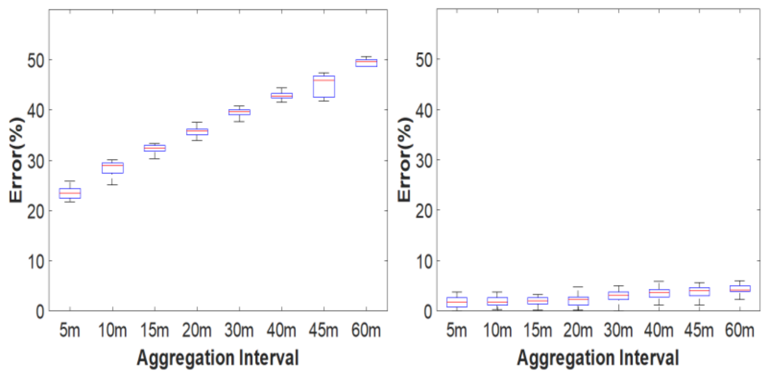

(a) Estimation error ***not*** considered (b) Estimation error considered

Figure 3.14 Comparison of estimated and actual number of tap changes

A similar trend is observed for the number of tap changes as well. However, the online tap-changing operations model provided better accuracy than the power-loss computation model. This can be attributed to the discrete count in the online tap-changing operation computation compared to the actual power-loss computation.

When the aggregation interval is increased, the percentage of error increases. This is because when a higher AI is used, more information is lost. As clearly shown, the AI impacts accurate load estimating and managing. The error trend in both the power-loss computation model and the online tap-changing operation estimation model are similar. Therefore, to achieve operational decisions with reasonable accuracy, the proposed seasonal deviation estimation model can be used. The proposed models can be used to optimize the demand AIs based on operational needs and accuracy requirements.

4. Interactive Distributed Energy Resource Management

4.1 Introduction

Recent trends in the literature facilitate co-optimized operation of transmission and distribution systems [3]-[6]. This is feasible through data sharing between transmission and distribution systems at the common coupling points [6]. However, conflicting interests among different stakeholders, privacy and security concerns, and data storage hinder data sharing between transmission and distribution operations [7]. This in turn limits practical viability of coordinated operation of transmission and distribution networks.

To overcome this challenge, regulated data sharing rules/guidelines are established when distribution operators need to share data or use a third party for managing consumer demand. For example, the California Public Utilities Commission's rule on Demand Response Provider (DRP) permits aggregators to assist retail customers with energy market participation [31]. These aggregators have an agreement with entities who will interface with the wholesale market. Rule 24/32 limits aggregators from sharing energy usage data with any entity and requires them to maintain privacy and security of any consumer data [31].

As motivated by the DRP rule, the two critical components of coordinated management of transmission and distribution systems are proper load distribution among the aggregators and effective information sharing among multiple stakeholders while preserving privacy. To achieve effective mechanism to support a DRP, it is essential to develop appropriate load clustering and load scheduling algorithms which are combined as load management in this work. A comprehensive literature review ([6]-[18]) on existing aggregation methods is shown in Table I. Techniques presented in Table I consider aggregator-based approach, however, the gap in the literature is that these approaches lack the emphasis on distributing/clustering the load among aggregators.

Table 4.1 Existing Literature on Aggregation based Load Management.

Domain	Objective	Aggregation
Market Strategy	Pricing mechanism considering customer satisfaction and system operator benefits [9]	EV customers cluster together as a virtual power plant [9]
	Framework for aggregator-based demand management [10] [11]	Each aggregator is assigned a zone (set of nodes) [11]
System Operations	Optimizing residential energy usage [12]	Regional aggregator accumulates demand in a locality [7], [12]-[18]
	System loss reduction [13]	
	Voltage optimization [13] [14]	Aggregation based on demand behavior [6] [8]
	Peak shaving/valley filling [7] [15]	

Load Clustering techniques for aggregator formation in the literature apply techniques that are used for load forecasting. For example, techniques such as k-means [58], fuzzy k means [59], C-means [58], support vector machine (SVM) [60], and classification and regression trees (CART) [60] are utilized for load forecasting. The objective in those is to form homogeneous clusters (similar customers grouped together).

Load management, unlike load forecasting, requires load in a cluster to be flexible to meet the load management objective, such as valley filling, peak clipping or load shifting. Thus, clustering only based on homogeneity of load profile is not the ideal solution for load management [61], which is also demonstrated in this chapter.

To overcome this limitation, **this work proposes** a two-part framework.

Part 1: Formation of aggregators through consumer fairness and privacy driven load clustering. The novelties of the proposed clustering algorithm are: (i) using heterogeneity for clustering; and (ii) integrating load characteristics and system operational requirements into data driven clustering.

Part 2: A decentralized load scheduling algorithm tailor made for aggregator-based load scheduling. The novelty of the proposed scheduling algorithm is the ability to obtain near optimal schedule without information interchange between the aggregators to meet the privacy requirements. In this work discrete time scheduling is proposed as the focus of this work is to develop the aggregators who can enable DRP to participate in the market.

4.2 Background and Motivation

Limited literature exists on techniques for formation of aggregators to manage load. An aggregator-based load management through formation of clusters is proposed by Hu et. al. [8]. They proposed a hierarchical control with aggregators to manage the thermostatically controllable loads (TCLs). Where, each aggregator is formed by collection of similar TCLs and they are controlled together. The major drawback of such techniques is that all the loads are controlled to reduce the peak, but they do not optimally smoothen the load curve as explained in subsections *A* and 4.2.1 and 4.2.2.

4.2.1 Load Clustering and Control Flexibility

Load aggregation could be based on spatial attributes, such as geographical location; temporal attributes, such as loading; or a combination of both. Figure 4.1 illustrates the three possible approaches for load clustering to support aggregator driven load control like the DRP model developed by California Public Utilities Commission.

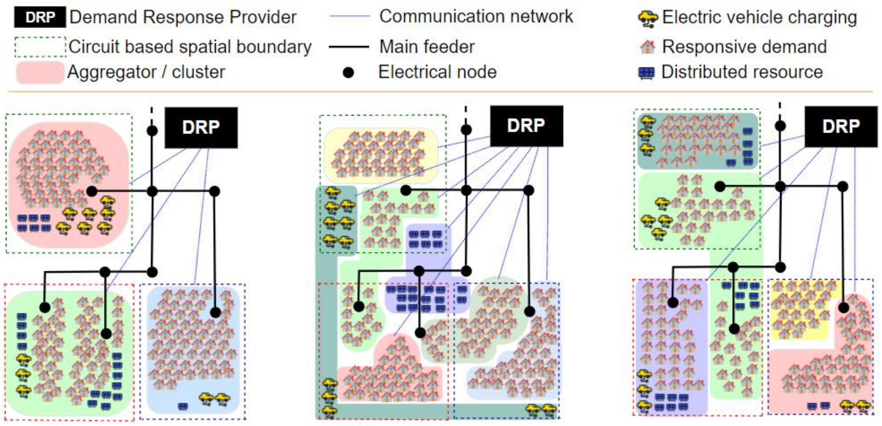

(a) spatial (b) temporal (c) spatio-temporal

Figure 4.1 Clustering approaches based on the spatial and temporal attributes

In figure 4.1 (a) load clusters are developed using spatial attributes [12] – [18]. This approach follows the conventional distribution system models. The main limitation of spatial boundaries is that load flexibility in spatially bounded aggregators heavily depend on the customers in the specific location. Not all aggregators would have sufficient flexibility for optimal operation of DRPs. Flexibility within an aggregator will be related to the benefits received by the aggregator This creates unfairness to the consumers when different aggregators have dissimilar flexibility.

To overcome this limitation, attributes based on demand pattern/usage are used to cluster the load [7] – [9] as shown in figure 4.1 (b). Aggregators are formed based on consumer load behavior where similar loads are grouped together. The major challenge with such an approach is that this does not consider consumer location in the distribution network, thus affecting the effective implementation. In addition, when similar consumers are clustered together, the load pattern of individual consumer can be easily projected by adversaries affecting the privacy of the individual consumers [62], [63].

A third approach as proposed in this work is shown figure 4.1 (c). Both spatial and temporal attributes are considered in creating the load clusters / aggregators. The advantages of this approach are two folded: (*a*) If the customers in a certain node are diverse enough, they would be clustered to form one aggregator. When the load flexibility is significantly larger multiple clusters / aggregators can be created within a node. On the other hand, when the load flexibility is not sufficient adjacent nodes are combined to create a super-node. This will improve the fairness and provide sufficient flexibility at each node; (*b*) When the diversified consumers are combined then the aggregated load will mask individual consumer load behavior. This will preserve consumer privacy when the data is shared between multiple stakeholders. A demonstration of this phenomenon is given in the following sub section.

4.2.2 Motivation Example: Heterogeneous Clustering

Consider 20 EVs with the availability for charging as shown in figure 4.2(a) as obtained from 2017 National Household Travel Survey (NHTS) data [64]. To illustrate the impact of cluster formation, two aggregators, referred as cluster A and B, are formed based on homogeneity and heterogeneity.

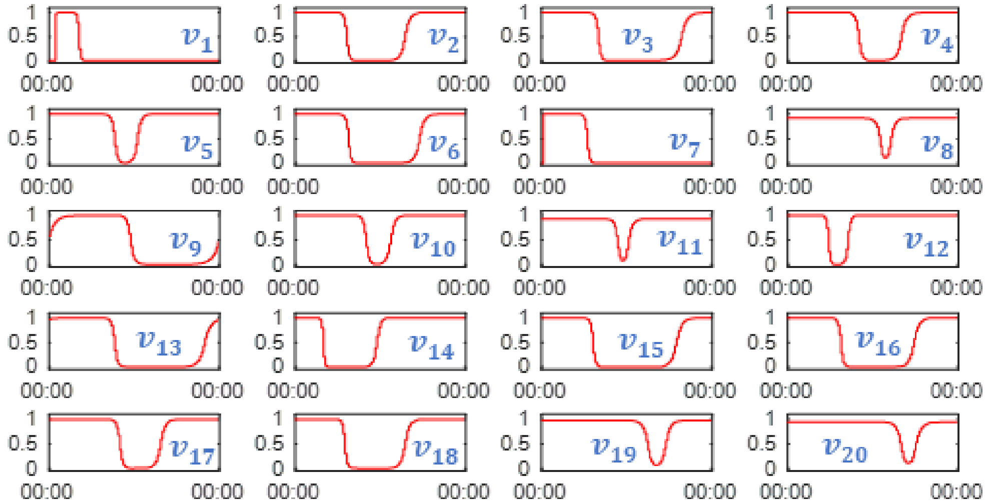

(a) probability of availability of 20 EVs for charging

Cluster	Homogenous	Heterogeneous
A	$v_1, v_3, v_7, v_9, v_{13}, v_{15}$	$v_1, v_3, v_4, v_9, v_{10}, v_{11}, v_{14}, v_{16}, v_{18}, v_{19}$
B	$v_2, v_4, v_5, v_6, v_8, v_{10}, v_{11}, v_{12}, v_{14}, v_{16}, v_{17}, v_{18}, v_{19}, v_{20}$	$v_2, v_5, v_6, v_7, v_8, v_{12}, v_{13}, v_{15}, v_{17}, v_{20}$

(b) cluster membership

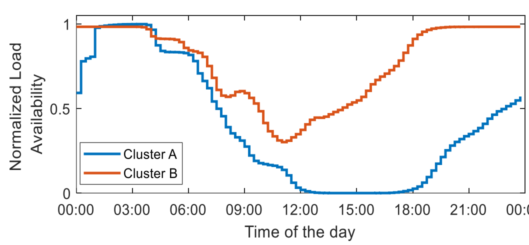

(c) clustering homogenous EVs

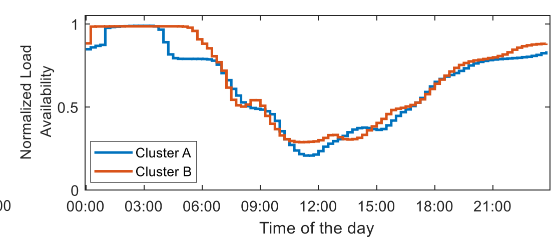

(d) clustering heterogeneous EVs

Figure 4.2 Clustering comparison based on homogeneity and heterogeneity.

The resulting aggregator memberships are given in the figure 4.2(b). As seen in the figure 4.2(b) when the aggregator is formed using homogeneity, members are unequally distributed, creating an unfairness. Figures 4.2(c) and 4.2(d) show the average aggrege load that is available for scheduling. In figures 4.2(c), clusters A and B have vastly different availabilities—specifically in cluster A none of the vehicles are available at home for charging from 12:00 pm until 6:00 pm. From an aggregator point of view, it is unfair for the aggregator that gets cluster A because it cannot provide any service for a certain period of the day, compared to the aggregator that gets cluster B. In addition, this sensitive information could be inferred based on the cluster load profile.

On the other hand, both clusters A and B have almost similar average availability when they are formed by clustering EVs with heterogeneous availability as shown in figure 4.2(d). Also, in this case, it will be difficult to decipher any individual customer information.

4.3 Context-Aware Heterogeneous Clustering

The existing clustering techniques are developed to cluster homogeneous members as clustering typically means creating groups (clusters) of similar members out of a given population [65].

An approach to obtain heterogeneous clusters is by using an existing clustering technique in a two-stage process as proposed in [62]. The *stage 1* creates clusters with similar *members such as k-*means clustering; and *stage 2 will* equally distribute the members from each cluster in *stage 1* among the aggregators. This will result in aggregators with heterogeneous members. The limitations of this method are: (i) unequal distribution of load among the aggregators (ii) the number of aggregators must be predefined and (iii) not considering the customers willingness to change their behavior to meet the grid needs.

An alternative approach is to develop a single stage heterogeneous clustering algorithm. *To the best of the authors' knowledge, there have been no efforts toward heterogeneous load clustering*. This work proposes a single stage heterogeneous clustering algorithm as described in the next submissions. *Subsection A* focuses on developing an approach cluster dissimilar members and *Subsection B* focuses on incorporating consumer and grid requirements/limitations.

4.3.1 Fundamentals of single stage heterogeneous clustering

Grouping similar members is achieved by grouping members with least distance between attributes together. However, heterogeneous clustering requires additional information such as:

a. What defines the dissimilarity?
b. How to define the distance between clusters to meet the required allocation?

a) Proposed dissimilarity metric for clustering

Li et. al. showed that cosine similarity is more suitable distance metric for time series data such as load profile, [66]. The cosine similarity captures the correlation between the changes (rise and fall) of two vectors. Also, cosine similarity is ideal for sparse vectors, such as load flexibility curves. The cosine distance between *n*-dimensional vectors $\boldsymbol{a}_i$ and $\boldsymbol{a}_j$ can be given as [66],

$$cosine_{i,j} = \frac{\boldsymbol{a}_i \cdot \boldsymbol{a}_j}{|\boldsymbol{a}_i||\boldsymbol{a}_j|}$$

In classical homogeneous clustering techniques members with larger cosine similarity will be grouped together. However, the objective in load management is to group diverse loads together. Therefore, the clusters should be created with members having lower cosine similarity.

In the context of load management, $\boldsymbol{a}_i$ is defined as the *availability vector* that represents the availability of i^{th} responsive demand. in the scheduling horizon with n intervals as shown in figure 4.2(a) as represented as:

$$\boldsymbol{a}_i = [p_i^1 \quad p_i^2 \quad \cdots \quad p_i^k \quad \cdots \quad p_i^n]^T$$

where, p_i^k is the historic probability of load availability at the time *k* for the *i*th responsive demand.

In terms of load management, the significance of load profile is captured at the time when a load becomes either available or unavailable. Therefore, a two-state (binary) model is developed in this work to represent the load availability vector. The *binarized availability vector* is formed where for the *i*th responsive demand at *k*th time the state of availability is given by,

$$\Psi_i^k = \begin{cases} 1 & if\ p_i^k \geq \epsilon \\ 0 & if\ p_i^k < \epsilon \end{cases}$$

where, ϵ chosen heretically based on customer behavior or historic data. Upon computing the binarized availability vector the similarity between those vectors needs to be computed. Jaccard coefficient is a well-known matric used to measure the distance two vectors. It is computed by the ratio of intersection of two vectors over their union. For example, in the case of binary vectors $(\boldsymbol{\Psi}_i \,\&\, \boldsymbol{\Psi}_j)$ intersection is defined as the sum of instances where both vectors have same value.

$$\boldsymbol{\Psi}_i \cap \boldsymbol{\Psi}_j = F(0,0) + F(1,1)$$

$F(0,0)$ and $F(1,1)$ give the number of instances where both the vectors $\boldsymbol{\Psi}_i$ & $\boldsymbol{\Psi}_j$ have the value of 0 and 1 respectively. Similarly, the union is given by the summation of all the instances.

$$\boldsymbol{\Psi}_i\ U\ \boldsymbol{\Psi}_j = F(0,0) + F(0,1) + F(1,1) + F(1,0)$$

Therefore, the Jaccard coefficient or similarity measure between vectors $\boldsymbol{\Psi}_i$ & $\boldsymbol{\Psi}_j$ is given as,

$$Jaccard\ Coefficeint_{i,j} = \frac{\boldsymbol{\Psi}_i \cap \boldsymbol{\Psi}_j}{\boldsymbol{\Psi}_i \cup \boldsymbol{\Psi}_j}$$

From the context of responsive demand, availability is the critical metric to determine the similarity. Therefore, the similarity can be determined by comparing the overlapping availability and total individual availability. This work proposes modification to Jaccard Coefficient, *binary similarity index* (BSI), for similarity measure.

To find the intersection the overlapping unavailable duration is excluded, and the relationship is given by:

$$\boldsymbol{\Psi}_i \,\tilde{\cap}\, \boldsymbol{\Psi}_j = F(1,1)$$

The union is considered as the instance in which at least one responsive demand is available, and the relationship is given by,

$$\boldsymbol{\Psi}_i \,\tilde{\cup}\, \boldsymbol{\Psi}_j = F(0,1) + F(1,0) + +F(1,1)$$

BSI for *i*th and *j*th responsive demands is given by:

$$BSI_{i,j} = \frac{\boldsymbol{\Psi}_i \,\tilde{\cap}\, \boldsymbol{\Psi}_j}{\boldsymbol{\Psi}_i \,\tilde{\cup}\, \boldsymbol{\Psi}_j}$$

In addition to better representing the load availability, the two-state representation will effectively capture dissimilarity as shown in Table 4.2.

Table 4.2 Distance Metric Comparison

Distance Metric	**Cosine Similarity**	**Jaccard Coefficient**	**BSI**
v_1 & v_7	0.7454	0.8750	0.5200
v_6 & v_7	0.6901	0.6875	0.4545
v_{10} & v_{11}	0.9780	0.9375	0.9318
v_{10} & v_{19}	0.8849	0.7292	0.7292

b) Proposed metric to define the distance between clusters

For fair aggregator formation, in addition to the diversity within one cluster, it is important to have similar load diversity among multiple clusters. Therefore, the proposed heterogeneous clustering should result in clusters (in turn aggregators) with similar load diversity. To ensure fair cluster formation, a metric, *load diversity distribution* (LDD) factor, is proposed in this work. The following illustrates the formulation of the LDD.

For the cluster m cluster average availability of the N_m responsive demands at instance k is defined as the number of average responsive demand available in one instant and is given as,

$$A_m^k = \frac{\sum_{i=1}^{N_m} p_i^k}{N_m}$$

Similarly, system average availability of the N responsive demands at instance k, which is given as,

$$A^k = \frac{\sum_{i=1}^{N} p_i^k}{N}$$

For each cluster, the average availability is allocated based on the number responsive demands in each cluster and the allocation factor given as,

$$w_m = \frac{N_m}{N}$$

The objective is to have each cluster availability as close as possible to the allocated average availability. Therefore, the LDD is defined as,

$$LDD_m^t = \left(\frac{A_m^t - w_m A^t}{w_m A^t}\right)$$

The average availability plotted for clusters A and B, shown in figures 4.2(c) and 4.2(d) for demonstration, was calculated using the relationship shown in the equation above. It is formulated to capture the difference between the availability of all the responsive demands considered for load management and the response demands in cluster during a time interval k. LDD factor of a cluster j for time t is given by,

$$LD_j^t = \left(\frac{A_j^t - A^t \left(\frac{N_j}{N}\right)}{A^t \left(\frac{N_j}{N}\right)} \right)$$

Where, N_j is the number of responsive demands allotted to cluster j; N is the total number of responsive demands considered for clustering and A_j^t & A^t are the availability of demand in the cluster and the total set during time t respectively.

c) Definition of Context/Context-Awareness

This work utilizes the basic the concept of *context/context-awareness* for defining the cluster formation. *Context/context-awareness* initially proposed for handheld device applications by Abowd et al. [67]. The following subsections provide detailed modeling of context-aware heterogeneous clustering that is proposed in this work.

Abowd et al. define the term context as information about the users' environment [67]. Moreover, they define the need for context-awareness to improve the user experience without asking the user for extensive information.

From the standpoint of load management, context-awareness could be defined as fair distribution of load. This work defines the context from both customer and grid perspectives. From the customer perspective, availability (desired time to use the load) and flexibility (the ability to start earlier later than the preferred time) of the load are considered as contexts. From the grid perspective, transformer loadability and non-responsive demand (demand not considered for load management) is considered as the context. The rationale behind this approach is to cluster customers with less coinciding availability as possible, at the same time ensuring not to cluster inflexible customers in the same cluster, which may result in less flexibility at the cluster level load management.

4.3.2 Proposed algorithm

The block diagram in figure 4.3 shows the concept of the proposed context-aware heterogeneous clustering (CAHC) algorithm. As in figure 4.3, the procedure of CAHC algorithm can be divided into the following 3 blocks,

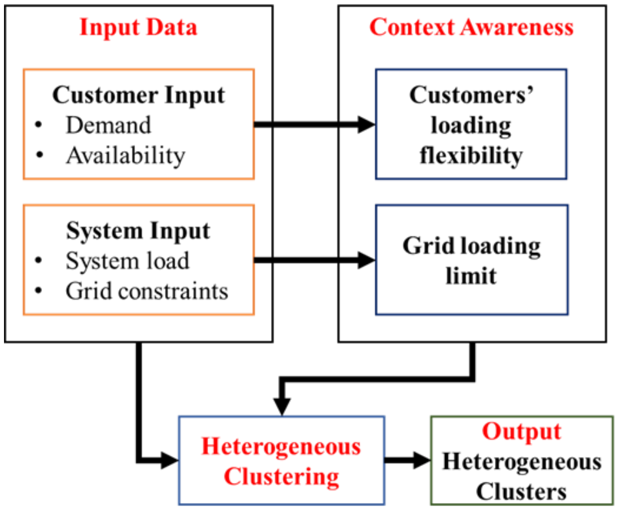

Figure 4.3 Concept of proposed CAHC algorithm

Input Data: Get the inputs: $\boldsymbol{N} -$ total responsive demands connected at the node; $\boldsymbol{K}_{-} -$ minimum number of clusters allowed; $\boldsymbol{K}_{+} -$ maximum number of clusters allowed; $\boldsymbol{a} -$ availability of all responsive demands during each time interval; $\boldsymbol{d} = [\boldsymbol{d_1}, \boldsymbol{d_2}, \dots, \boldsymbol{d_N}] -$ rated demand of all responsive demands; $\boldsymbol{c} = [\boldsymbol{c_1}, \boldsymbol{c_2}, \dots, \boldsymbol{c_T}] -$ cost/weight given by the system for each time interval based on the transformer loadability and other non-responsive demand in the system.

Matrix $\boldsymbol{a}$ is of the dimension $(T \times N)$, where each $\boldsymbol{a_1}, \boldsymbol{a_2}, \dots, \boldsymbol{a_N}$ is a $(T \times 1)$ column vector, as given by equation (4):

$$\boldsymbol{a} = [\boldsymbol{a_1}, \boldsymbol{a_2}, \dots, \boldsymbol{a_N}]$$

Adding Context-Awareness: Once the input data is made to the required form, the context awareness is given by the following step:

Using $\boldsymbol{a_i}$, determine the probability of available duration for each responsive demand from the following relationship, for the i^{th} responsive demand:

$$pa_i = \frac{\sum_{t=1}^{T} d_i * a_i^t}{\sum_{t=1}^{T} c_t}$$

$$p_{labels_i} = \frac{pa_i}{pt_i}$$

where pt_i is the number of time slots required for operation of the i^{th} responsive demand, i.e., duration of demand represented as time slots required. Then, arrange all responsive demand labels in an array $\boldsymbol{p_{labels}}$ such that $pa_i < pa_{i+1}$ (ascending probability of available duration).

Heterogeneous Clustering: After the input data is provided the context-awareness the heterogeneous clustering is done through the following steps:

Step 1: Pick the first k responsive demands from the list $\mathbf{p_{labels}}$, and assign them to each cluster $\mathbf{W_1}$ to $\mathbf{W_k}$. Update $\mathbf{p_{labels}}$.

Step 2: Make a new array for all responsive demands, $i \in \boldsymbol{p_{labels}}$, by giving a binary value for availability during a time period t, using the relation given in equation (2)

Step 3: Consider the cluster $\boldsymbol{W_1}$, and determine the next responsive demand to put in the cluster by finding the one that produces,

$$min\left(\sum_{t=1}^{T} \boldsymbol{\Psi}_{\boldsymbol{W_1^t}} + \boldsymbol{\Psi}_{\boldsymbol{a_i^t}}\right)$$

Step 4: Update $\boldsymbol{p_{labels}}$ after allotting the responsive demand to the cluster. Update $\boldsymbol{\Psi_{W_1}}$by adding $\boldsymbol{\Psi_{a_i}}$ of the SL_i that is allotted to cluster $\boldsymbol{W_1}$ in step 2**.**

Step 5: Repeat steps 2 & 3 until every cluster is allotted with one responsive demand.

Step 6: Repeat steps 2 to 4 until all responsive demands are allotted to a cluster.

Step 7: Once all responsive demands are allotted, compute the LD factor for all clusters 1 through k, as in equation (9).

$$LD_j^t = \left(\frac{A_j^t - A^t\left(\frac{N_j}{N}\right)}{A^t\left(\frac{N_j}{N}\right)}\right), j = 1,2, \dots, k$$

Step 8: Check to see if,

$$\|\boldsymbol{LD_j}\| \leq \tau, for\ j = 1,2, \dots, k$$

where $\boldsymbol{LD_j} = \left[LD_j^1, LD_j^2, \dots, LD_j^T\right] -$ LD vector of cluster W_j.

If yes, then go to step 12; else, check if,

$$k = K_+$$

If yes, then go to step 8; else, increment k by one and go to step 1.

Step 9: Output the cluster index for all responsive demands and STOP.

The output of the proposed CAHC algorithm will be k clusters with N_j members allotted to them. The CAHC algorithm is formulated in such a way that it will allot an equal number of responsive demands to each cluster unless $mod(N/k) \neq 0$. In that case, the additional responsive demand will be placed in the cluster where it best fits (adds to heterogeneity).

4.3.3 Metrics to evaluate heterogeneous clustering

Traditionally, the metrics used to evaluate the clustering efficiency (such as, silhouette coefficient and Hopkins statistic) are formulated to test the homogeneity between the members of the same cluster [24]. But the goal of the proposed CAHC algorithm is to form clusters with heterogeneous members, for load management. Therefore, the evaluation metric to evaluate the heterogeneous clustering should measure how well the clusters exhibit these phenomena. This can be calculated as how well the cluster availability coincides with the valley in the system demand, as given by,

$$Clustering\ Score\ (CS_j) = \frac{\sum_{t=1}^{T} TA_j^t * DL^t}{\sqrt{\sum_{t=1}^{T} {TA_j^t}^2 * \sum_{t=1}^{T} DL^t}}$$

where $TA_j^t = \sum_{n=1}^{N_j} a_i^t$ is the total availability of the cluster j at time t given as the summation of availability of all responsive demands in j during time period t, and DL^t is the demand limit given by the system operator to the aggregator for time t.

$$Normalized\ CS_j = \frac{\sum_{t=1}^{T} A_j^t * DL^t}{\sqrt{\sum_{t=1}^{T} {A_j^t}^2 * \sum_{t=1}^{T} DL^t}}$$

4.4 Proposed Load Scheduling Algorithm

Each heterogeneous cluster generated using the CAHC will be allotted to an aggregator. The role of the aggregator is to schedule the responsive demands allotted to it. A priority-led best first search (P-BFS) algorithm is developed for the aggregator level load scheduling. P-BFS is inspired by water-filling technique used for optimal resource allocation [68].

4.4.1 Problem Formulation

The objective of load scheduling is to obtain the plan for every responsive demand in the aggregator such that the demand intervals do not coincide as much i.e., to distribute the load as much as possible. According to water filling technique it can be represented as in the equation below, where the maximum value will be obtained by the plan ($\boldsymbol{selcPlan_{i\epsilon W_j}}$) that best fits the aggregator (W_j) demand limit ($\boldsymbol{depth_{W_j}}$).

$$max\left(\sum_{t=1}^{T} depth_{W_j}^t * \sum_{i=1}^{N_j}\left(selcPlan_{i\epsilon W_j}^t * d_{i\epsilon W_j}\right)\right)$$

Where, $selcPlan_{i\epsilon W_j}^t -$ 0 or 1 variable that gives the decision to turn OFF or ON the responsive demand i in aggregator W_j during time t; $d_{i\epsilon W_j} -$ demand kW of responsive demand i and $depth_{W_j}^t -$ aggregator demand limit of time t.

The depth information is given by the system operator to each aggregator. In this context, the depth is calculated as,

$$depth_{W_j}^t = \frac{N_j}{N} * \min(\psi_t, P_t)$$

Where, P_t is the node level demand limit based on the line loading and ψ_t gives the limit based on the voltage drop allowed at a particular node in the system. ψ_t is computed from the K_{drop} factor and maximum voltage drop allowable as,

$$\psi_t = \frac{\%V_{drop}^{MAX}}{K_{drop} * Distance\ from\ the\ Substation}$$

The system operator determines the demand limit $\min(\psi_t, P_t)$ based on the other demand and renewable generation at the node and the rest of the system for a time slot. The demand limit constraint for aggregator W_j is given by,

$$\sum_{i=1}^{N_j} selcPlan_i * d_{i\epsilon W_j}^{t} \leq depth_{W_j}^{t}$$

In addition to this constraint, there is also the constraint that ensures that all responsive demands obtain the desired operational duration at the end of the scheduling horizon T. It is implemented by equating the sum of slots allotted the selected plan of the i^{th} responsive demand in an aggregator during time slots T to the desired slots.

$$\sum_{t=1}^{T} selcPlan_i^t \ = \ slots$$

4.4.2 Discrete Search Strategy

While the objective function in evaluates the fit of the plan i, and provide the feasibility check. The search procedure starts with finding the deepest time interval to schedule the responsive demand. The selection of responsive demand to be scheduled in this deepest time interval is selected based on the priority, and finally, the direction that fills the maximum depth is chosen. This procedure based on the traditional water filling approach is represented in figure 4.4.

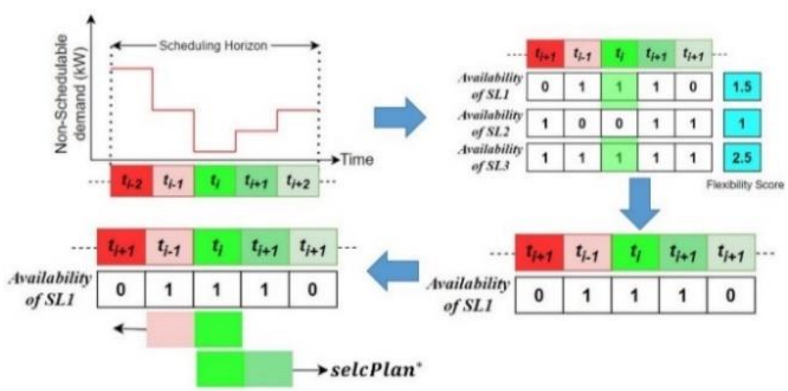

Figure 4.4 Sequence per traditional water-filling approach (starting from top left).

Since the control variable ($selcPlan_i^t$) is a 0 or 1 type variable the search space becomes discrete. Like any other discrete space search this load scheduling problem also poses the challenge of finding the optimal (or near optimal) solution in polynomial time. For instance, if a responsive demand is available for γ time slots in the scheduling horizon T and must be operated for α slots, then the possible ways it can be scheduled would be $\gamma!/\alpha!\,(\gamma-\alpha)!$. The worst-case scenario for this problem is, all responsive demands to be scheduled have $\alpha = \gamma/2$, resulting in the highest number of possibilities. However, this worst-case can be avoided by using CAHC algorithm as it results in mix of responsive demand with different flexibility and availability in a cluster. In addition, the search is further optimized by the water-filling based search procedure used given in figure 4.4.

4.4.3 Modification to improve global solution

In the real-time scenario the scheduling will be done simultaneously by all the aggregators. In that case multiple aggregators operating at the same node might create similar scheduling plan. This may lead the aggregators consuming (or not consuming) at the same time. To account for this, the water-filling approach is modified to start with the responsive demand with highest priority (least flexible), then the time with the most depth (lowest load) in which that demand is available is chosen. The procedure of the proposed P-BFS algorithm is shown in figure 4.5. This modification makes significant difference when scheduling demand in parallel without information transfer among aggregators.

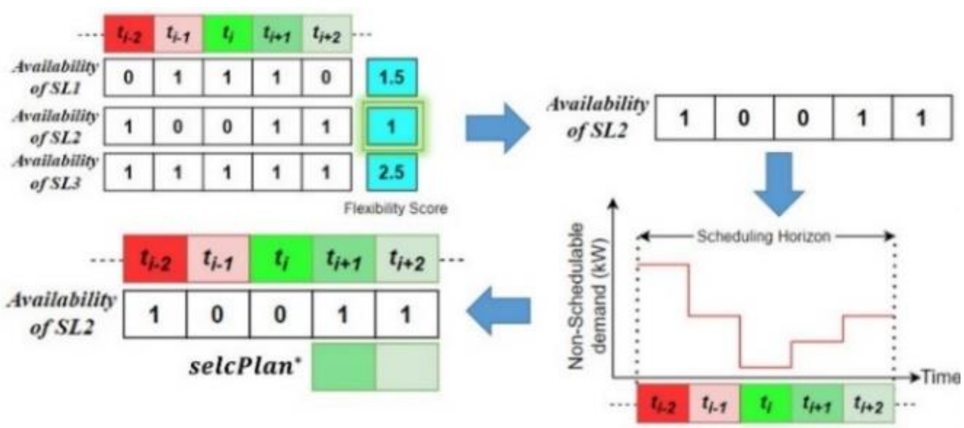

Figure 4.5 Sequence per proposed P-BFS algorithm (starting from top left).

Although, it is impossible to prove the optimality and convergence of the algorithm, the numerical analysis done shows the feasibility of obtaining a near-optimal solution. The proposed scheduling algorithm is given below:

Algorithm: Priority led Best First Search

Input:

1. $Agg_j = \left\{v_{p1}, v_{p2}, \dots v_{N_j}\right\}$: set of load availability data with priority (p_{labels}) in aggregator j
2. $slots$: Number of slots required for user to operate their load
3. DL : Demand limit (depth) for each time slot

Output: Schedule for all responsive demands in aggregator j

1: **Procedure** $SCHEDULE(n, slots, DL, availability)$
2: $Agg' \leftarrow Agg_j$
3: $FinalSchedule = 0$
4: $Plans = 0$
5: **while** $Agg' \neq NULL$ ***do***
6: $plans = GeneratePlans(v_{pi}, slots)$
7: $selcPlan = PlanRanking(v_{pi}, slots, EVDL, choice)$
8: **if** $(DL \backslash selcPlan) \geq 0$ **then**
9: $FinalSchedule = finalSchedule \cup \{selcPlan\}$
10: $Agg' = Agg' \backslash v_{pi}$
11: **else**
12: **for** $i = 0$ to $|selcPlan|$
13: $selcPlan = selcPlan \backslash selcPlan_i$
14: go to 8
15: **end for**
16: **end if**
17: **end while**
18: **return** $FinalSchedule$
19: **end procedure**

4.5 Numerical Analysis and Results

In this section, the proposed clustering algorithm and scheduling algorithm are implemented using EVs as the responsive demand. The rationale for choosing EVs for the implementation is that they are one of the (if not the) increasing loads that the grid will see in the future. Also, they come in different sizes (charging demand) and connect to the grid at different times (demand availability). Thus, EVs were chosen as being representative of a responsive demand. For the purpose, 100 EVs from the same geographical location were chosen from the NHTS data [64]. These EVs were assumed to be connected to Node 675 in the IEEE 13-bus system. System demand at that node is shown in figure 4.6. This graph was obtained by subtracting the renewable generation injected at the node from the net non-responsive demand.

The two variants of the proposed context-aware heterogeneous clustering algorithm are compared with the two-stage process implemented using k-means, mean-shift, optics, and hierarchical clustering algorithms. The reason for choosing these methods was to have at least one algorithm based on spherical clustering (k-means and mean-shift), density-based clustering (optics), and hierarchical clustering. The effectiveness of the resulting heterogeneous clusters in each of these methods is evaluated using the index defined in subsection 4.3.3

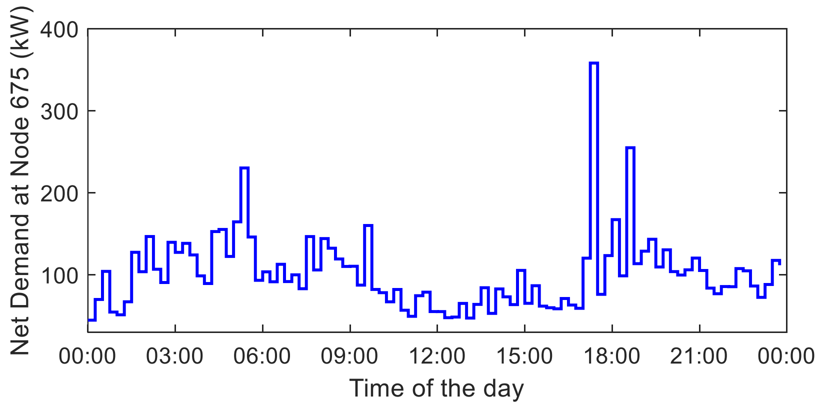

Figure 4.6 Node-level demand data used for analysis.

4.5.1 Proposed CAHC Algorithm (vs) Two-Stage Clustering

The first step in the proposed method is to allot the EVs to aggregators. The two variants of the proposed context-aware heterogeneous clustering algorithm are compared with the two-stage process implemented using k-means, mean-shift, optics, and hierarchical clustering algorithms. The reason for choosing these methods was to have at least one algorithm based on spherical clustering (k-means and mean-shift), density-based clustering (optics), and hierarchical clustering. The effectiveness of the resulting heterogeneous clusters in each of these methods is evaluated using the index given in subsection 4.3.3.

For performing this allocation, as provided in Section III, along with the input data mentioned above, the following parameters were chosen: $K_{-} = 10$; $K^{+} = 10$; $c_t = 1$. The rationale behind choosing these values was to have the same number of clusters in both the CAHC algorithm and the two-stage clustering process for comparison, as the two-stage process requires a predefined number of aggregators. The cost/weight for each time period was chosen to be equal for the same reason. figure 4.7, gives the resulting probable EVs available under different methods. The tighter the graphs are more similar the aggregators and so is the fairness in distribution of EVs for demand response. From this figure we can say that the CAHC: Binarized has the least variation between the aggregators throughout the day. The boxplot shown in figure 4.8 indicates the variation in number of EVs among the clusters when clustered using the two-stage process. This unequal distribution would be unfair for aggregators and would result in increased scheduling complexity for the aggregator with more EVs. The effect of clustering on the final schedule is given in the following subsection.

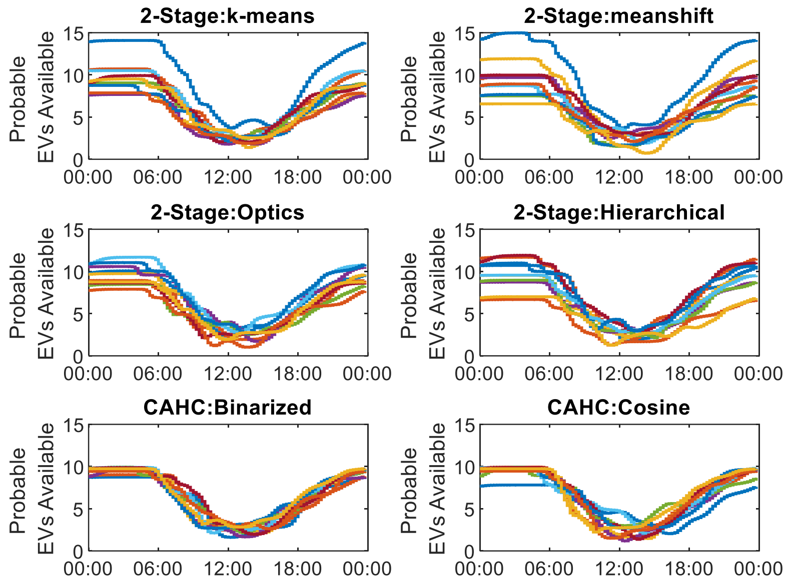

Figure 4.7 Aggregators obtained from corresponding methods.

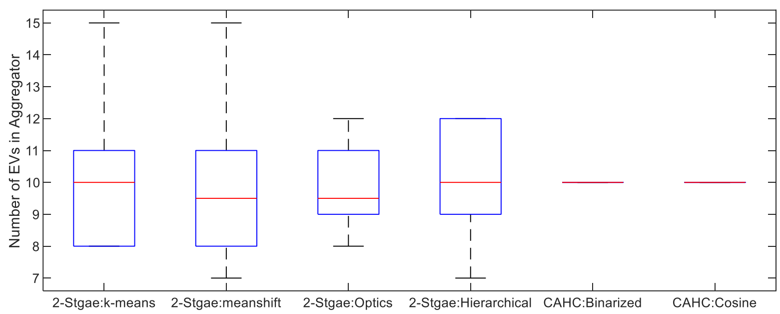

Figure 4.8 Distribution of EVs among aggregators in corresponding methods

Based on the metrics defined the clusters obtained from each method were evaluated, and the sum of the scores are represented in Table II. From this table, the two variants of the proposed CAHC algorithm have the same score with and without normalization using the number of vehicles in the cluster. This is because the proposed CAHC algorithm provides equal distribution of load among the clusters, whereas the two-stage process results in clusters with different numbers of EVs.

Table 4.3 Clustering Score Obtained Using Different Methods

Method	**Sum of Cluster Scores**	**Sum of Normalized Cluster Score**
2 Stage: k-means	9.102	7.7023
2 Stage: Optics	9.092	7.8915
2 Stage: Mean shift	9.095	7.2954
2 Stage: Hierarchical	**9.103**	7.7034
CAHC: Binarized	9.091	**9.091**
CAHC: Cosine	9.080	9.080

4.5.2 Water-Filling (vs) P-BFS Approach

To establish the effectiveness of the proposed P-BFS algorithm, two separate analysis were done: (i) applying the water-filling and P-BFS techniques for the whole dataset (100 EVs at a time with no clustering), and (ii) applying the water-filling and P-BFS techniques to the aggregators (clustering from CAHC: binarized). The resulting EV demand from analyses (i) and (ii) are presented in figures 4.9 and 4.10. It is evident that the water-filling technique works better for centralized scheduling, but when applied to aggregator-level scheduling, it creates an artificial peak, as shown in figure 4.10. The P-BFS technique performs better because it reduces the EV demand during the peak period of the day (compared to on-arrival charging) and does not create artificial peaks (as in the water-filling technique). This is because of the modification explained in Section IV that makes it suitable for aggregator-level scheduling, which is done simultaneously.

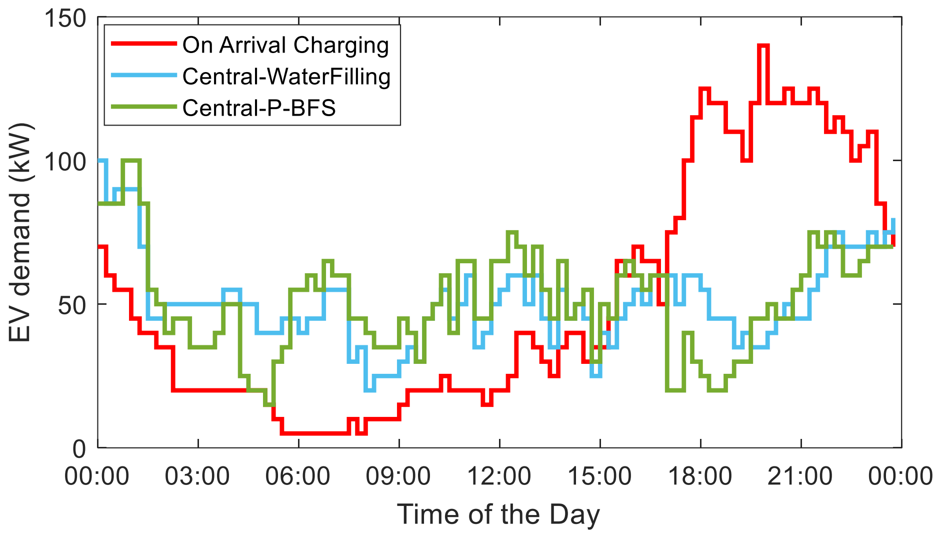

Figure 4.9 Scheduling without clustering.

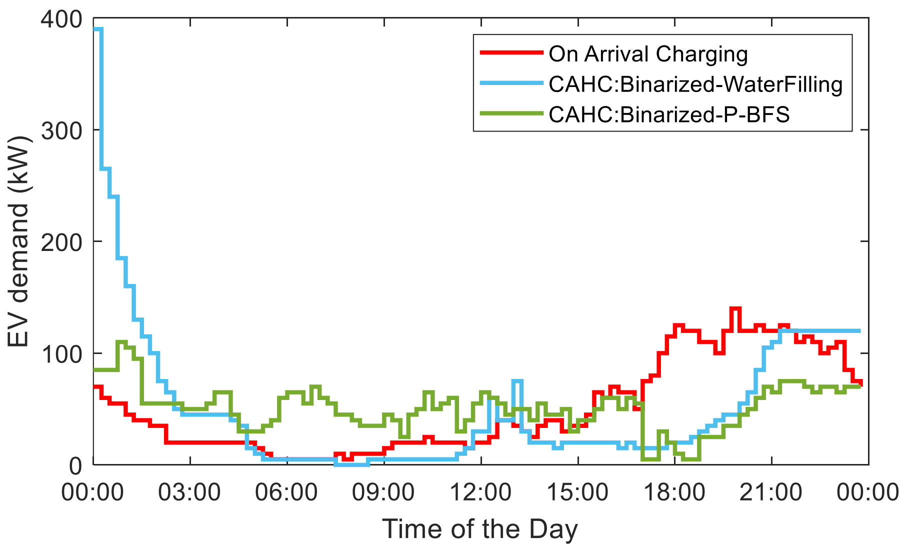

Figure 4.10 Scheduling with clustering

To analyze the effectiveness of the proposed methods (CAHC + P-BFS), the following cases are considered: (i) on-arrival charging, (ii) two-stage process: hierarchical with BFS (iii) CAHC: cosine with P-BFS and (iv) CAHC: binarized with BFS. From figure 4.11, on-arrival charging results in the highest EV demand that too during the peak hours. However, it is hard to visualize the difference between the other cases from figure 4.11. To analyze the effectiveness of these schedules, they are implemented on a distribution test system in the following sub section.

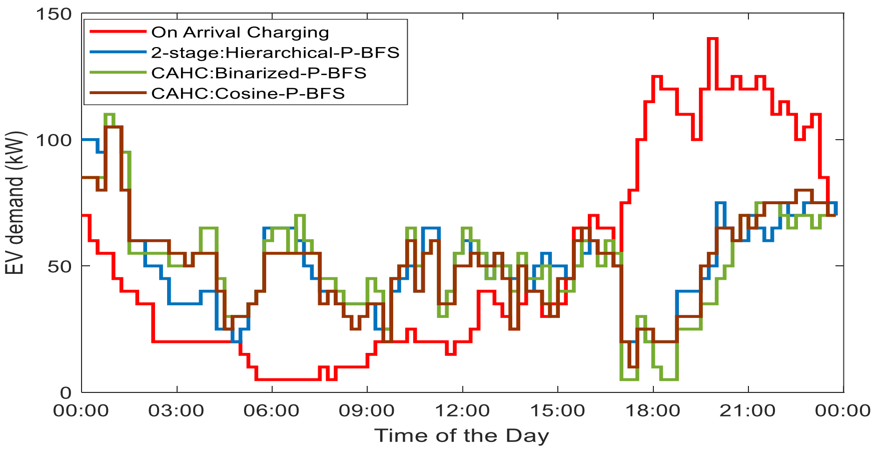

Figure 4.11 Proposed scheduling under different clustering procedures.

4.5.3 Implementing Schedule in IEEE 13-Bus System

The four schedules presented in figure 4.11 where implemented (one at a time) at node 675 of IEEE 13 bus test system. The demand in the rest of the nodes were considered non-responsive. The power flow analysis was carried out with the above arrangement and the results are shown in figure 4.12. In this figure, the system performance is shown in terms of no. of tap changes and power loss during the day. Both these parameters are presented as a percentage of the corresponding values when no EV charging is considered. From figures 4.12 and 4.13 the schedule with CAHC: binarized and P-BFS result in the least impact to the system. Thus, the proposed techniques when implemented only in one node provide considerable benefit to the overall system. This shows the significance of the proposed methods.

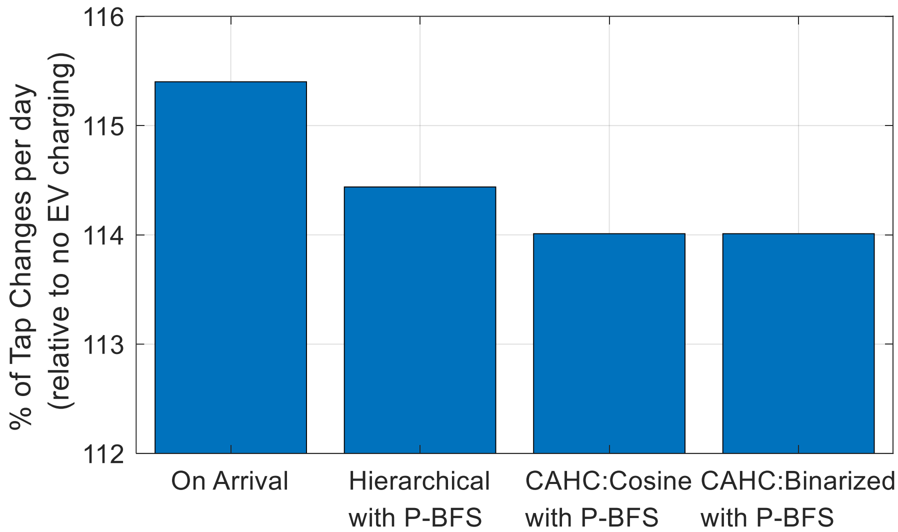

Figure 4.12 Number of tap operations in different methods

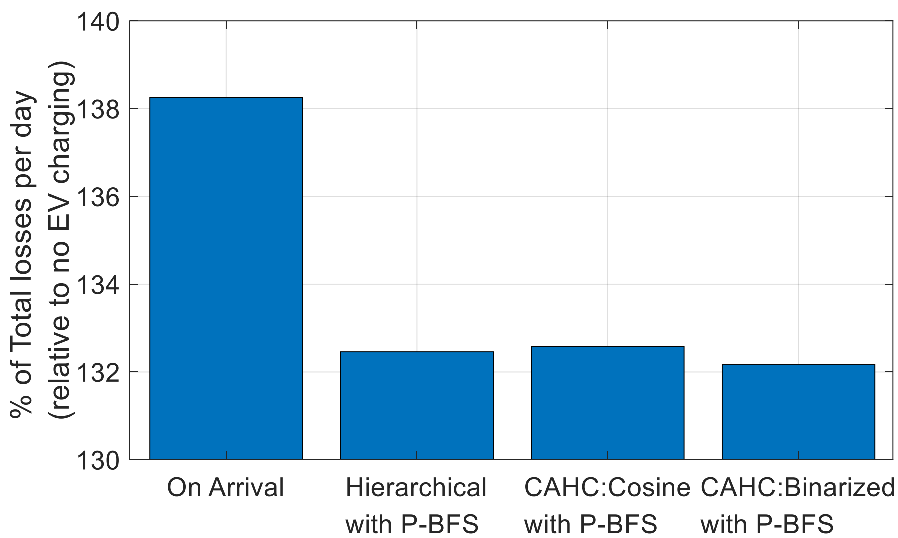

Figure 4.13 System power loss in different methods

5. Conclusion

Based on the preliminary study conducted by this work, the significance of distribution system load and data aggregation were found to be one of the key elements (that were not addressed in the existing literature) for effective coordination of transmission and distribution systems. Following are the conclusions and final remarks from this work:

This work presented the initial benchmark for quantifying the loss of important details when data is aggregated. Based on the literature review, to our best knowledge the effect of data granularity on control accuracy is not quantified or modeled for the power system problems. The main contribution of this work is to provide an outlook on the idea to quantify the data granularity on power system control accuracy.

Based on the results, it is evident that the effect of the data aggregation interval is significant, and a generic model for any distribution network is not effective. Therefore, any model that incorporates data must consider the network topology, network unbalance, consumer type, etc. In summary, this work evaluated and presented a technique to assess the importance of the data AI for power system applications, with the focus on closing the gap to better understand communication requirements and power-system needs. The resulting modeling technique from this work can be applied to a wide variety of applications:

- Improved distribution-level asset management: For example, low-resolution data obtained by the utility can be used to estimate online tap-changer remaining life.
- Enhancement of demand-response programs: Identification of the effective aggregation interval based on consumer comfort requirements can be used as a guide for the demand response.
- Active consumer participation: The next-generation distribution system with distributed generation can be operated better using low-resolution data with estimated deviation.

In addition to the above a novel heterogeneous load clustering technique for responsive demand management is developed in this work. Furthermore, a best first scheduling algorithm is developed for managing responsive demand within a cluster (aggregator). The proposed method improves consumer privacy and aggregation efficiency (fairness and scheduling). The proposed context-aware heterogeneous clustering algorithm has superior performance as it considers both power system properties and consumer preferences. Along with the clustering algorithm, the priority-led best first scheduling algorithm schedules responsive demand such that the distribution system loss and tap operations are minimized. This proposed approach can be applied in future aggregator driven retail markets and for effective integrated operation of transmission and distribution systems.

Appendix

A. Tap-Changing Operations Prediction Model

During normal operation, the bandwidth of the voltage regulators is set at 2V on the base of 120V. The maximum voltage drop is calculated at the furthest node from the feeder. Voltage at node 1 can be evaluated as

$$V_1 = A_1 V_S - B_1 \sum_{j=1}^{n} I_j$$

Voltage at node 2 can be evaluated as,

$$V_2 = A_2 V_1 - B_2 \sum_{j=2}^{n} I_j$$

Therefore,

$$\Delta V_2 = A_1 A_2 V_S - A_2 B_1 \sum_{j=1}^{n} I_j - B_2 \sum_{j=2}^{n} I_j$$

Hence, the voltage drop between the substation and node 2 is

$$\Delta V_2 = (1 - A_1 A_2) V_S + A_2 B_1 \sum_{j=1}^{n} I_j + B_2 \sum_{j=2}^{n} I_j$$

The generalized voltage drop between the substation and node *i* is

$$\Delta V_i = \left(1 - \prod_{k=1}^{i} A_k\right) V_s + \sum_{k=1}^{n} \left(\sum_{m=1}^{\min(k,i-1)} \left(\prod_{r=m+1}^{i} A_r \right) B_m \right) I_k + B_i \sum_{k=i}^{n} I_k$$

When the length of the feeder sections is small, $A_i = 1$, the following approximated model can be used:

$$\Delta V_i = \sum_{k=1}^{n} \left(\sum_{m=1}^{\min(k,i-1)} B_m \right) I_k + B_i \sum_{k=i}^{n} I_k$$

When multiple branches are present in a feeder, the voltage drop must be computed for every end node (n_e). The maximum voltage drop at the kth time interval is

$$\Delta V_m(k) = \max_{\forall n_e} \left| \Delta V_{n_e} \right|$$

B. Line-Loss Prediction Model

Using a similar approach, the line loss between source node and node 1 can be evaluated as

$$P_{loss,s-1} = B_1 \left(\sum_{j=1}^{n} I_j \right)^2$$

Similarly, power loss can be evaluated as

$$P_{loss} = B_1 \left(\sum_{j=1}^{n} I_j \right)^2 + B_2 \left(\sum_{j=2}^{n} I_j \right)^2 + \cdots B_{n-1} \left(\sum_{j=n-1}^{n} I_j \right)^2 + B_n I_n^2$$

which could be further simplified as

$$P_{loss} = \sum_{j=1}^{n} \left(B_j \sum_{i=j}^{n} I_i \right)$$

References

[1] B. Palmintier, et al., “Integrated Distribution-Transmission Analysis for Very High Penetration Solar PV,” NREL/TP-5D00-65550, 2016.

[2] EPRI, “The Integrated Grid: Realizing the Full Value of Central and Distributed Energy Resources,” Available:https://energy.gov. [Accessed August 2020].

[3] Palmintier, Bryan, et al. "Experiences integrating transmission and distribution simulations for DERs with the Integrated Grid Modeling System (IGMS)." Power Systems Computation Conference (PSCC), 2016. IEEE, 2016.

[4] Schneider, Kevin P., et al. Modern grid initiative distribution taxonomy final report. No. PNNL-18035. Pacific Northwest National Lab.(PNNL), Richland, WA (United States), 2008.

[5] Aliprantis, Dionysios, et al. "Integrated retail and wholesale power system operation with smart-grid functionality." IEEE PES General Meeting. IEEE, 2010.

[6] Evans, P. "New Power Technologies,“Regional Transmission and Distribution Network Impacts Assessment for Wholesale Photovoltaic Generation,” California Energy Commission." tech. rep., CEC-200-2014-004 (2014).

[7] J. Tu, M. Zhou, H. Cui, and F. Li, “An Equivalent Aggregated Model of Large-Scale Flexible Loads for Load Scheduling,” in *IEEE Access*, vol. 7, pp. 143431-143444, 2019.

[8] M. Ghanavati and A. Chakravarthy, "Demand-Side Energy Management by Use of a Design-Then-Approximate Controller for Aggregated Thermostatic Loads," in *IEEE Trans. on Control Systems Technology*, vol. 26, no. 4, pp. 1439-1448, July 2018.

[9] J. Hu et al., “Load Following of Multiple Heterogeneous TCL Aggregators by Centralized Control,” in *IEEE Trans. on Power Systems*, vol. 32, no. 4, pp. 3157-3167, July 2017.

[10] S. G. Argade, V. Aravinthan, I. E. Buyuktahtakın, and S. Joseph, “Performance and consumer satisfaction-based bi-level tariff scheme for EV charging as a VPP,” in *IET Generation, Transmission & Distribution*, vol. 13, no. 11, pp. 2112-2122, 4 6 2019.

[11] C. Zhang, Q. Wang, J. Wang, P. Pinson, J. M. Morales, and J. Østergaard, “Real-Time Procurement Strategies of a Proactive Distribution Company with Aggregator-Based Demand Response,” in *IEEE Trans. on Smart Grid*, vol. 9, no. 2, pp. 766-776, March 2018.

[12] K. Bruninx, H. Pandžić, H. Le Cadre, and E. Delarue, “On the Interaction between Aggregators, Electricity Markets and Residential Demand Response Providers,” in *IEEE Trans. on Power Systems*, vol. 35, no. 2, pp. 840-853, March 2020.

[13] Y. Ozturk, D. Senthilkumar, S. Kumar, and G. Lee, “An Intelligent Home Energy Management System to Improve Demand Response,” in *IEEE Trans. on Smart Grid*, vol. 4, no. 2, pp. 694-701, June 2013.

[14] S. Deilami, A. S. Masoum, P. S. Moses, and M. A. S. Masoum, “Real-Time Coordination of Plug-In Electric Vehicle Charging in Smart Grids to Minimize Power Losses and Improve Voltage Profile,” in *IEEE Trans. on Smart Grid*, vol. 2, no. 3, pp. 456-467, Sept. 2011.

[15] H. Xing, M. Fu, Z. Lin, and Y. Mou, “Decentralized Optimal Scheduling for Charging and Discharging of Plug-In Electric Vehicles in Smart Grids,” in *IEEE Trans. on Power Systems*, vol. 31, no. 5, pp. 4118-4127, Sept. 2016.

[16] Z. Xu, W. Su, Z. Hu, Y. Song, and H. Zhang, “A Hierarchical Framework for Coordinated Charging of Plug-In Electric Vehicles in China,” in *IEEE Trans. on Smart Grid*, vol. 7, no. 1, pp. 428-438, Jan. 2016.
[17] Palmintier, Bryan, et al. "Design of the HELICS high-performance transmission-distribution-communication-market co-simulation framework." Proc. 2017 Workshop on Modeling and Simulation of Cyber-Physical Energy Systems, Pittsburgh, PA. 2017.
[18] Daily, Jeff, et al. "Framework for network co-simulation." *3rd workshop on next-generation analytics for the future power grid*. Vol. 17. 2014.
[19] Pilatte, Nicolas, Petros Aristidou, and Gabriela Hug. "TDNetGen: An Open-Source, Parametrizable, Large-Scale, Transmission, and Distribution Test System." IEEE Systems Journal (2017).
[20] Schmidt, Hernán Prieto, et al. "Interchangeable balanced and unbalanced network models for integrated analysis of transmission and distribution systems." IEEE Transactions on Power Systems 30.5 (2015): 2747-2754.
[21] Huang, Qiuhua, and Vijay Vittal. "Integrated transmission and distribution system power flow and dynamic simulation using mixed three-sequence/three-phase modeling." IEEE Transactions on Power Systems 32.5 (2017): 3704-3714.
[22] Li, Zhengshuo, et al. "Transmission contingency analysis based on integrated transmission and distribution power flow in smart grid." IEEE Transactions on Power Systems 30.6 (2015): 3356-3367.
[23] Velaga, Yaswanth Nag, et al. "Transmission-Distribution Co-Simulation: Model Validation with Standalone Simulation." *2018 North American Power Symposium (NAPS)*. IEEE, 2018.
[24] Kadavil, Rahul, Timothy M. Hansen, and Siddharth Suryanarayanan. "An algorithmic approach for creating diverse stochastic feeder datasets for power systems co-simulations." Power and Energy Society General Meeting (PESGM), 2016. IEEE, 2016.
[25] Abhyankar, S., K. Balasubramaniam, and B. Cui. "Load Model Parameter Estimation by Transmission-Distribution Co-Simulation." 2018 Power Systems Computation Conference (PSCC). IEEE, 2018.
[26] Balasubramaniam, K., and S. Abhyankar. "A combined transmission and distribution system co-simulation framework for assessing the impact of Volt/VAR control on transmission system." Power & Energy Society General Meeting, 2017 IEEE. IEEE, 2017.
[27] Singhal, Nikita G., and Kory W. Hedman. "An integrated transmission and distribution systems model with distribution-based LMP (DLMP) pricing." North American Power Symposium (NAPS), 2013. IEEE, 2013.
[28] Elliott, Ryan T., et al. "Sharing Energy Storage Between Transmission and Distribution." *IEEE Transactions on Power Systems* 34.1 (2019): 152-162.
[29] Mohseni-Bonab, Seyed Masoud, et al. "Investigation of BESSs' benefits in transmission and distribution systems operations using integrated power grid co-optimization." Electrical Power and Energy Conference (EPEC), 2017 IEEE. IEEE, 2017.
[30] P. Mancarella and G. Chicco, “Real-Time Demand Response from Energy Shifting in Distributed Multi-Generation,” *IEEE Trans. Smart Grid*, vol. 4, no. 4, Dec. 2013.
[31] California Public Utilities Commission, “Rule 21 Interconnection,” [Online]. Available: https://www.cpuc.ca.gov/Rule21/. [Accessed January, 2021].
[32] California Public Utilities Commission, “Direct Participation with a DRP Aggregator,” [Online]. Available: https://www.cpuc.ca.gov. [Accessed September, 2020].

[33] J. Ponoćko and J. V. Milanović, "Forecasting Demand Flexibility of Aggregated Residential Load Using Smart Meter Data," in *IEEE Transactions on Power Systems*, vol. 33, no. 5, pp. 5446-5455, Sept. 2018.

[34] V. Sarkar and S. Khaparde, “Improving Demand Response and Bid-Consistency of Price Outcome in the Security-Constrained Dispatch Scheduling,” *IEEE Trans. on Power Systems*, vol. 28, no. 3, Aug. 2013.

[35] A. Rabiee, A. Soroudi, B. Mohammadi-ivatloo, and M. Parniani, “Corrective Voltage Control Scheme Considering Demand Response and Stochastic Wind Power,” *IEEE Trans. Power Systems*, early access.

[36] Y. Ozturk, D. Senthilkumar, S. Kumar, and G. Lee “An Intelligent Home Energy Management System to Improve Demand Response,” *IEEE Trans. Smart Grid*, vol. 4, no. 2, June 2013.

[37] N. Forouzandehmehr, M. Esmalifalak, H. Mohsenian-Rad and Z. Han, "Autonomous Demand Response Using Stochastic Differential Games," in *IEEE Transactions on Smart Grid*, vol. 6, no. 1, pp. 291-300, Jan. 2015.

[38] M. Parvania, M. Fotuhi-Firuzabad, and M. Shahidehpour, “ISO’s Optimal Strategies for Scheduling the Hourly Demand Response in Day-Ahead Markets,” *IEEE Trans on Power Systems*, vol. 29, no. 6, Nov. 2014.

[39] J. Wang, S. Kennedy, and J. Kirtley Jr. “Optimization of Forward Electricity Markets Considering Wind Generation and Demand Response,” *IEEE Trans. Smart Grids*, vol. 5, no. 3, May 2014.

[40] A. Safdarian, M. Fotuhi-Firuzabad, M., and M. Lehtonen, M., “Benefits of Demand Response on Operation of Distribution Networks: A Case Study,” *IEEE Systems Journal*, vol. 10, no. 1, pp. 189-197, 2016.

[41] A.L.A. Syrri and P. Mancarella, “Reliability Evaluation of Demand Response to Increase Distribution Network Utilization,” *International Conference on Probabilistic Methods Applied to Power Systems* (*PMAPS*), July 7-10, 2014.

[42] S. Puradbhat and R. Banerjee, “Estimating Demand Side Management Impacts on Buildings in Smart Grid,” 2014 IEEE Innovative Smart Grid Technologies—Asia (ISGT Asia), May 20-23, 2014, pp. 635-640.

[43] V. Gungor, D. Sahin, T. Kocak, S. Ergut, C. Buccella, C. Cecati, and G. Hancke, “A Survey on Smart Grid Potential Applications and Communication Requirements,” *IEEE Trans. Industrial Informatics*, vol. 9, no.1, pp. 28-42, Feb. 2013.

[44] J. McHann, “Grid Analytics: How Much Data Do You Really Need?” *2013* IEEE Rural Electric Power Conference, April 28, 2013–May 1, 2013, pp. C3-1–C3-4.

[45] S. Chakraborty, T. Balachandran, and V. Aravinthan, “Worst-Case Reliability Modeling and Evaluation in Cyber-Enabled Power Distribution Systems,” 2017 North American Power Symposium (NAPS), Morgantown, WV, September 2017.

[46] V. C. Dev et al., “Towards Application-Aware Data Concentration Schemes for Advanced Metering Infrastructures,” 2015 IEEE International Conference on Smart Grid Communications (SmartGridComm), Miami, FL, 2015, pp. 440-445.

[47] S. Elphick, V. Gosbell, S. Perera, “The Effect of Data Aggregation Interval on Voltage Results,” Australian Universities Power Engineering Conference 2007, Dec. 9-12, 2007, pp. 1-7.

[48] Wang Li-yong, Zhang Bao-hui, Ren Jin-feng, Zhou De-cai, Yao Feng, Zhang Wen-hao, Xie Huan, and Yu Guang-liang, “A Solution to Lower Tap Changing or Capacitors

Regulator Times in Reactive Power Control in Distribution Systems," 2005 IEEE/PES Transmission and Distribution Conference and Exhibition: Asia and Pacific, 2005, pp. 1-5.

[49] R. Jongen, E. Gulski, P. Morshuis, J. Smit, and A. Janssen, "Statistical Analysis of Power Transformer Component Life Time Data," 2007 International Power Engineering Conference, Dec. 3-6, 2007,.

[50] H. Markiewicz and K. Antoni, Klajn, "Voltage Disturbances Standard EN 50160—Voltage Characteristics in Public Distribution Systems, Wroclaw University of Technology, 2004.

[51] K. Dehghanpour, Z. Wang, J. Wang, Y. Yuan and F. Bu, "A Survey on State Estimation Techniques and Challenges in Smart Distribution Systems," in *IEEE Transactions on Smart Grid*.

[52] W. H. Kersting, *Distribution System Modeling and Analysis*, CRC Press, Boca Raton, FL, 2002.

[53] I. Richardson and M. Thomson, "One-Minute Resolution Domestic Electricity Use Data, 2008-2009" [computer file]. UK Data Archive [distributor], Colchester, Essex, October 2010. SN: 6583, http://dx.doi.org/10.5255/UKDA-SN-6583-1

[54] A. R. Malekpour and A. Pahwa, "Reactive Power and Voltage Control in Distribution Systems with Photovoltaic Generation," North American Power Symposium (NAPS), Sept. 9-11, 2012, pp. 1-6.

[55] National Renewable Energy Laboratory, "Transmission Grid Integration," available online at http:// www.nrel.gov/electricity/transmission/solar_integration_dataset.html.

[56] American Society of Quality, "Design of Experiments Tutorial," available online at http://asq.org/learn-about-quality/data-collection-analysis-tools/overview/design-of-experiments-tutorial.html.

[57] NIST, *Engineering Statistics Handbook,* available online at http://www.itl.nist.gov/div898/handbook/index.html

[58] F. L. D. Silva, C. E. H. Nishida, D. M. Roijers, and A. H. R. Costa, "Coordination of Electric Vehicle Charging through Multiagent Reinforcement Learning," in *IEEE Trans. on Smart Grid*, vol. 11, no. 3, pp. 2347-2356, May 2020

[59] Q. Chen *et al.*, "Dynamic Price Vector Formation Model-Based Automatic Demand Response Strategy for PV-Assisted EV Charging Stations," in *IEEE Trans. on Smart Grid*, vol. 8, no. 6, Nov. 2017.

[60] G. J. Tsekouras, N. D. Hatziargyriou, and E. N. Dialynas, "Two-Stage Pattern Recognition of Load Curves for Classification of Electricity Customers," in *IEEE Trans. on Power Systems*, vol. 22, no. 3, pp. 1120-1128, Aug. 2007.

[61] C. L. Shek, A. Manoharan, S. Gampa, T. Chandrappa and V. Aravinthan, "A Diversity-Based Clustering Technique for Implementing Decentralized Node Level Charge Scheduling Of Electric Vehicles," at *2019 North American Power Symposium (NAPS)*, pp. 1-6

[62] J. Cao, B. Carminati, E. Ferrari, and K. Tan, "CASTLE: Continuously Anonymizing Data Streams," in *IEEE Trans. on Dependable and Secure Computing*, vol. 8, no. 3, pp. 337-352, 2011.

[63] Z. Tu, K. Zhao, F. Xu, Y. Li, L. Su, and D. Jin, "Protecting Trajectory from Semantic Attack Considering k-Anonymity, l-Diversity, and t-Closeness," in IEEE Trans. on Network and Service Management, vol. 6, no. 1, pp. 264-278, 2019.

[64] U.S. Department of Transportation Federal Highway Administration, "National Household Travel Survey," 2017. [Online]. Available: https://nhts.ornl.gov/. [Accessed January 2020]

[65] A.K. Jain, "Data clustering: 50 years beyond K-means," in Pattern recognition letters, 31(8), pp.651-666, 2010.

[66] W. Li, J. Zhou, X. Xiong, and J. Lu, "A Statistic-Fuzzy Technique for Clustering Load Curves," in IEEE Trans. on Power Systems, vol. 22, no. 2, pp. 890-891, May 2007.

[67] Abowd, G.D., Dey, A.K., Brown, P.J., Davies, N., Smith, M., and Steggles, P., "Towards a Better Understanding of Context and Context-Awareness," in *International Symposium on Handheld and Ubiquitous Computing* (pp. 304-307). Springer, Berlin, Heidelberg, September 1999.

[68] P. He, L. Zhao, S. Zhou, and Z. Niu, "Water-Filling: A Geometric Approach and Its Application to Solve Generalized Radio Resource Allocation Problems," in *IEEE Trans. on Wireless Communications*, vol. 12, no. 7, pp. 3637-3647, July 2013.

Part II

Modeling Distributed Rooftop Solar Generation

Ward Jewell
Sandhya Nadipalli, Graduate Student

Wichita State University

For information about this project, contact

Ward Jewell
Wichita State University
216 Jabara Hall
Wichita, Kansas 67260
Phone: (316) 978-6340
Email: ward.jewell@wichita.edu

Power Systems Engineering Research Center

The Power Systems Engineering Research Center (PSERC) is a multi-university Center conducting research on challenges facing the electric power industry and educating the next generation of power engineers. More information about PSERC can be found at the Center's website: http://www.pserc.org.

For additional information, contact:

Power Systems Engineering Research Center
Arizona State University
527 Engineering Research Center
Tempe, Arizona 85287-5706
Phone: 480-965-1643
Fax: 480-727-2052

Notice Concerning Copyright Material

Table of Contents

List of Figures

1. Introduction

Solar photovoltaic (PV) generation systems installed on residential and commercial buildings are providing increasing levels of energy generation—generation about which operators have little information. Increasingly sophisticated load models give generation and transmission operators accurate forecasts of load. But the amount of solar generation is relatively unknown, making it difficult to schedule system resources. “Masked load” refers to the load that is not seen by upstream components because its presence is masked by PV or any other form of distributed generation. Generators on the distribution side are usually not monitored in real time so their status is unknown to operators.

It is important that the masked load instead of actual total load is not used for planning and operations. Figure 1.1 [1] shows an example. The actual load (peak ckt load) is much higher than the measured load (peak ckt measured) because the measured load is the actual load minus the PV generation (total PV). If operators are unaware of PV generation and decisions are made based on measured instead of actual load, then significant overloads may occur when the PV system disconnects unexpectedly for any reason. This example highlights the importance of the issue and stresses the need for modeling PV generation on distribution systems.

This report presents the details of a new modeling and simulation technique developed to provide accurate estimates of rooftop solar generation at the distribution substation level. The only information needed about solar generation is the total area of solar panels present in the distribution system supplied by the substation. This can be estimated from the information provided to the distribution utility by PV owners. It can alternately be estimated using signal processing techniques on satellite images of the distribution service area. The orientation and tilt of the panels will be unknown, but the technique developed in this project estimates those values. Real-time or forecast solar radiation data is then used to estimate the aggregated output of the PV generators.

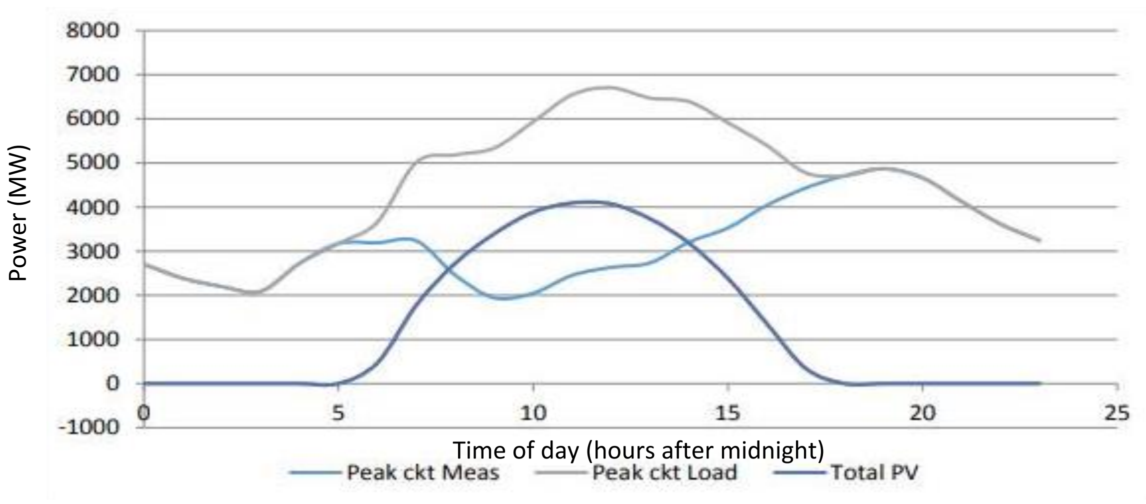

Figure 1.1 Actual load, measured load, and PV generation on peak load day [1].

1.1 Organization of Report

This report is organized as follows: Chapter 2 presents the literature search on relevant solar generation modeling techniques. Chapter 3 explains development of the new model. Chapter 4 presents a case study demonstrating the technique. Conclusions are provided in Chapter 5, and future work is addressed in Chapter 6.

2. Literature Search

2.1 Solar PV Modeling

There are standard models for solar farms that have a generation of more than 1 MW, but there is a gap in the literature about modeling rooftop solar generation because of its small scale and non-uniformity. According to FERC Order 2222, Distributed Energy Resources (DERs) with capacities from 1 kW to 10 MW are allowed to participate along with traditional resources in regional organized markets through aggregation [2]. Many of these DERS are located on distribution systems and may be behind a customer meter. Most are not monitored in real time, so they must be modeled to estimate their instantaneous and forecast generation.

Techniques that exist in the literature use various data dimension-reduction techniques such as K-means and principal component analysis (PCA). In [4], a variety of data reduction techniques are implemented and compared for accuracy and efficiency. K-means techniques cluster DERs, but the center of the cluster may not accurately represent the capacity that the cluster is actually holding. PCA may give more weight to a particular single point that has more generation, but at some other place, there can be more generation by combining multiple generators, which PCA will not recognize. PCA is effective at reducing the number of dimensions, but it is a linear technique. If the data is not organized in a linear fashion, then PCA fails to model it accurately.

A data-driven learning-based approach for disaggregating behind-the-meter PV generation using only smart meter data is proposed in [5]. Smart meter data are used to build libraries and exemplars that constantly update their weight in real time, which requires significant computing power.

Disaggregation algorithms are proposed in [6]. Net active power at the point of common coupling and local global horizontal solar irradiance are the data used. This is demonstrated for high penetrations of rooftop PV generation but will not perform well for lower penetrations.

In [7], net load readings and a proposed unsupervised framework to disaggregate PV generation are used. The algorithm iteratively estimates PV generation with a physical model and electrical load with the hidden Markov model regression. Disaggregating the net load into load and PV generation at every individual home is again very computationally challenging, and that level of granularity is not needed for transmission planning and operation.

Another disaggregation technique is proposed in [8]. Here, the model is trained with historical advanced meter infrastructure (AMI) data but only requires (supervisory control and data acquisition) SCADA data from substations in real time. This algorithm works well for a very small number of houses, but error increases with the increasing number of houses, making it unsuitable for the entire distribution system of one substation.

Another estimation technique for distributed PV is presented in [9]. The model uses customer net load based on support vector machines. Like other algorithms, it requires historical data to train the data sets. The authors in [10] used regression models in a contextually supervised source separation optimization algorithm to disaggregate load data at a substation into a sum of unobserved signals. A data decoupling method to estimate customer base load in the presence of demand response by first clustering similar customer groups and then estimating actual load power is presented in [11]. The algorithm performance depends on the duration for which demand response is implemented.

In [12], a different approach is used to calculate the potential of PV generation using a light detection and ranging (LiDAR) tool and Environmental Systems Research Institute (ESRI) solar modeling tools. This method needs extra data to calculate the amount of solar irradiance in the distribution service area. The data is unavailable for most systems now, but almost all distribution utilities do have basic information about installed rooftop solar systems. This report presents a method developed to use this limited but available data to estimate the output of PV generation on a distribution system for each time interval throughout the day.

3. New Model of Distributed Rooftop Solar PV Generation

3.1 Introduction

The total capacity of distributed PV generation installed on a distribution system is known by the distribution utility to which the generators are connected. This information is required from any customer who wishes to connect a system to the distribution system. Often capacity is the only information known about each system.

The output of a solar generator can be estimated accurately using solar radiation forecasts or data, but the area, efficiency, azimuth angle, and tilt angle of each panel are needed. Azimuth angle is the directional orientation of the panel; 90^{o} indicates the panel is oriented due east, 0^{o} is due south, and -90^{o} (270^{o}) is due west. This section describes the technique to determine assumed values for each of these for a limited number of simulated PV systems that provide an accurate forecast of PV generation for a much greater number of PV systems actually present on a distribution system.

3.2 Estimating Solar Panel Area

The total area of solar panels for each rooftop PV system can be estimated using system capacity and panel efficiency, as shown in equation (3.1):

$$Panel\ area\ (m^2) = \frac{Capacity\ (kw)}{efficiency\ (\%) \times \frac{1\ kW}{m^2}} \tag{3.1}$$

where 1 kW/m^2 is the standard value of solar radiation used to rate PV panels.

Most PV panels have efficiencies in the range of 15–18%, although they can vary more widely. Because most are in this fairly small range, a value is assumed for each system in order to estimate the size of the panels in that system. The same value is used in estimating the system generation using solar radiation forecast data. This minimizes the error caused by unknown efficiency.

3.3 Solar Irradiance

Global horizontal irradiance (GHI) is the total amount of solar radiation at any time on a horizontal plane. It includes both direct normal irradiance (DNI) and diffuse horizontal irradiance (DHI), as shown in Fig. 3.1. Reflected radiation is included in DHI. All of these values can be calculated using standard techniques [13] or recorded historical data, or real-time measured data can be used. Calculated or historical data will be used for planning purposes, and real-time measured data will be used for operations.

Global tilt irradiance **(**GTI) is total solar radiation received on a surface with defined tilt and azimuth angles. This is the sum of scattered radiation, direct and reflected:

$$GTI = DNI_t + DHI$$

where DNI_t is the DNI on a tilted surface with tilt *t*.

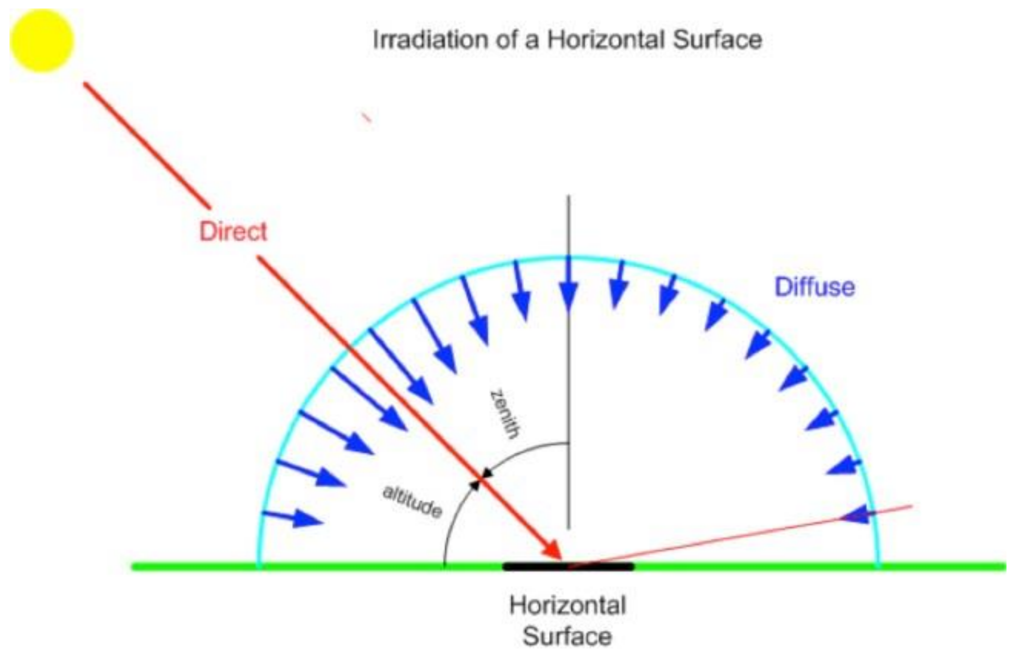

Figure 3.1 Direct and diffuse horizontal irradiance [3].

Calculation of DNI_t

1. Declination angle δ is the angle of the sun relative to the equator. Positive values are north of the equator, and negative values are south of the equator. This depends on the day of the year *N*.

$$\delta = 23.45 * \sin\left(\frac{N + 284}{365} * 360\right) degrees$$

   where *N* is the day of the year: 1 is January 1 and 365 is December 31.

2. Solar altitude angle β_{sun} is the angle of the sun above a horizontal plane. It is 0^o at sunrise and sunset, and 90^o when the sun is directly overhead.

3. Solar zenith angle θ is the angle of the sun from vertical and is the complement of solar altitude angle:

$$\theta = 90 - \beta_{sun}$$

4. The solar azimuth angle is the angle between a horizontal line running north and south, and the shadow cast by a vertical rod. An angle of zero indicates the shadow falls on the line. The angle is positive if the shadow is east of the horizontal line, and negative if it is west.

$$\alpha_{sun} = \cos^{-1}\left(\frac{\sin(\beta_{sun}) * \sin(L) - \sin(\delta))}{\cos(\beta_{sun}) * \cos(L)}\right)$$

where L is the latitude of the rod on earth.

5. Collector angle is the angle between a line normal to the surface of the collector and the sun's rays, $\theta_{collector}$:

$$\theta_{collector} = \cos^{-1}\left(\sin\left(\beta_{sun}\right) * \cos\left(\beta_{panel}\right) + \cos\left(\beta_{sun}\right) * \sin\left(\beta_{panel}\right) * \cos\left(\alpha_{sun} - \alpha_{panel}\right)\right)$$

where α_{panel} is the panel's azimuth angle, and β_{panel} is the panel's tilt angle.

6. Direct normal irradiance is calculated by

$$DNI_t = DNI * \cos(\theta_{collector})$$

7. Global tilt irradiance is calculated by

$$GTI = DNI_t + DHI$$

3.4 Estimating Azimuth and Tilt Angles

Possible azimuth angles for a panel are continuous between 0^o and 360^o. Possible tilt angles above horizontal are continuous between 0^o and 90^o. Not all azimuth angles, however, are practical for PV generation for a given latitude. Figures 3.2 to 3.5 show the effects of varying tilt and azimuth angles for a system in Wichita, Kansas (latitude 37.7^o north) on November 3, 2019, for a total panel area of 1,000 m^2.

Figure 3.2 shows that the azimuth angle is meaningless for a horizontal PV panel because the panel simply rotates in the horizontal plane. Output increases from sunrise to solar noon when the output peaks and then decreases until sunset. Figures 3.3 to 3.5 demonstrate the effects of varying panel azimuth angles for panels tilted above the horizontal. Angles between 90^o and 270^o indicate the panels are starting to face north, with 180^o being due north, and their output becomes significantly reduced.

Figure 3.6 shows the total energy generated on this day by the system as the tilt and azimuth angles are varied. As shown, for azimuth angles between 100^o and 260^o, generation is less than half of the more optimal azimuth angles. It is unlikely that it would be economical to install a system with these configurations, so they are not considered in this model. Similarly, tilt angles between 30^o and 70^o are considered as the practical range in this model. A tilt angle of 0^o is also included if there are flat roofs in the service area. Typically, rooftops dictate the tilt and azimuth angles of rooftop PV systems, which are rarely installed if the available values are not economical for PV generation. This information sets the limits of configurations that are considered when estimating the orientations of PV panels in a service area.

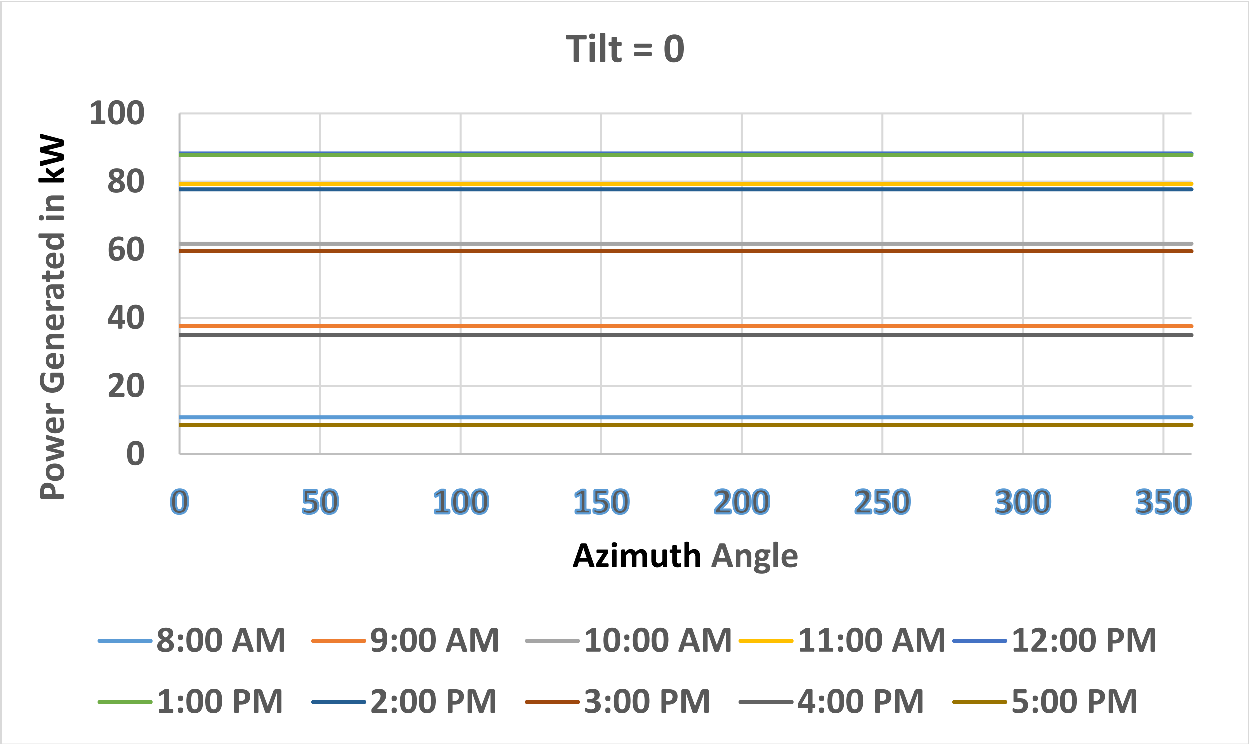

Figure 3.2 PV system output with horizontal panels.

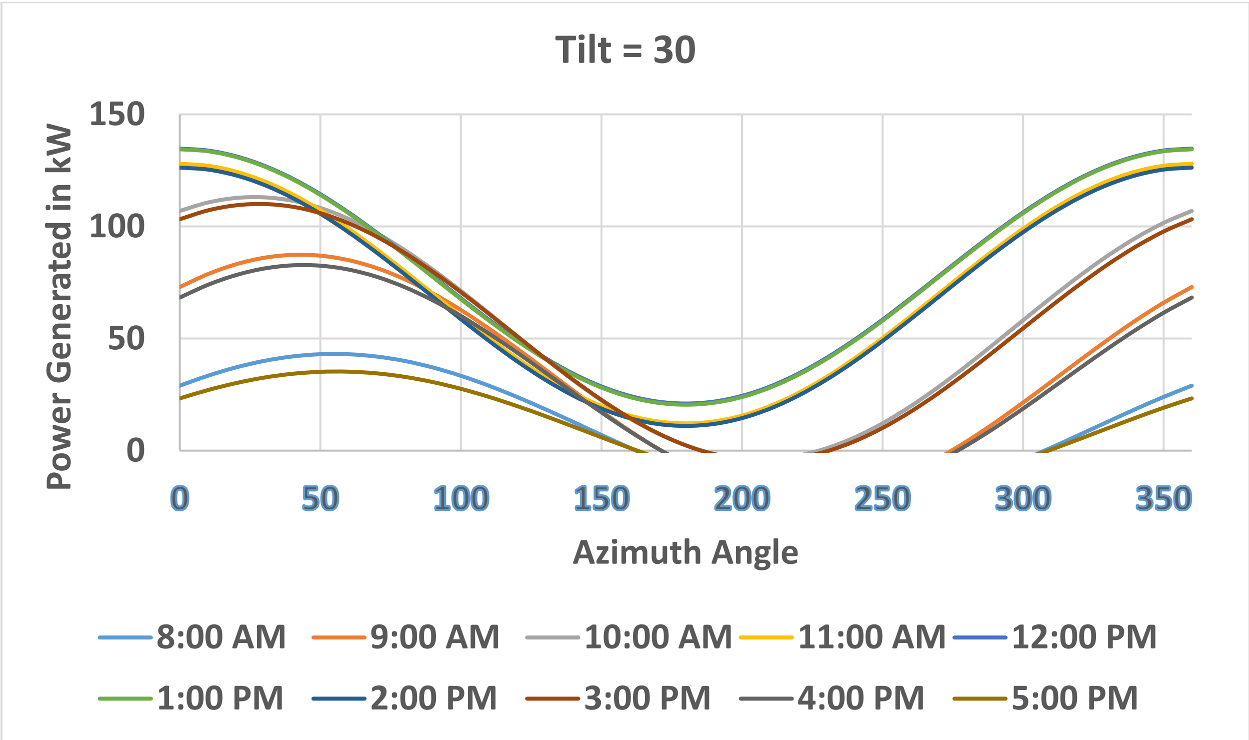

Figure 3.3 PV system output with panels tilted 30° above horizontal.

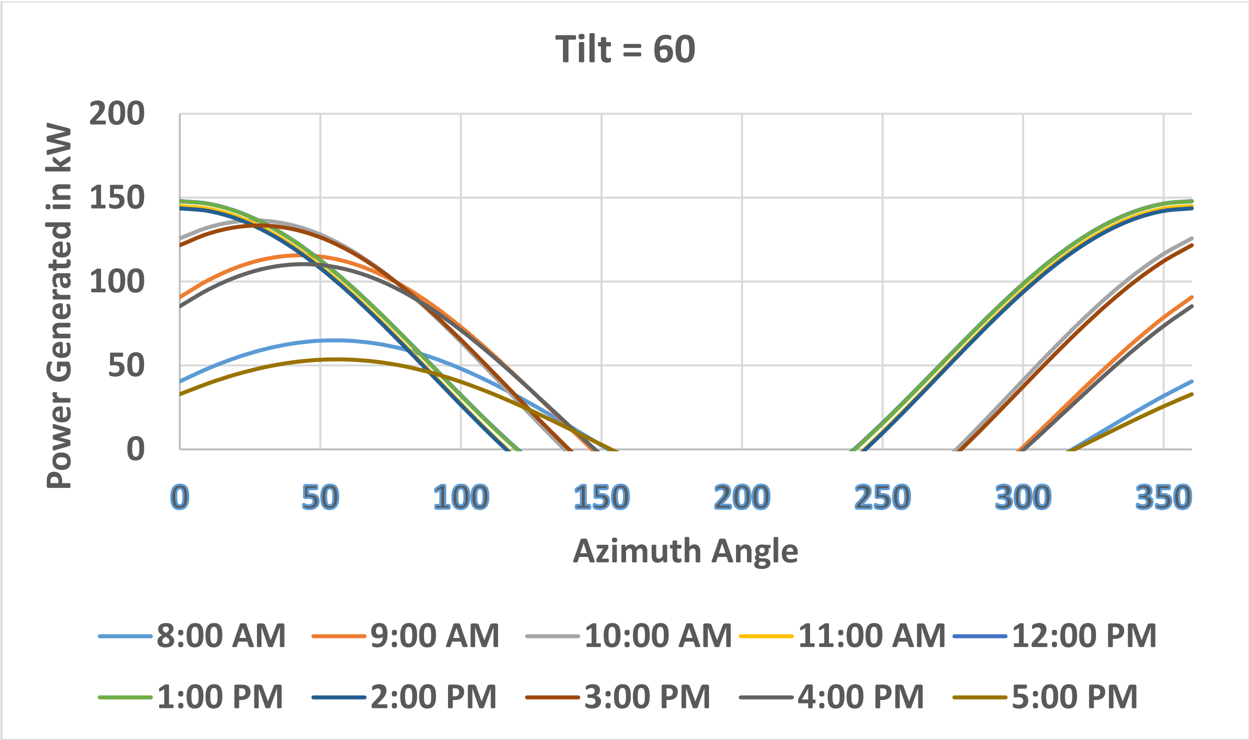

Figure 3.4 PV system output with panels tilted 60° above horizontal.

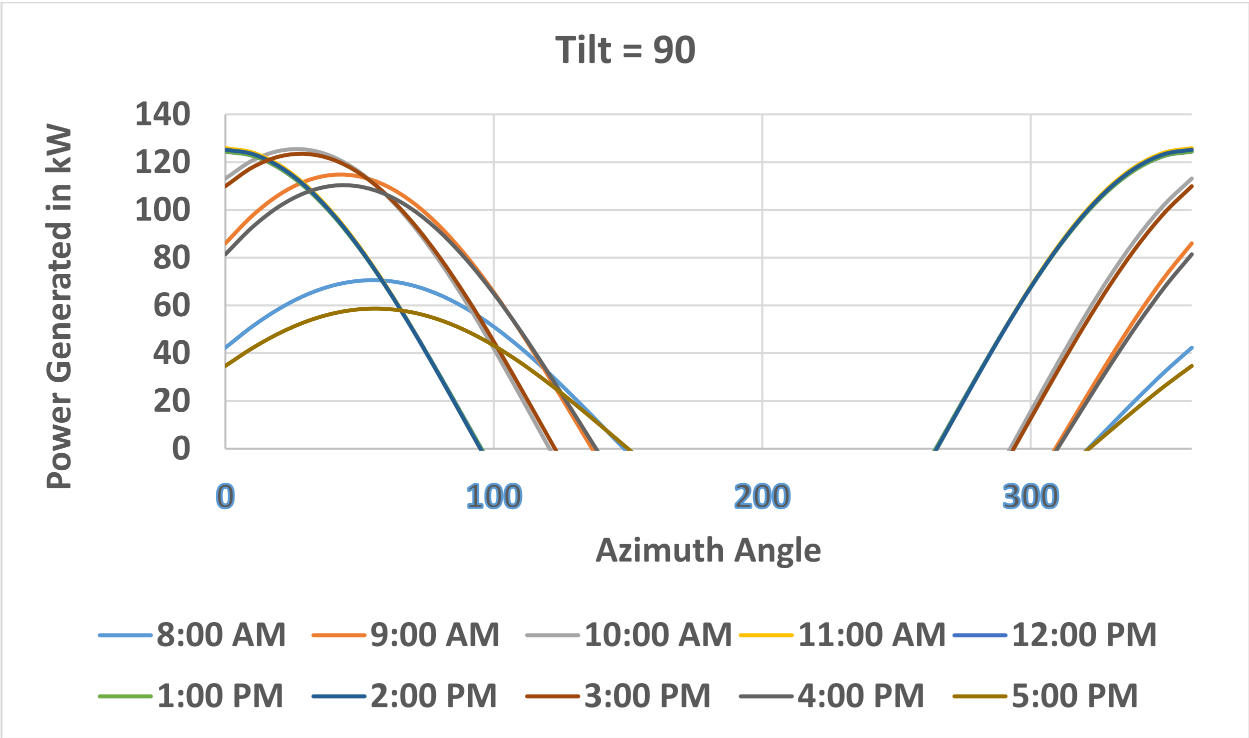

Figure 3.5 PV system output with panels tilted 90° above horizontal.

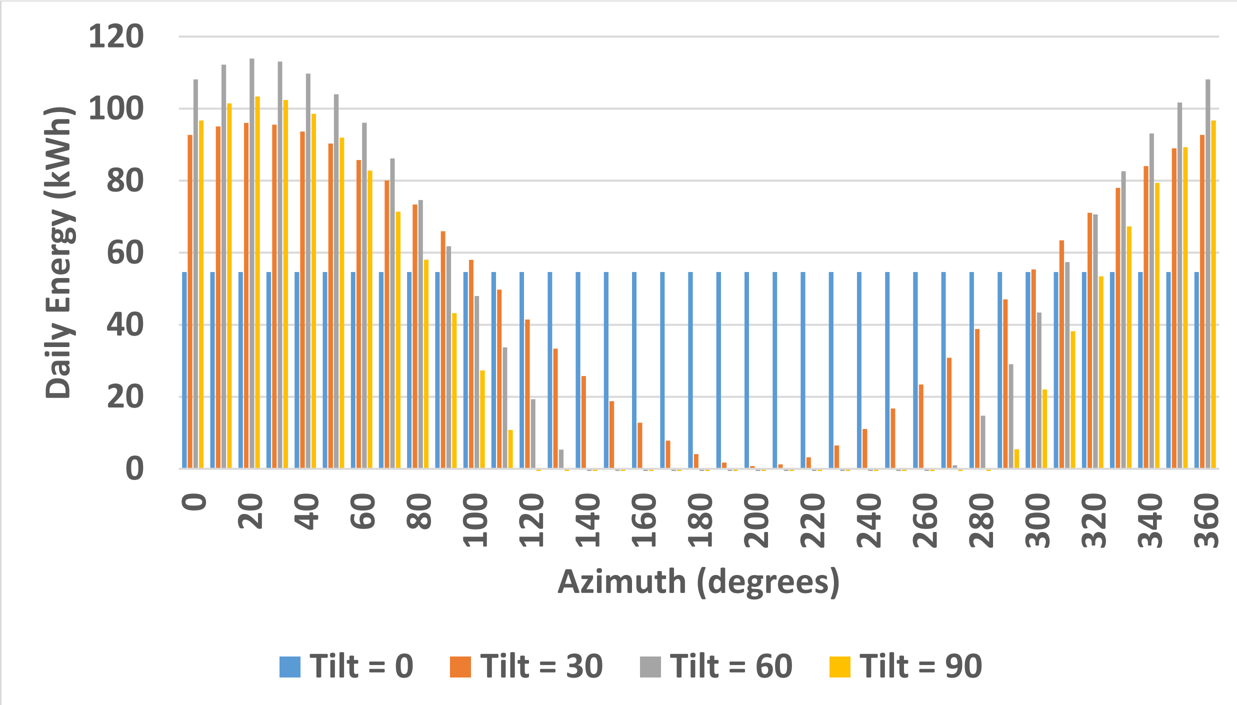

Figure 3.6 Daily PV energy generated.

When panels are horizontal with a tilt angle of 0°, generation is the same for all azimuth angles. Horizontal panels are on flat roofs. This case is included in the model if it is likely or known that horizontal panels exist in the service area.

A solar farm that consists of all the rooftop PV panels in the distribution service area of a substation is modeled. Only practical configurations are considered, and to reduce computational time, those are limited.

Equation 3.2 is used to determine the minimum number of panels:

$$\sum_{i=1}^{N} P_{i,k} = \sum_{j=1}^{J} \hat{P}_{j,k} \tag{3.2}$$

where N is the actual number of PV systems with a given configuration, J is the assumed number of PV systems in the model (the goal is to limit J to significantly less than N), $P_{i,k}$ is the actual power generated by a PV system with the i^{th} configuration in the k^{th} time interval, and $\hat{P}_{j,k}$ is the estimated power generated by a PV system in the assumed j^{th} configuration in the k^{th} interval.

The goal is to determine the minimum number of J configurations whose generation is within an error value of the actual N systems.

3.5 Numerical Analysis

The procedure for determining the number of PV systems *J* and the azimuth and tilt angles of each of those configurations is outlined here.

1. The sum shown on the left side of equation 3.2 represents the actual measured generation from all PV generators in the service area. This is historical measured data from smart meters for the service area.

2. The procedure to determine the configurations in the reduced model is iterative. Configurations considered are those that produce at least 70% of the maximum possible energy using the procedure described in section 3.4. The model begins with two configurations that are linearly distributed over tilt and azimuth angle within these configurations. The known area of the panels, from distribution system data, is divided equally among the configurations. Based on Wichita's latitude location, tilt angles are between 30^{o} and 65^{o}, and azimuth angles are between 20^{o} and 90^{o}.

3. Solar generation for the model configurations is calculated using historical measured solar radiation data [14].

4. Energy generated by the modeled systems is compared with the historical measured generation. The root mean squared error (RMSE) is calculated, and the modeling process ends when the RMSE is less than a pre-defined threshold.

5. If the RMSE exceeds the predefined threshold, then the number of configurations is increased by one, and steps 3 and 4 are repeated until the RMSE is below the threshold value.

A flow chart of the modeling technique is presented in Figure 3.7.

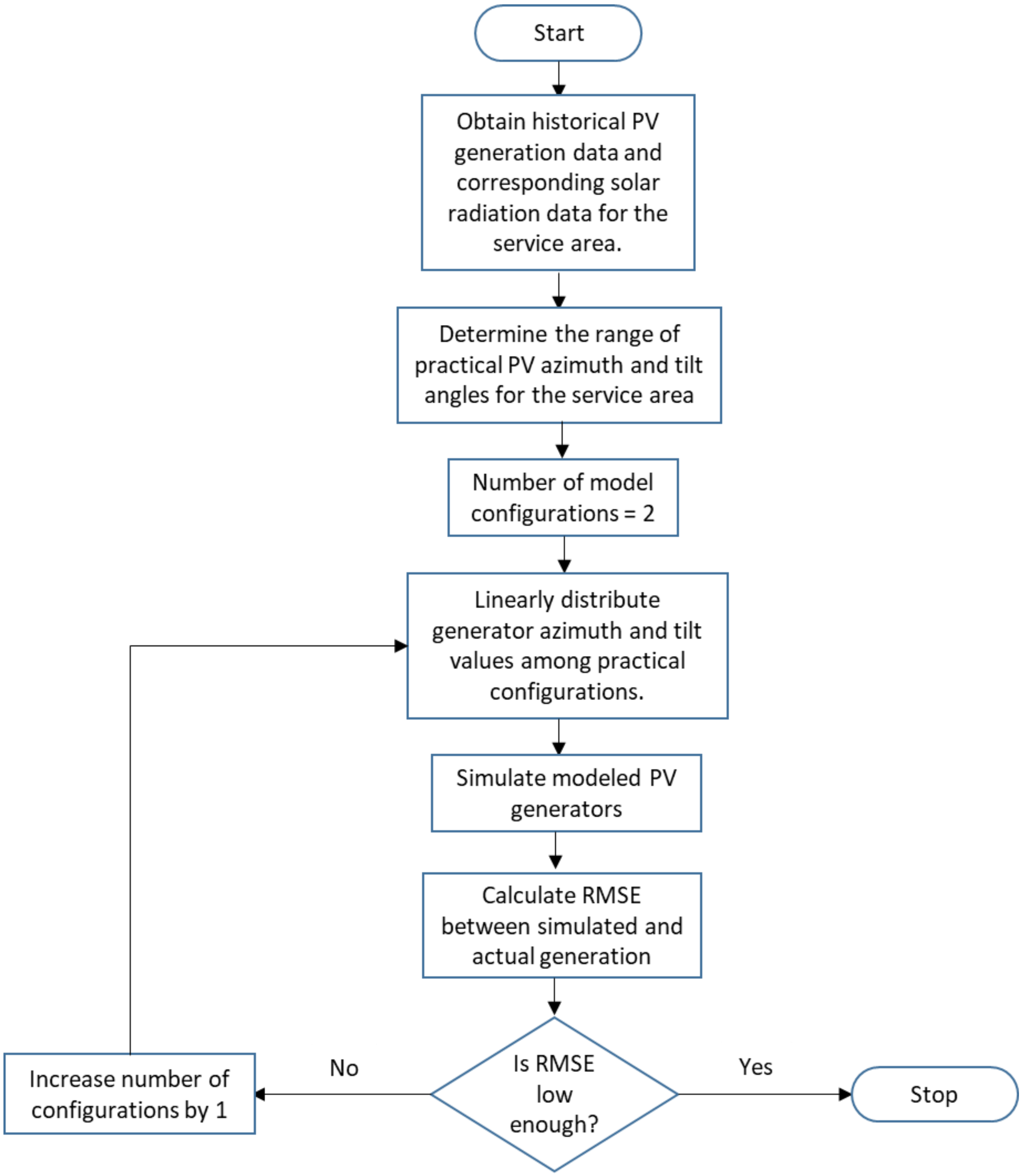

Figure 3.7 Modeling technique.

4. Demonstration of the Technique

The technique described in this project is demonstrated on a simulated distribution service area in Wichita, Kansas, with 1,000 m^2 of PV panels. For this project, the actual historical data for PV generators was not available, so the "measured" values were simulated with a model of solar panels with 100 different tilt and azimuth angles. Each system has 10 m^2 of panels. The efficiency of the systems was varied from 13% to 17%. Inverter efficiency was randomly taken from 93% to 97%. Historical measured DHI, DNI, and zenith angle data [14] were used to simulate the output of those PV systems. Data were generated for January, June, and November 2019, in order to realize the seasonal variations.

Nine configurations of PV panels produced the results presented in Figures 4.1 to 4.3. These nine configurations resulted in an RMSE value for June of 15.8%. For November, the RMSE is lower at 4.9%, and for January it is 18.5%. In this case study, the algorithm performs better for winter with its lower solar radiation. These figures also show that the error is higher during the middle part of the day when solar radiation is highest. The algorithm can be improved with more advanced load estimators, an increased number of PV configurations, and advanced optimization techniques.

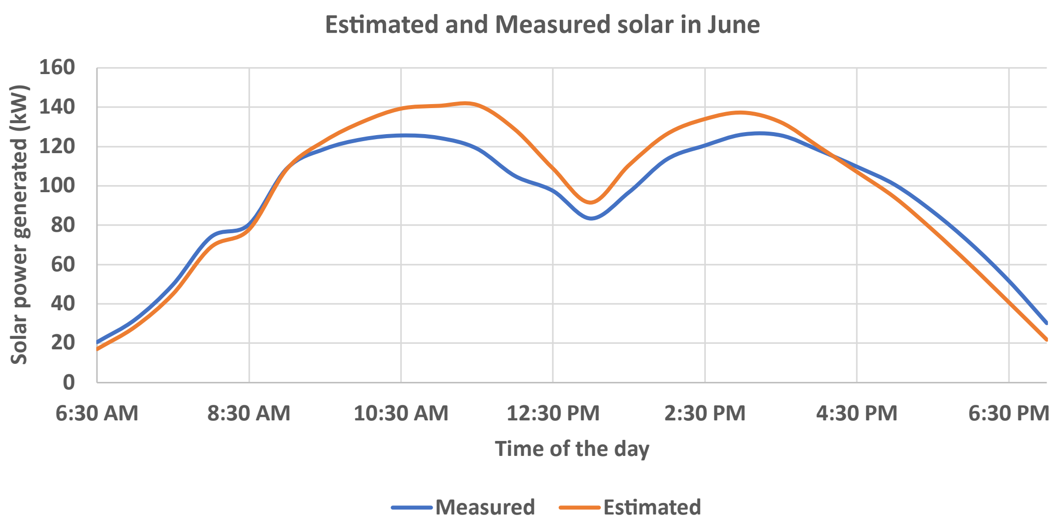

Figure 4.1 Simulated and estimated PV generation data for June 2019.

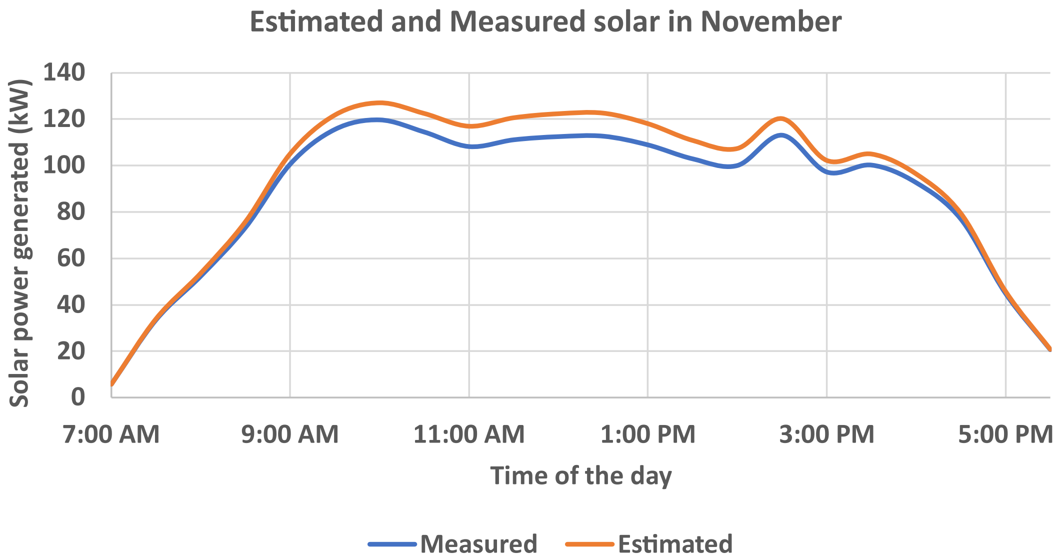

Figure 4.2 Simulated and estimated PV generation data for November 2019.

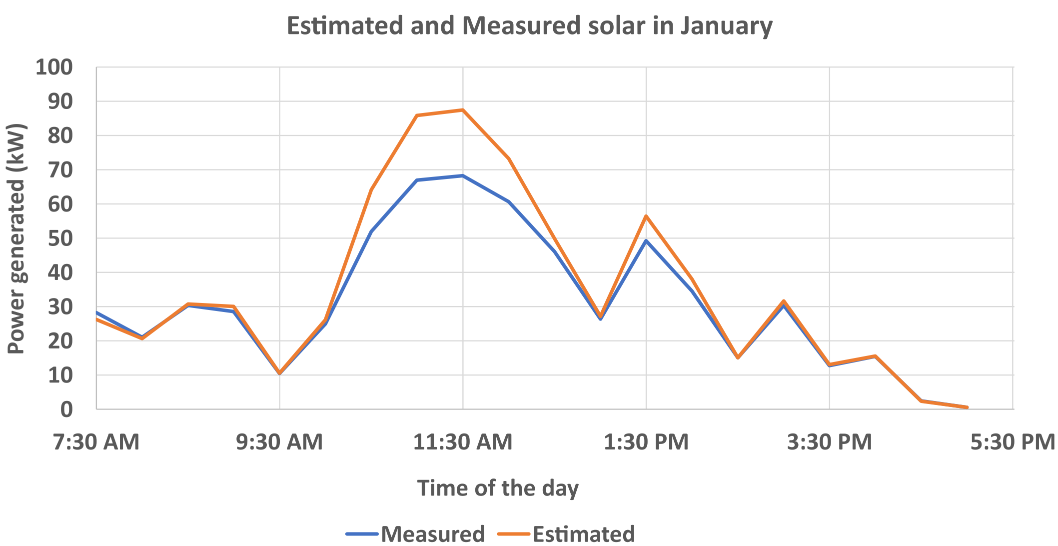

Figure 4.3 Simulated and estimated PV generation data for January, 2019.

5. Conclusions

Accurate estimates of unmonitored distributed PV generation on a distribution system can be made for transmission operator planning and operation using the technique presented and demonstrated in this report. For operations, the estimates can be made in real time.

The data required are the total capacity of distributed PV generation on the distribution system being modelled and historical data of the output of those systems. Distribution operators collect capacity data for all interconnected generators. Smart meters can provide historical data on the actual energy generated. Once the model is developed for a feeder or substation, it should be updated annually. To provide generation estimates, the model uses real-time or historical solar radiation data as its only input.

The model will be developed by the distribution operator and provided to the transmission operator for their use. The limited data needed for the model is all aggregate data for a service area, and the actual model provided to the transmission operator should pose no privacy concerns for customers.

6. Future Work

The model presented in this report uses a manual technique to estimate the azimuth and tilt angles for PV panels on the system. Several optimization techniques will be tested, and calculation of the model parameters will be automated using the technique that provides the best combination of accuracy and computational efficiency.

Thus far, no smart meter data on rooftop PV generation were available for the project. While smart meters have the capability of collecting this data, most are not being used to do so in order to limit the amount of data collected and communicated. Only limited data are needed, and the investigators will determine how that can best be collected from existing smart meters. Once this is done, the model will be tested using actual generation data. If an entire year’s data can be collected and used, then the model’s accuracy can be determined in greater detail.

Electric vehicles are a growing load on distribution systems and have different characteristics than conventional loads. This model will be expanded to include electric vehicle loads, and a market model for PV and electric vehicles will be developed.

References

[1] Rich Seguin, Jeremy Woyak, David Costyk, Josh Hambrick, and Barry Mather, *High Penetration PV Integration Handbook for Distribution Engineers,* NREL/TP-5D00-63114, January 2016, National Renewable Energy Laboratory, www.nrel.gov/publications.

[2] *Participation of Distributed Energy Resource Aggregations in Markets Operated by Regional Transmission Organizations and Independent System Operators,* Order No. 2222, US Federal Energy Regulatory Commission, Issued September 17, 2020, https://www.ferc.gov/sites/default/files/2020-09/E-1_0.pdf

[3] *PV System Performance: GHI to PoA,* EcoSmart Foundation, Vancouver, BC, Canada, https://ecosmartsun.com/pv-system-performance-3/pv-system-performance-ghi-to-poa/

[4] H. Shaker, H. Zareipour, and D. Wood, "A Data-Driven Approach for Estimating the Power Generation of Invisible Solar Sites," in *IEEE Transactions on Smart Grid*, vol. 7, no. 5, pp. 2466-2476, Sept. 2016, doi: 10.1109/TSG.2015.2502140.

[5] F. Bu, K. Dehghanpour, Y. Yuan, Z. Wang, and Y. Zhang, "A Data-Driven Game-Theoretic Approach for Behind-the-Meter PV Generation Disaggregation," in *IEEE Transactions on Power Systems,* vol. 35, no. 4, pp. 3133-3144, July 2020, doi:10.1109/ TPWRS.2020.2966732.

[6] F. Sossan, L. Nespoli, V. Medici, and M. Paolone, "Unsupervised Disaggregation of Photovoltaic Production from Composite Power Flow Measurements of Heterogeneous Prosumers," in *IEEE Transactions on Industrial Informatics*, vol. 14, no. 9, pp. 3904-3913, Sept. 2018, doi: 10.1109/TII.2018.2791932.

[7] F. Kabir, N. Yu, W. Yao, R. Yang, and Y. Zhang, "Estimation of Behind-the-Meter Solar Generation by Integrating Physical with Statistical Models," *2019 IEEE International Conference on Communications, Control, and Computing Technologies for Smart Grids* (SmartGridComm), 2019, pp. 1-6, doi: 10.1109/SmartGridComm.2019.8909743.

[8] Michaelangelo Tabone, Sila Kiliccote, and Emre Can Kara, "Disaggregating Solar Generation behind Individual Meters in Real Time," 2018 5th Conference on Systems for Built Environments, Association for Computing Machinery, New York, NY, USA, 43–52. DOI:https://doi.org/10.1145/3276774.3276776

[9] F. Wang, K. Li, X. Wang, L. Jiang, J. Ren, Z. Mi, M. Shafie-khah, and J. P. S. Catalao, "A Distributed PV System Capacity Estimation Approach Based on Support Vector Machine with Customer Net Load Curve Features," *Energies* , vol. 11, p. 1750, 2018.

[10] Z. Xuan, X. Gao, K. Li, F. Wang, X. Ge, and Y. Hou, "PV-Load Decoupling Based Demand Response Baseline Load Estimation Approach for Residential Customer with Distributed PV System," in *IEEE Transactions on Industry Applications*, vol. 56, no. 6, pp. 6128-6137, Nov.–Dec. 2020, doi: 10.1109/TIA.2020.3014575.

[11] E. Vrettos, E. C. Kara, E. M. Stewart, and C. Roberts, "Estimating PV Power from Aggregate Power Measurements within the Distribution Grid," *Journal of Renewable and Sustainable Energy*, vol. 11, iss. 2, April 2019, https://doi.org/10.1063/1.5094161.

[12] Caroline Carl, *Calculating Solar Photovoltaic Potential on Residential Rooftops in Kailua Kona, Hawaii*, MS Thesis, University of Southern California, May 2014, https://spatial.usc.edu/wp-content/uploads/2014/03/CarlCarolineThesis.pdf

[13] Kirk D. Hagen, *Introduction to Renewable Energy for Engineers*, Pearson, 2016, www.vitalsource.com/referral?term=9780133404111

[14] *National Solar Radiation Database*, National Renewable Energy Laboratory, nsrdb.nrel.gov.

Part III

Co-optimization of Transmission & Distribution Operations

C. Lindsay Anderson
Jialin Liu, Graduate Student
Luckny Zéphyr, Postdoctoral Associate

Cornell University

Judith Cardell

Smith College

For information about this project, contact

C. Lindsay Anderson
Cornell University
111 Wing Dr, 316 Riley-Robb Hall
Ithaca, New York 14853
Phone: (607) 255-4533
Email: cla28@cornell.edu

Power Systems Engineering Research Center

The Power Systems Engineering Research Center (PSERC) is a multi-university Center conducting research on challenges facing the electric power industry and educating the next generation of power engineers. More information about PSERC can be found at the Center's website: http://www.pserc.org.

For additional information, contact:

Power Systems Engineering Research Center
Arizona State University
527 Engineering Research Center
Tempe, Arizona 85287-5706
Phone: 480-965-1643
Fax: 480-727-2052

Notice Concerning Copyright Material

Table of Contents

List of Figures

List of Tables

1. Introduction

The interconnected power system was originally developed with centralized power generating facilities connected to a meshed high voltage network that delivered power to customers predominantly connected via passive, radial, distribution systems. A gradual deregulation and restructuring of the electric power industry began in the 1970s and continues at a measured pace today [1]. This process has facilitated the inclusion of alternate distributed energy resources (DER) such as small-scale distributed and renewable generation, flexible demand technologies, along with moderate autonomy for independent power producers [2]. These changes challenge the centralized system control paradigm of the legacy power system.

Distributed and smart energy resources have been poised to transform the power system for decades. Costs for renewable energy steadily decrease. Customers' desire to limit negative impacts of power generation and transmission increases. A wary fascination of electric vehicles as well as home automation is ever present. What then explains the continued dominance of centralized generating facilities and passive customer engagement in the power industry? The causes of slow system evolution are numerous and often well-justified. Nonetheless, society as a whole will benefit from DER and smart technology penetration expanding as rapidly as possible. Equally important to this evolution of physical devices on the power system are the software algorithms and protocols used to analyze and operate the system. The historical operating strategies assumed the historical power system structure, e.g., active and highly meshed central generating facilities serving customers located in passive, radial distribution systems. In this system configuration, high resolution energy data from distribution systems was neither available nor necessary for reliable system operation. The current direction for system evolution promotes a significant increase in both distributed and renewable energy generating technologies. Advances in automation, personal area networking and communications technologies facilitate both increased flexible load across end-use devices as well as two-way communication of high resolution energy usage and system state data from customers and low voltage systems to the grid operators. Faced with this mixture of legacy system elements and newer, advanced technologies, algorithms for system analysis and operations need to evolve to fully exploit the benefits of, and also avoid potential negative impacts of new DER and renewable energy technologies.

Transmission and distribution are traditionally modeled and analyzed separately from each other, emphasizing networked versus radial systems, and the use of substations to aggregate load for the transmission system, while maintaining greater resolution for load at the distribution level. With the expanding integration of distributed energy resources, DER, these active distribution systems more heavily influence transmission system operations. As a result, there is a growing motivation to integration decisions and operations of T&D systems together using coordinated models. The challenge is to provide the necessary and sufficient information to both the transmission and the distribution level models, while minimizing the computational complexity of accurately representing both levels. A fully combined transmission-plus-distribution model would be excessively complex, suggesting that two separate models are still needed: a transmission model that includes needed information from distribution, and distribution model that includes relevant information from transmission.

This part of the project developed a framework for partially-coupled T&D system models where sufficient but limited information is shared. The partially-coupled network will use cooptimization to coordinate the systems, providing additional information from transmission into distribution model and distribution into transimission model. A bi-level optimization modeling framework was developed and used to analyze (simulated) system costs and the deployment of demand response, including the ability of demand response to balance wind forecasting errors. With this view of the existing and near-future power system, this project investigated the use of bi-level co-optimization algorithms for system analysis. Specifically, at what level of DER penetration does it become important to use the proposed optimization algorithms in order to fully capture the expected benefits of DER to system performance. Results compare the simulated system performance as determined by single-level, traditional optimization to that determined by the proposed bi-level optimization that incorporates detailed knowledge of the distribution system as a microgrid with multiple DER installed.

The bi-level optimization provides a framework to co-ordinate distribution and transmission decisions. This part of the report investigates the concept that the benefits of DER, including distributed generation and demand response, will be realized only with intentionally coordinated operations between transmission and distribution. In particular, the impact of pricing decisions on the use of demand response is quantified, and compared between the use of traditional single level and the proposed bi-level optimization frameworks.

It could appear that this framework takes the already complex problem of transmission system modeling, and makes it more complex by adding detailed distribution system models at substation buses. However, through the use of the algorithm to co-optimize the two system levels with the bi-level modeling framework (See figure 1.1 below), we can explore the benefits of the proposed approach.

A significant amount of the research into integrated T&D simulation and analysis derives from a co-simulation perspective. The project additionally considers the optimal decisions that arise from a leader-follower algorithm of optimization under uncertainty. This means that the problem is formulated as a leader-follower problem where the transmission system is leader and the distribution system(s) are followers. Note that these are two distinct optimization problems that are solved simultaneously – each system maintains some autonomy of perspective in the structure of the problem.

The co-optimization modeling framework proposed here is based on the transmission system at the upper level and distribution system(s) as the lower level problem. This structure can be reformulated into a single level using the Karush–Kuhn–Tucker conditions, known to apply when Slater’s condition are satisfied for convex optimization [1,2] The framework includes the distribution system constraints into a transmission system level (single-level) model, without losing the distribution system objective within the resulting single-level optimization.

Figure 1.1 represents a conceptual diagram of the proposed modeling framework that highlights the bi-level structure of the problem, where the transmission system is the upper-level problem and the distribution system is the lower level. The right side of the diagram shows the high-level information flow between the systems, in which the transmission system determines and communicates the demand response and energy prices to the distribution system. Using this price information, the distribution system then determines the dispatch of the distributed energy resources and communicates this information back to the transmission system. The optimization thus includes, at the transmission level, both the unit commitment and economic dispatch problems. The distribution then optimizes its own local, economic dispatch for the embedded distributed resources along with necessary energy imports, using the upper-level price information. Additional internal decisions made include the generation dispatch and reserve quantities at the transmission system level.

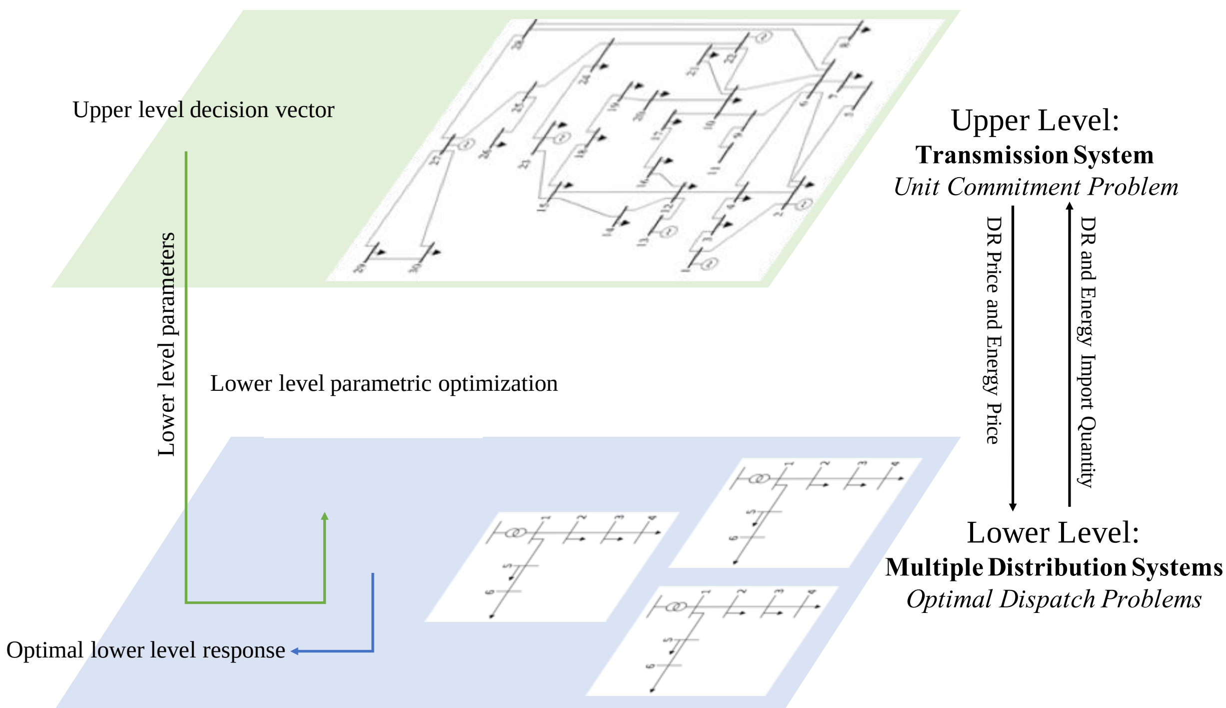

Figure 1.1 Conceptual diagram of T&D Bilevel Optimization Structure

1.1 Report Part III Organization

The remainder of Part III of this report is organized with the following sections. In Section 2, we describe the individual models for the transmission and distribution systems and the structure of these decisions within the bi-level optimization framework, followed by the formulation of the optimization problem and description of the models for renewables uncertainty and dynamic storage decisions. In Section 4, the single-level reformulation of the original problem is described in the context of the case study, followed by comparison of results between the cooptimization and traditional optimization approaches.

2. Model Formulation

Nomenclature

Paremeters	
T	length of the planning horizon
G	total number of generators in the transmission system
$\overline{R}_g/\underline{R}_g$	upper/lower ramp rate limit of transmission system generator g
$\overline{P}_g/\underline{P}_g$	generation upper/lower bound of transmission system generator g
$\overline{L}$	transmission system line limit
C_g^1/C_g^2	linear/quadratic cost coefficient (\$/MW) of transmission system generator
C_g^c	commitment cost coefficient (\$/MW) of transmission system generator g
C_g^r	reserve cost coefficient (\$/MW) of transmission system generator g
GSF	generation shift factor matrix for transmission system
W_t^f	transmission forecasted wind power in period t
W_t^{up}/W_t^{dn}	upward/downward deviation from the forecast wind power in period t in the transmission system
N_b	number of buses in the transmission system
L_t	transmission system load power vector in period t
$\underline{L}_t^d/\overline{L}_t^d$	lower/upper bound for microgrid aggregated dispatchable load in period t
L_t^i	microgrid inelastic load in period t
$\overline{B}/\underline{B}$	max/min level of microgrid storage energy state
C^b	microgrid storage energy maintenance cost coefficient (\$/MW)
C^{m1}/C^{m2}	microgrid generation linear/quadratic cost coefficient (\$/MW)
C^d	microgrid utility for consuming dispatchable load
C^{dr1}/C^{dr2}	microgrid linear/quadratic demand response cost coefficient
$\overline{P}^m/\underline{P}^m$	upper/lower bound on microgrid generation
$\underline{P}^b/\overline{P}^b$	microgrid storage discharging/charging limit
Variables	
$r_{g,t}^{up}/r_{g,t}^{dn}$	upward/downward reserve of transmission system generator g in period t
p_t^{dr}	microgrid demand response price,in period t (\$/MW)
$p_{g,t}$	generation of transmission system generator g in period t
p_t^m	microgrid generation in period t
b_t	microgrid storage energy state at the beginning of period t
p_t^{ex}/p_t^{im}	microgrid exported/imported power in period t
c_t^{ex}/c_t^{im}	price of microgrid exported/imported power in period t
p_t^b	microgrid storage power (charging/discharging) output in period t
l_t^d	microgrid aggregated dispatchable load in period t
dr_t^{up}/dr_t^{dn}	upward/downward demand response of microgrid dispatchable load in period t
$pinj_t$	transmission bus power injection vector in period t
$w_{g,t}$	transmission system generator commitment variable for generator g in period t

The transmission system model solves the unit commitment and economic dispatch problems. The distribution system model implements an optimal power dispatch problem for the resources within the distribution system. Developing the framework for the co-operation, and co-optimization, of the systems is the focus of this study. The model formulation is presented below, with the nomenclature introduced above.

2.1 Transmission System Day-Ahead Unit Commitment Problem

The transmission system is modeled as a network of transmission lines and buses. Traditional and renewable generation units, loads, and microgrids are connected to buses in the network. The transmission system solves a day-ahead unit commitment problem, which involves the energy and ancillary services markets. The objective of this problem is to find cost-effective operation schedules for the energy resources to meet the load considering renewable generation uncertainty. Specifically, for the energy market, the transmission system aims to minimize the cost of meeting the system demand with its own generation or energy imported from microgrids. For the ancillary services market, the goal is to minimize the cost of providing reserves to account for the renewable forecast uncertainty. The reserve resource is procured from a combination of the transmission system generators' reserve and the distribution system's DR. The energy and ancillary services market decisions are determined together. The interested reader is referred to [3] for a detailed treatment of the unit commitment problem.

2.2 Distribution System Optimal Dispatch Problem

The size of a distribution system could vary from a few kW to hundreds of MW [4]. The distribution system may be part of the distribution system or the entire distribution system and so directly connect to the transmission system through the substation. The case of direct connection to the transmission system is considered in this work. The distribution system has an aggregated dispatchable load and a non-dispatchable load, an energy storage unit, and a distributed generator. This model provides sufficient detail to capture distribution system interaction with the bulk transmission system. In the day-ahead market, the distribution system solves an optimal dispatch problem. The dispatchable load is scheduled at a level between its upper and lower bounds. The difference between the upper/lower bound and its preset load level could be used to provide upward/downward DR. The objective of the distribution system is to minimize the cost of meeting its demand either via its distributed generation or energy import from the transmission system, and to maximize the revenue from providing DR and optional energy export. For a detailed description of the distribution system optimal dispatch problem, see [5].

2.3 Transmission System and Distribution System Operation Modes

The integrated system, including the transmission system and the distribution system, may operate in two modes. The first one of these is the standalone mode, in which the systems are disconnected and can neither exchange energy, nor allow the distribution system to provide DR to the transmission system. In the second (co-operative) mode, the two systems have the capability to transact. Specifically, the transmission system determines the price of distribution system energy import and export as well as the price for the distribution system DR purchases, and the distribution system responds to the prices by determining the amount of energy exchange and provision of DR to the transmission system.

2.4 Bi-level Optimization Model

Bi-level optimization is a common game-theoretic approach to analyze the interactive behavior between market entities [6] with a two-level, or leader-follower, problem structure. Specifically, the leader makes the first move with some expectation for the follower's move. The follower then reacts to the leader's move optimally. The co-optimization modeling framework for the two power system levels, representing the two physical voltage levels in the power system. This is shown in the following general formulation:

$$
\begin{aligned}
\text{Upper-Level Problem: } & \min_{x \in X} F(x,y) \\
\text{s.t.: } & G_i(x,y) \leq 0,\ i \in \{1,2,\ldots,I\} \\
& H_k(x,y) = 0,\ k \in \{1,2,\ldots,K\} \\
\text{Lower-Level Problem: } & \min_{y \in Y} f(x,y) \\
\text{s.t.: } & g_j(x,y) \leq 0,\ j \in \{1,2,\ldots,J\}, \\
& h_m(x,y) = 0,\ m \in \{1,2,\ldots,M\}
\end{aligned}
\tag{1}
$$

In (1), the variable set of the upper/lower-level problem is X/y, $F(x,y)/f(x,y)$ is the objective function, and $(G_i,H_k)/(g_j,h_m)$ are the constraints. In this work, bi-level optimization is a natural approach to co-optimize the transmission system and distribution system in the power markets. The co-operative behavior between the two systems is illustrated in a bi-level optimization structure in Fig. 2.1.

The integrated system of the transmission system and microgrids can operate either in islanded or cooperative modes. In islanded mode, the microgrids do not interact with the bulk power system and so do not exchange energy with the transmission system. In the cooperative mode, the two systems are co-optimized such that they do exchange energy and reserves services, to the extent that these are part of an optimal, least cost, solution. The transmission system optimization phase determines the locational marginal pricing (LMP) to be used as the price of microgrid energy import and export as well as the price for the microgrid DR purchases. The microgrid responds to the price by determining the amount of energy exchange and provision of DR to the transmission system. This exchange of energy provides feedback to the transmission system level, and affects the determination of the LMP.

$$x_t = [w_{g,t}, p_{g,t}, r_{g,t}^{up}, r_{g,t}^{dn}, p_t^{dr}, c_t^{im}, c_t^{ex}]$$

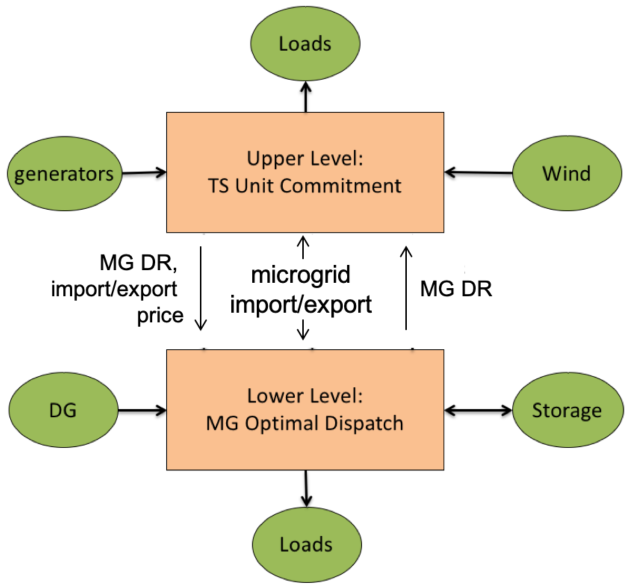

$$y_t = [p_{g,t}^{m}, p_t^{b}, p_t^{im}, p_t^{ex}, dr_t^{up}, dr_t^{dn}, l_t^{d}, b_t]$$

Figure 2.1 The upper-level transmission system decides the energy and demand response price signals, and the lower-level distribution system problem responds by deciding the quantity of energy exchanged and the demand response.

The specifics of the bi-level optimization model in this study are given below.

2.5 Upper-Level Problem: Transmission Day-Ahead Unit Commitment Problem

For the upper level transmission system unit commitment decision, central station generation and aggregated low-voltage system loads are connected to generation and load buses, respectively. In this framework, microgrids are modeled as detailed networks with distributed energy resources (generation, responsive demand and storage), connected to the high voltage grid at specified buses. This upper level problem solves the day-ahead unit commitment for both energy and reserves. The objective function represents costs for all energy resources, central stations, renewable generation and distributed resources, and is minimized while accounting for uncertainties. The transmission system will either use power from central generating units or power exported from microgrids. In the reserves market, the objective is to minimize the cost of reserves while accounting for renewable energy (specifically wind energy) uncertainty. Reserves can be provided from transmission system generating resources as well as from low-voltage system demand response. Energy and ancillary services are co-optimized for the unit commitment problem. For this upper-level day-ahead unit commitment problem, the operation schedule minimizes the cost of operation of the transmission system, *i.e.*, the generator commitment status $w_{g,t}$, generation output $p_{g,t}$, the generator's upward and downward reserve $r_{g,t}^{up}$, $r_{g,t}^{dn}$, the distribution system DR price p_t^{dr}, and the prices of the distribution system's imported and exported energy c_t^{im}, c_t^{ex}. The optimization variables are denoted by the vector x_t:

$$x_t = [w_{g,t}, p_{g,t}, r_{g,t}^{up}, r_{g,t}^{dn}, p_t^{dr}, c_t^{im}, c_t^{ex}]$$

The objective of the upper-level optimization problem is to minimize the transmission system operation cost including the cost of operation of the transmission system, the generation cost, the reserve cost, the cost of energy exchange with the distribution system, and the distribution system DR cost. The objective function is

$$F(\{x_t\}_{t=1}^{T}) = \sum_{t=1}^{T} \sum_{g=1}^{G} \Big(C_{gc} w_{g,t} + C_{g1} p_{g,t} + C_{g2}(p_{g,t})^2 + C_{gr}(r_{g,t}^{up} + r_{g,t}^{dn}) - c_t^{im} p_t^{im} + c_t^{ex} p_t^{ex} + p_t^{dr}(dr_t^{up} + dr_t^{dn})\Big) \quad (2)$$

and is minimized under the following constraints:

- *Power Flow:*

$$-\overline{L} \leq GSF \times pinj_t \leq \overline{L}, \qquad t \in \{1, ..., T\} \quad (3)$$

$$-\overline{L} \leq GSF \times pinj_t^* \leq \overline{L}, \qquad t \in \{1, ..., T\} \quad (4)$$

$pinj_t$ is the nodal net power injection vector accounting for traditional generation, wind generation, and demand for all the buses in period t. $pinj_t^*$ incorporates the error in the forecasted wind power, generator reserves and distribution system DR into the base $pinj_t$. Eqs. (3) and (4) bound the power flows through the transmission lines.

- *Generation Capacity:*

$$\underline{P}_g \times w_{g,t} \leq p_{g,t} \leq \overline{P}_g \times w_{g,t}, \qquad t \in \{1, \ldots, T\}, g \in \{1, \ldots, G\} \quad (5)$$

$$(p_{g,t} + r_{g,t}^{up}) - (p_{g,t-1} - r_{g,t-1}^{dn}) \leq \overline{R}_g, \qquad t \in \{2, \ldots, T\}, g \in \{1, \ldots, G\} \quad (6)$$

$$\underline{R}_g \leq (p_{g,t} - r_{g,t}^{dn}) - (p_{g,t-1} + r_{g,t-1}^{up}), \qquad t \in \{2, \ldots, T\}, g \in \{1, \ldots, G\} \quad (7)$$

Eq. (5) restricts the generators' outputs to lie within their capacities. The generator ramping limits are represented in Eqs. (6) and (7). The ramp limit is in terms of MW/hour as the time frame for the dispatch and wind estimation is per hour.

- *Power Balance:*

$$\sum_{g=1}^{G} p_{g,t} - (\mathbf{1}_{1.Nb} \cdot L_t) + W_t^f = p_t^{im} - p_t^{ex} \quad t \in \{2, ..., T\}, g \in \{1, ..., G\} \quad (8)$$

where $\mathbf{1}_{1\times N_b}$ is an N_b-dimensional vector filled of 1's. The dot product $\mathbf{1}_{1\times N_b} \cdot L_t$ gives the total load on the system. Eq. (8) balances the system's power supply and demand.

- *Wind Power Forecast Uncertainty:*

  The wind power generation is all located in windfarms, at the high-voltage system level. The wind data are from the NREL-Eastern Wind Integration Study dataset [7]. Using three years of data, 24-hour trajectories are grouped to identify a set of 54 trajectories representing possible wind realizations. The central trajectory of the group is selected as the wind power forecast, and the remaining trajectories are used to estimate the distribution of forecast errors. Based on the forecast error distribution, 10,000 scenarios are generated to represent an uncertainty set of wind realizations, each of which would introduce error with respect to the base case wind forecast. Those error scenarios are then added to the forecast to create wind generation scenarios [8]. For the wind generation forecast and a set of possible wind generation scenarios, the upward/downward wind power deviation from the forecast W_t^{up}/W_t^{dn} is calculated by taking the difference between the maximum/minimum generation scenario and the forecast for period t. The downward/upward transmission generation reserve $r_{g,t}^{dn}/r_{g,t}^{up}$ and upward/downward distribution system DR dr_t^{up}/dr_t^{dn} are used to offset the upward/downward wind power deviation from the forecast. dr_t^{up}/dr_t^{dn} indicates the amount of increase/decrease in the distribution system dispatchable load consumption relative to its baseline l_t^d. This is essentially robust optimization under the bi-level framework as the reserve allocation is optimized to handle the worst wind scenarios.

$$W_t^{up} \leq dr_t^{up} + \sum_{g=1}^{G} r_{g,t}^{dn}, \qquad t \in \{1, ..., T\} \tag{9}$$

$$W_t^{dn} \leq dr_t^{dn} + \sum_{g=1}^{G} r_{g,t}^{up}, \qquad t \in \{1, ..., T\} \tag{10}$$

  Eqs. (9) and (10) ensure that there is enough generator reserve and distribution system DR to compensate for wind forecast deviation. Finally, the transmission system unit commitment problem can be expressed as follows:

$$\min_{\{x_t\}_{t=1}^T} F\left(\{x_t\}_{t=1}^T\right)$$

$$\text{s.t. } (3) - (10)$$

2.6 Lower-Level Problem: Distribution system Operation Optimization

The distribution system modeled in this work is designed to exchange power with the main grid, and consists of distributed generation (DG) with traditional resources, an energy storage unit, an aggregated dispatchable load, and a non-dispatchable load. Each microgrid has some dispatchable, or flexible load and some non-dispatchable, non-responsive load. The modeling framework is designed to allow the microgrid and the high-voltage transmission system to exchange power with bi-directional flow. For the dispatchable load, any margin between the upper or lower bounds and its dispatch point is available to provide upward or downward demand response as needed by the transmission system (particularly to balance wind uncertainties). The objective of the microgrid is to minimize the cost of meeting its load either with its own distributed generation or with energy import from the transmission system, as well as to maximize revenue from providing demand response and energy export to the transmission system [9].

The objective of the distribution system dispatch problem is to determine the generation schedule $p^m{}_t$, the energy storage power output $p^b{}_t$ (*i.e.*, the energy storage charging and discharging decision), the distribution system energy import schedule $p^{im}{}_t$ and export schedule $p^{ex}{}_t$, the dispatchable load profile $l_t{}^d$, the upward/downward demand response $dr_t{}^{up}/dr_t{}^{dn}$ provided by the dispatchable load, and the energy storage energy state b_t. The lower-level optimization variables are collected in the vector y_t:

$$y_t = [p_t^m, p_t^b, p_t^{im}, p_t^{ex}, dr_t^{up}, dr_t^{dn}, l_t^d, b_t]$$

In this problem, the cost of operation of the distribution system, consisting of generation, energy storage, energy exchange with the transmission system, and DR, is minimized. The dispatchable load consumption utility, energy export, and DR revenue, which are negative costs, are maximized. The objective function to be minimized is given by:

$$\begin{aligned} f(\{y_t\}_{t=1}^T) \;\; &= \;\; \textstyle\sum_{t=1}^T (C^{m1}p_t^m + C^{m2}(p_t^m)^2 + C^b b_t + c_t^{im}p_t^{im} - c_t^{ex}p_t^{ex} \\ &+ \;\; C^{dr1}(dr_{g,t}^{up} + dr_{g,t}^{dn}) + C^{dr2}((dr_t^{up})^2 + (dr_t^{dn})^2) \\ &- \;\; C^d l_t^d - p_t^{dr}(dr_t^{up} + dr_t^{dn})) \end{aligned} \tag{12}$$

Similar to the transmission system problem, the distribution system problem is subject to constraints, as described below. For clarity, the dual variables corresponding to the inequality constraints are denoted by λ and those for the equality constraints are denoted by μ.

- *Generation Limits:*

$$\underline{P}^m \leq p^m{}_t \leq P^m, \qquad \lambda_{1,t},\ \lambda_{2,t},\ t \in \{1,...,T\} \tag{13}$$

Eq. (13) limits the distribution system's generation to lie between the upper and lower bounds.

- *Dispatchable Load Capacity:*

$$\underline{L}_t^d \leq l_t^d \leq \overline{L}_t^d, \qquad \lambda_{3,t},\ \ \lambda_{4,t},\ t \in \{1,...,T\} \tag{14}$$

The dispatchable loads are constrained within predefined bounds shown in Eq. (14).

- *Demand Response:*

$$l_t^d + dr_t^{up} \leq \overline{L}_t^d, \qquad \lambda_{5,t}, \quad t \in \{1, ..., T\} \tag{15}$$

$$l_t^d - dr_t^{dn} \geq \underline{L}_t^d, \qquad \lambda_{6,t}, \quad t \in \{1, ..., T\} \tag{16}$$

$$0 \leq dr_t^{up} \leq W_t^{up}, \qquad \lambda_{7,t} \ \ \lambda_{8,t}, \quad t \in \{1, ..., T\} \tag{17}$$

$$0 \leq dr_t^{dn} \leq W_t^{dn}, \qquad \lambda_{9,t} \ \ \lambda_{10,t}, \quad t \in \{1, ..., T\} \tag{18}$$

Eqs. (15) and (16) limit the DR of the dispatchable load to lie between the upper and lower bounds on the dispatchable load. Additionally, the DR cannot exceed the wind power deviation from the forecast, as specified in Eqs. (17) and (18).

- *Energy Storage Dynamics:*

$$\underline{P}^b \leq p_t^b \leq \overline{P}^b, \qquad \lambda_{11,t}, \ \ \lambda_{12,t}, \quad t \in \{1, ..., T\} \tag{19}$$

$$\underline{B} \leq b_t \leq \overline{B}, \qquad \lambda_{13,t}, \ \ \lambda_{14,t}, \quad t \in \{1, ..., T\} \tag{20}$$

$$b_t = b_{t-1} + p_{t-1}^b, \qquad \mu_{1,t}, \quad t \in \{1, ..., T\} \tag{21}$$

Eqs. (19) and (20) update the energy storage's output power and the energy state and limit them to lie between their upper and lower bounds. The energy storage state transition from one period to the next is described in Eq. (21). A positive/negative p_{t-1}^b value corresponds to charging/discharging of the energy storage.

- *Import and Export Limits:*

$$0 \leq p_t^{im}, \qquad \lambda_{15,t}, \ t \in \{1,...,T\} \tag{22}$$

$$0 \leq p_t^{ex}, \qquad \lambda_{16,t}, \ t \in \{1,...,T\} \tag{23}$$

The distribution system import and export power is defined to be non-negative, as shown in Eqs. (22) and (23).

- *Power Balance:*

$$p_{mt} - p_{bt} - L_{it} - l_{td} = p_{ext} - p_{tim}\,, \qquad \mu_{2,t},\ t \in \{1,...,T\} \tag{24}$$

Eq. (24) ensures that the power is balanced within the distribution system system.

Thus the distribution system dispatch problem can be formulated as follows:

$$\min_{\{y_t\}_{t=1}^{T}} f\left(\{y_t\}_{t=1}^{T}\right)$$

$$\text{s.t. } (13)-(24)$$

Therefore, the bi-level optimization of the transmission system and distribution system can be expressed as follows:

$$\min_{\{x_t\}_{t=1}^{T}} F\left(\{x_t\}_{t=1}^{T}\right)$$

s.t. (3) − (10)

$$\min_{\{y_t\}_{t=1}^{T}} f\left(\{y_t\}_{t=1}^{T}\right)$$

$$\text{s.t. } (13)-(24)$$

3. Single-Level Reformulation of the Bi-level Problem

Two strategies are usually used to solve bi-level optimization problems. The first employs classical methods, including single-level reduction [10], descent [11], penalty function [12], and trust-region methods [13]. Those methods generally exploit mathematical properties of the problems such as convexity, continuous differentiability, and lower semi-continuity. The second category employs evolutionary methods such as genetic algorithms [14], particle swarm optimization [15], differential evolution [16], and metamodeling-based methods [17]; those methods require considerable computational effort and do not provide performance guarantee [6]. For a detailed review of various bi-level optimization techniques, see [6, 18].

The single-level reformulation is commonly applied when the lower-level problem is a convex optimization problem and satisfies Slater's constraints qualifications [19]. The single-level reformulation replaces the lower-level problem with its corresponding Karush-Kuhn-Tucker (KKT) conditions, which are combined with the upper-level problem to devise the single-level reformulation. One thing to note is that this technique simply reformulates the problem, it does not change the original problem solution. As the lower-level problem in this study meets these requirements, its associated KKT conditions namely (stationarity, dual feasibility and complementary slackness), which are described below, are used to reformulate the transmission system and distribution system co-operation problem into a single-level optimization problem.

- *Stationarity*

  The Lagrangian function associated with the distribution system problem is:

$$
\begin{aligned}
L\left(x,y,\lambda,\mu\right) \;&=\; f(x,y)+\lambda_{1,t}(\underline{P}^m-p_t^m)+\lambda_{2,t}(p_t^m-\overline{P}^m)+\lambda_{3,t}(l_t^d-\overline{L}_t^d)\\
&+\;\lambda_{4,t}(\underline{L}_t^d-l_t^d)+\lambda_{5,t}(dr_t^{up}+l_t^d-\overline{L}_t^d)+\lambda_{6,t}(dr_t^{dn}-l_t^d+\underline{L}_t^d)\\
&+\;\lambda_{7,t}(-dr_t^{up})+\lambda_{8,t}(dr_t^{up}-W_t^{up})+\lambda_{9,t}(-dr_t^{dn})+\lambda_{10,t}(dr_t^{dn}-W_t^{dn})\\
&+\;\lambda_{11,t}(p_t^b-\overline{P}^b)+\lambda_{12,t}(\underline{P}_t^b-p^b)+\lambda_{13,t}(b_t-\overline{B})\\
&+\;\lambda_{14,t}(\underline{B}-b_t)+\lambda_{15,t}(-p_t^{im})+\lambda_{16,t}(-p_t^{ex})+\mu_{1,t}(b_t-b_{t-1}-p_{t-1}^b)\\
&+\;\mu_{2,t}(p_t^m-p_t^b-L_t^i-l_t^d-p_t^{ex}+p_t^{im})
\end{aligned}
$$

Stationarity describes a set of first-order optimality conditions, *i.e.*, the first derivative of the Lagrangian function with respect to each decision variable is 0. Thus the following conditions associated with the decision variables (p^m_t, l_t^d, b_t, p^{im}_t, p^{ex}_t, p^b_t, dr_t^{up}, dr_t^{dn}) are needed:

$$C^{m1} + 2C^{m2}p_t^m + \lambda_{2,t} - \lambda_{1,t} + \mu_{2,t} = 0, \qquad t \in \{1,...,T\} \tag{27}$$

$$-C_{td} - \lambda_{4,t} + \lambda_{3,t} - \lambda_{6,t} + \lambda_{5,t} - \mu_{2,t} = 0, \qquad t \in \{1,...,T\} \tag{28}$$

$$C_b + \lambda_{13,t} - \lambda_{14,t} + \mu_{1,t} = 0, \qquad t \in \{1,...,T\} \tag{29}$$

$$c_t^{im} - \lambda_{15,t} + \mu_{2,t} = 0, \qquad t \in \{1,...,T\} \tag{30}$$

$$-c_{ext} - \lambda_{16,t} - \mu_{2,t} = 0, \qquad t \in \{1,...,T\} \tag{31}$$

$$\lambda_{11,t} - \lambda_{12,t} - \mu_{1,t+1} - \mu_{2,t} = 0, \qquad t \in \{1,...,T-1\} \tag{32}$$

$$-p_t^{dr} + \lambda_{8,t} - \lambda_{7,t} + \lambda_{5,t} = 0, \qquad t \in \{1,...,T\} \tag{33}$$

$$-p_t^{dr} + \lambda_{10,t} - \lambda_{9,t} + \lambda_{6,t} = 0, \qquad t \in \{1,...,T\} \tag{34}$$

- *Dual feasibility*:

  All dual variables associated with the inequality constraints need to be non-negative.

$$\lambda_{i,t} \geq 0, \qquad i \in \{1,...,16\}, t \in \{1,...,T\} \tag{35}$$

- *Complementary slackness*:

  The complementary slackness conditions require the product of each inequality and the corresponding variable to be 0. Indeed, it is known from linear programming theory that a dual price is 0 if the corresponding inequality is not saturated, and non-zero otherwise. Therefore, in this context the following conditions associated with the constraints Eqs. (13)-(20), (22) and (23) are necessary:

$$\lambda_{1,t}(\underline{P}^m - p_t^m) = 0, \qquad t \in \{1, ..., T\}$$

$$\lambda_{2,t}(p_t^m - \overline{P}^m) = 0, \qquad t \in \{1, ..., T\}$$

$$\lambda_{3,t}(l_t^d - \overline{L}_t^d) = 0, \qquad t \in \{1, ..., T\}$$

$$\lambda_{4,t}(\underline{L}_t^d - l_t^d) = 0, \qquad t \in \{1, ..., T\}$$

$$\lambda_{5,t}(dr_t^{up} + l_t^d - \overline{L}_t^d) = 0, \qquad t \in \{1, ..., T\}$$

$$\lambda_{6,t}(dr_t^{dn} - l_t^d + \underline{L}_t^d) = 0, \qquad t \in \{1, ..., T\}$$

$$\lambda_{7,t}(-dr_t^{up}) = 0, \qquad t \in \{1, ..., T\}$$

$$\lambda_{8,t}(dr_t^{up} - W_t^{up}) = 0, \qquad t \in \{1, ..., T\}$$

$$\lambda_{9,t}(-dr_t^{dn}) = 0, \qquad t \in \{1, ..., T\}$$

$$\lambda_{10,t}(dr_t^{dn} - W_t^{dn}) = 0, \qquad t \in \{1, ..., T\}$$

$$\lambda_{11,t}(p_t^b - \overline{P}^b) = 0, \qquad t \in \{1, ..., T\}$$

$$\lambda_{12,t}(\underline{P}^b - p_t^b) = 0, \qquad t \in \{1, ..., T\}$$

$$\lambda_{13,t}(b_t - \overline{B}) = 0, \qquad t \in \{1, ..., T\}$$

$$\lambda_{14,t}(\underline{B} - b_t) = 0, \qquad t \in \{1, ..., T\}$$

$$\lambda_{15,t}(-p_t^{im}) = 0, \qquad t \in \{1, ..., T\}$$

$$\lambda_{16,t}(-p_t^{ex}) = 0, \qquad t \in \{1, ..., T\}$$

The complementary slackness constraints are complicated by the variable product terms embedded in them. Using the fact that either the dual variable or the primal constraint has to be 0 for their product to be 0, each complementary slackness constraint can be linearized by introducing sufficiently large constants M_i and binary variables φ_i. This method is commonly referred as the big-M method. The interested reader is referred to [20] for details. For each period t, the complementary conditions can be replaced by the following constraints:

$$p_t^m - \underline{P}^m \leq (1 - \phi_1) \times M_1, \qquad t \in \{1, ..., T\} \tag{36}$$

$$\overline{P}^m - p_t^m \leq (1 - \phi_2) \times M_2, \qquad t \in \{1, ..., T\} \tag{37}$$

$$-l_t^d + \overline{L}_t^d \leq (1 - \phi_3) \times M_3, \qquad t \in \{1, ..., T\} \tag{38}$$

$$l_t^d - \underline{L}_t^d \leq (1 - \phi_4) \times M_4, \qquad t \in \{1, ..., T\} \tag{39}$$

$$-dr_t^{up} - l_t^d + \overline{L}_t^d \leq (1 - \phi_5) \times M_5, \qquad t \in \{1, ..., T\} \tag{40}$$

$$- dr_t^{dn} + l_t^d - \underline{L}_t^d \leq (1-\phi_6) \times M_6, \qquad t \in \{1,...,T\} \qquad (41)$$

$$dr_t^{up} \leq (1-\phi_7) \times M_7, \qquad t \in \{1,...,T\} \qquad (42)$$

$$- dr_t^{up} + W_t^{up} \leq (1-\phi_8) \times M_8, \qquad t \in \{1,...,T\} \qquad (43)$$

$$dr_t^{dn} \leq (1-\phi_9) \times M_9, \qquad t \in \{1,...,T\} \qquad (44)$$

$$- dr_t^{dn} + W_t^{dn} \leq (1-\phi_{10}) \times M_{10}, \qquad t \in \{1,...,T\} \qquad (45)$$

$$- p_t^b + \overline{P}^b \leq (1-\phi_{11}) \times M_{11}, \qquad t \in \{1,...,T\} \qquad (46)$$

$$p_t^b - \underline{P}^b \leq (1-\phi_{12}) \times M_{12}, \qquad t \in \{1,...,T\} \qquad (47)$$

$$- b_t + \overline{B} \leq (1-\phi_{13}) \times M_{13}, \qquad t \in \{1,...,T\} \qquad (48)$$

$$b_t - \underline{B} \leq (1-\phi_{14}) \times M_{14}, \qquad t \in \{1,...,T\} \qquad (49)$$

$$p_t^{im} \leq (1-\phi_{15}) \times M_{15}, \qquad t \in \{1,...,T\} \qquad (50)$$

$$p_{ext} \leq (1-\varphi_{16}) \times M_{16}, \qquad t \in \{1,...,T\} \qquad (51)$$

$$\lambda_{i,t} \leq \varphi_i \times M_i \qquad i \in \{1,...,16\}, t \in \{1,...,T\} \qquad (52)$$

In addition, the bilinear terms $-c^{im}{}_t\, p^{im}{}_t + c^{ex}{}_t\, p^{ex}{}_t + p^{dr}{}_t\,(dr_t{}^{up} + dr_t{}^{dn})$ in the upper-level objective function Eq. (2) also pose challenges to solution of the problem. This can be circumvented by observing that the same bilinear terms also appear in the lower-level objective function Eq. (12) and that, by strong duality, the optimal value of the objective function of the primal problem is equal to that of the corresponding dual lower-level problem. The objective function of the dual of the lower-level problem is

$$\begin{aligned} D(\{\lambda_t, \mu_t\}_{t=1}^T) \;=\; & \textstyle\sum_{t=1}^T (-C^{dr2}(dr_t^{dn})^2 - C^{dr2}(dr_t^{up})^2 - C^{m2}(p_t^m)^2 \\ - \; & \mu_{2,t} L_t^i + \lambda_{1,t}\underline{P}^m - \lambda_{2,t}\overline{P}^m - \lambda_{3,t}\overline{L}_t^d + \lambda_{4,t}\underline{L}_t^d - \lambda_{5,t}\overline{L}_t^d + \lambda_{6,t}\underline{L}_t^d \\ - \; & \lambda_{8,t} W_t^{up} - \lambda_{10,t} W_t^{dn} - \lambda_{11,t}\overline{P}^b + \lambda_{12,t}\underline{P}^b - \lambda_{13,t}\overline{B} + \lambda_{14,t}\underline{B}) \end{aligned} \qquad (53)$$

Interested readers are referred to [21] for the formulation of the dual problem with a primal quadratic program. By equating the objective functions in Eqs. (12) and Eq. (53), and rearranging terms, the expression $-p_t^{im} c_t^{im} + p_t^{ex} c_t^{ex} + p_t^{dr}(dr_t^{up} + dr_t^{dn})$ in the upper-level objective function in Eq. (2) is equal to the following expression (which, after cancellation of pairs of terms that are of equal magnitude and opposite sign, is linear):

$$\sum_{t=1}^{T}(C^{m1}p_t^m + C^{m2}(p_t^m)^2 + C^b b_t + C^{dr1}(dr_t^{up} + dr_t^{dn}) +$$
$$+C^{dr2}((dr_t^{up})^2 + (dr_t^{dn})^2) - C_t^d l_t^d - D(\{\lambda_t, \mu_t\}_{t=1}^T)$$

As a result, the upper-level objective function Eq. (2) can be reformulated as

$$\begin{aligned} F'\left(\{x_t, y_t, \lambda_t, \mu_t\}_{t=1}^T\right) &= \textstyle\sum_{t=1}^T \sum_{g=1}^G (C_g^c w_{g,t} + C_g^1 p_{g,t} + C_g^2 (p_{g,t})^2 + C_g^r (r_{g,t}^{up} + r_{g,t}^{dn})) \\ &+ \textstyle\sum_{t=1}^T (C^{m1}p_t^m + C^{m2}(p_t^m)^2 + C^b b_t + C^{dr1}(dr_t^{up} + dr_t^{dn}) + \\ &+ C^{dr2}((dr_t^{up})^2 + (dr_t^{dn})^2) - C_t^d l_t^d - D(\{\lambda_t, \mu_t\}_{t=1}^T) \end{aligned}$$

The reformulated single-level problem can then be expressed as follows:

$$\min_{\{x_t, y_t, \lambda_t, \mu_t\}_{t=1}^T} F'\left(\{x_t, y_t, \lambda_t, \mu_t\}_{t=1}^T\right)$$
st: (3) − (10), (13) − (24), (27) − (52)

After removing the nonlinearity in the complementary slackness and upper-level objective function, the bi-level problem now becomes a single-level mixed-integer linear problem which can be solved with a wide range of commercial solvers such as CPLEX.

4. Solution Method and Results

To illustrate the benefits of implementing the proposed bi-level optimization framework, the results presented here compare costs and dispatch results obtained with the traditional single level formulation to those obtained with the proposed bi-level formulation. To further clarify this comparison, note that the single level framework (the traditional optimization) has a single model formulation incorporating both transmission and distribution levels. Within this framework, all demand response and energy exchanges are priced under the traditional LMP framework, with the LMP established as the single price for distribution system energy imports and local demand response.

In contrast, with the bi-level formulation, unit commitment and economic dispatch are run for the upper-level transmission system problem, and the price for energy exchange is determined by this first stage decision-making process. What is added in the cooptimization formulation a second stage decision making process in which the power flow model is run for the distribution system. Within this subproblem, the quantity of energy imported (purchased from the transmission grid) as well as the price and the quantity of demand response provided are determined by the distribution system. In the cooptimization approach, the distribution power flow is included in the formulation, and the demand response price is set by the distribution system as an optimization parameter, instead of using the LMP that is determined by the transmission system.

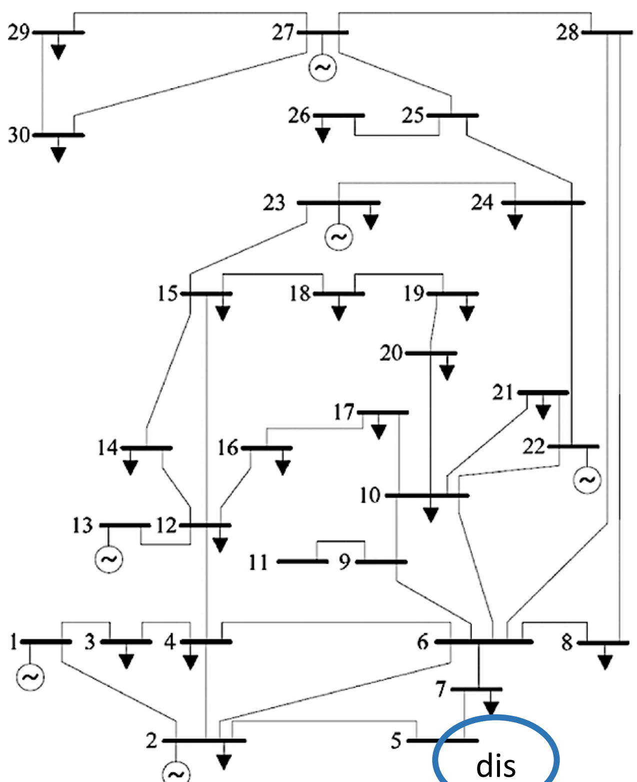

Figure 4.1 Test system diagram showing distribution system

4.1 Cost Comparisons with Single versus Bilevel Optimization

The first set of results compares the cost of electricity from simulations with proposed cooptimization versus the more traditional single level optimization. Figure 4.1 shows the one-line diagram for the high voltage grid, used in the optimizations. Figure 4.2 shows the distribution system model used in the bi-level optimization framework. As shown in Figure 4.1, this model is connected to bus 5. For the results discussed below the cost comparison is between the traditional optimization with no distribution system detail, compared to the bi-level optimization which includes a single detailed distribution system (at bus 5) for these results. The bi-level formulation can accommodate as many detailed distribution system models as desired.

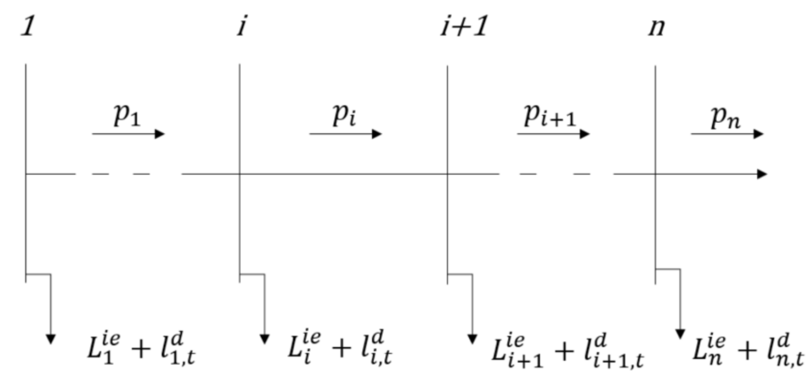

Figure 4.2 Test system diagram showing distribution system

In comparing costs determined by each formulation, recall that in the traditional single level optimization, the electricity price is the shadow price for both energy purchases by the distribution system from the transmission system, and for the demand response ***provided by*** the distribution system to the transmission system.

The results below consider two cases: the first with a small amount of demand response (15% of load and indicated by “drsize 1” in the figures), and a second with 20% more demand response (equal to 18% of load, and indicated by “drsize 1.2” in the figures).

Looking to Figure 4.3, in the traditional case, increasing demand improves the production cost for the distribution system – customers providing demand response make increased revenue from providing demand response. This is shown in the right-hand bar chart by comparing the gray and yellow bars. The gray bar represents the production cost in the distribution system when 15% of load is responsive, while the yellow bar shows the production cost when responsive load is increased by 20% from this base case, to a total of 18% response load. Comparing the gray and yellow bars in the left-hand bar chart in figure 4.3. shows that the transmission system gains nothing from an increased demand response capacity. The gray and yellow bars show that the transmission system experiences the same production cost with 15% responsive load and with 18% responsive load.

In contrast, under cooptimization, both system levels benefit a small amount. Though this result will become clearer with further investigation, the initial interpretation is that the improved, *i.e.*, more accurate, distribution of benefits, leads to overall improvement in system efficiency, and so provides benefits to both the transmission and the distribution systems. This result is seen by comparing the blue and orange bars in the left- and right-hand bar charts of figure 4.3.

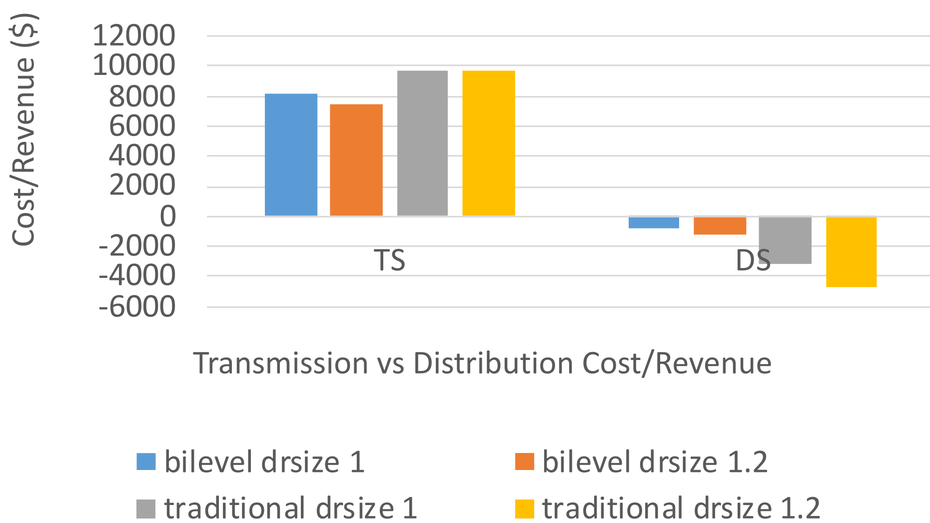

Figure 4.3 Bilevel versus Single level optimization cost comparison

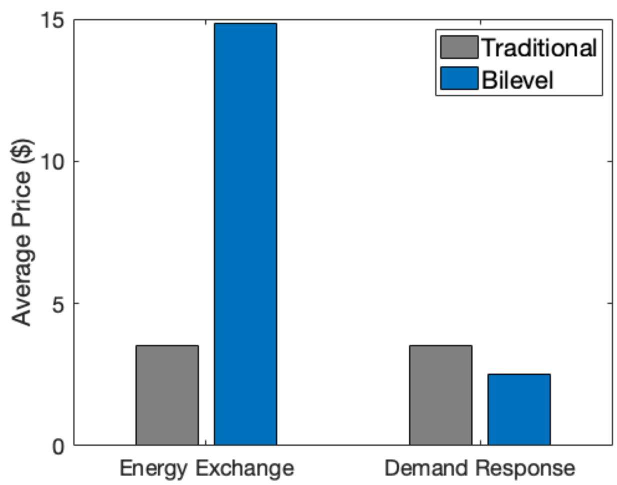

Figure 4.4 Bilevel versus Single level optimization cost comparison

Figure 4.4 investigates the price differences within the transmission and the distribution system. Looking at the gray bars, this figure shows that under the traditional case, and by definition, the energy exchange and demand response have the same price, as set by the LMP in stage 1.

With the bi-level optimization, the distribution system runs its own, local power flow and economic dispatch in order to determine the value to local load of providing demand response. In this bilevel case, the energy exchange price is seen to be significantly higher than the demand response price. Recall that the demand response price is determined by the 2nd stage of the optimization, run for the distribution system.

This figure 4.4 demonstrates the benefits to the system as a whole from using the bi-level cooptimization. The energy and demand response products are priced more accurately, and lead to greater system efficiency in dispatching available resources. The transmission system receives more benefit under the bi-level optimization with the increased flexibility from the demand response resources. The next section builds upon this result, demonstrating the benefits with the bi-level optimization when managing imbalance due to wind forecast errors.

4.2 Balancing Wind Forecast Errors

Figures 4.5 and 4.6 below compare the mix of reserves and demand response selected (on average over many scenarios) in the single-level and bi-level optimizations for real time mitigation of wind forecast errors. Reserves and demand response can both be utilized to balance wind forecast errors, and the proportion of reserves to demand response selected is different for the two different optimization frameworks.

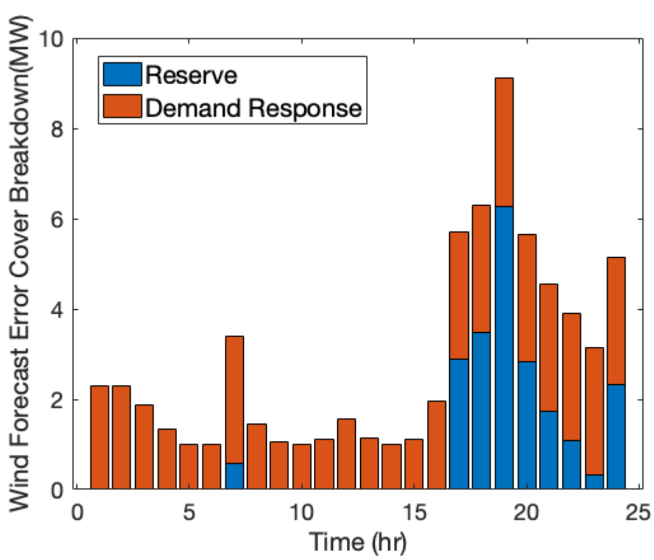

Figure 4.5 Balancing wind forecast errors with single level optimization

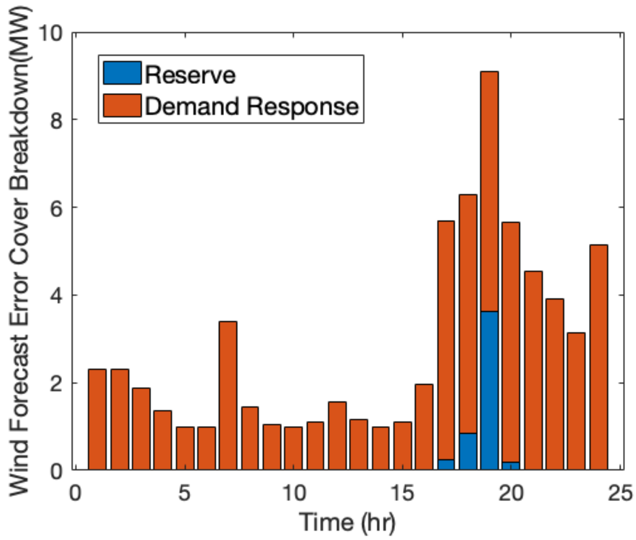

Figure 4.6 Balancing wind forecast errors with bilevel optimization

Specifically, the cooptimized decisions lead to using more demand response thank the traditional, single level approach, because the demand response price is often lower than the price for reserves with the bi-level optimization. In the single level optimization, all resources are priced equally at LMP.

Note that the wind forecast errors are realized strictly in the second stage (real time) since all dispatch decisions are set in the first stage. In the second stage of the optimization wind imbalances are mitigated by either reserves or demand response. In summary, the figures 4.5 and 4.6 demonstrate that under the bilevel co-optimization, demand response is (on average) less expensive and decreases the need for reserves; reserves that would be called upon if the single level optimization were to be used.

5. Case Study: Co-optimizing High and Low Voltage Systems

5.1 Case Study

5.1.1 Introduction to case study

In contrast with the results presented above, the focus of this section is a comparison between two common pricing schemes (*i.e.*, fixed vs dynamic) for the interactions between the transmission and microgrid systems. In addition, this case study analyzes the incremental benefit of utilizing the bi-level framework as the number of distribution systems modeled increases, to explore the impact of gradual system changes on operations, and potential challenges under the current (single-level) optimization framework. Finally, this case study analyzes the causes of incremental system cost changes as the number of microgrids increases. These simulations include data for the distributed generation and microgrid demand response under alternative system configurations.

5.1.2 Solution Approach

Bi-level optimization problems simulate the interaction of market players with conflicting objectives and constraints. The lower-level problem in this study has the advantage of being convex and satisfies Slater's constraints qualifications. These properties allow the lower level problem to be replaced by its associated Karush-Kuhn-Tucker conditions, and combined with the upper-level problem to form a single level problem that represents the optimization of each system appropriately [22]. The bi-linearity in the resulting single-level problem is circumvented by the big-M method and strong duality theorem. References [23], [24], [25] provide the technical details of this solution approach. The resulting problem is a mixed-integer linear problem which could be solved by various solvers in the market such as Gurobi and Cplex.

5.1.3 Power System Model

The transmission model described in Section II-A is applied to the IEEE 30-bus system shown in Figure 2. The total generation capacity of the system is 335 MW, with other system characteristics and parameters given in [26]. A wind farm is positioned at bus 5. For consistency with realistic market conditions, it is assumed that the energy buy-back price in the wholesale market is slightly lower than the energy sale price. As a result, the microgrid export cost, cex, is defined as 0.9 cim, which also ensures that the microgrid cannot participate in an illogical arbitrage strategy. A baseline 25 MW microgrid with parameters provided in Table 5.1 is used to demonstrate system operations under this bi-level framework. The six bus diagram for the low voltage system is shown in Figure 3. The microgrid includes a generator, a storage unit, aggregated dispatchable load, and non-dispatchable load, and is able to operate in islanded and grid-connected modes.

Parameter	Value	Parameter	Value
$\underline{L}_t^d$	6.6 MW	C^{dr1}	\$0.4/MW
$\overline{L}_t^d$	12 MW	C^{dr2}	\$0.3/MW
L_t^i	12 MW	C_t^d	\$6/MW
$\overline{B}$	10 MW	$\overline{P}_t^d$	\$1/MW
$\underline{B}$	0 MW	$\overline{P}^m$	25 MW
C^b	\$0.1/MW	$\underline{P}^m$	0 MW
C_t^{m1}	\$4/MW	$\underline{P}^b$	-5 MW
C_t^{m2}	\$0.07/MW	$\overline{P}^b$	5 MW

Table 5.1 Microgrid Parameter Values

5.2 Results

The purpose of these simulations is two-fold. First is the investigation of the degree to which the proposed bi-level optimization framework is effective in quantifying the appropriate cost allocation between the high and low voltage systems in the interconnected electric power system. Second is the analysis of a set of possible future configurations of the power system, focusing on increasing the number of microgrids interconnected with the transmission system. Results from the bi-level optimization framework are compared to those from the traditional single-level optimization. The single- and bi-level formulations differ in that the single-level optimization objective function is the sum of those from the upper and lower level problems under the bi-level framework, and the constraints are the combined set of the constraints from the upper and lower level problems.

The bi-level framework uses the KKT conditions to represent the leader-follower aspects of the co-optimized system, and also is capable of modeling the details of network constraints in the low voltage network. However these details are not included in the existing, traditional optimization framework. Therefore, to ensure a meaningful comparison between formulations, low-voltage network constraints are not implemented in either framework in the results presented below. This ensures that the differences in results presented here are entirely due to the differences in the problems structures. Figures 5.4 and 5.5 show the system costs as determined by the bi-level framework compared to those determined by the standalone single-level optimization framework.

The high voltage transmission system has interconnectged microgrids, modeled as active low voltage systems with distributed generation, demand response, and storage. The single-level optimization assumes islanded mode operation for the microgrids in as much as they do not actively interact with, or exchange energy bi-directionally with, the transmission system. In contrast, the bi-level co-optimization allows for bi-directional energy flow at each level. Three cases are simulated with each optimization framework, including one, three and five baseline microgrids at bus five. Since there is no congestion in the system, the locations of the microgrids are not critical to the results presented.

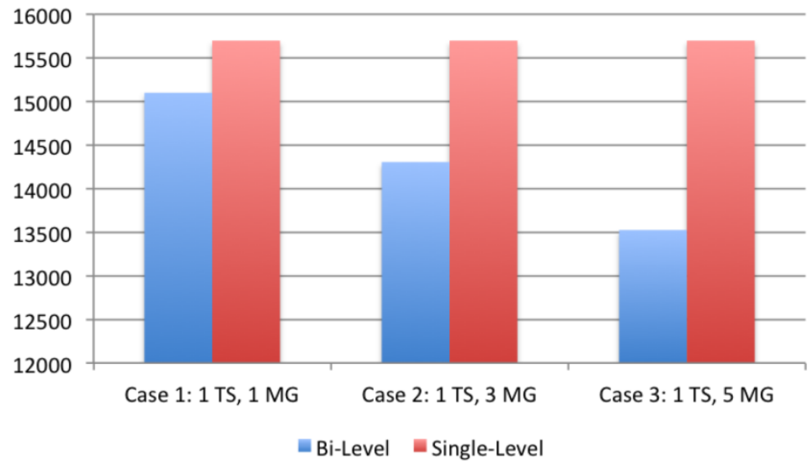

Figure 5.1 Comparison of Transmission System Cost between Bi-Level and Single-Level Optimization as Modeled with 1, 3 & 5 MicroGrids

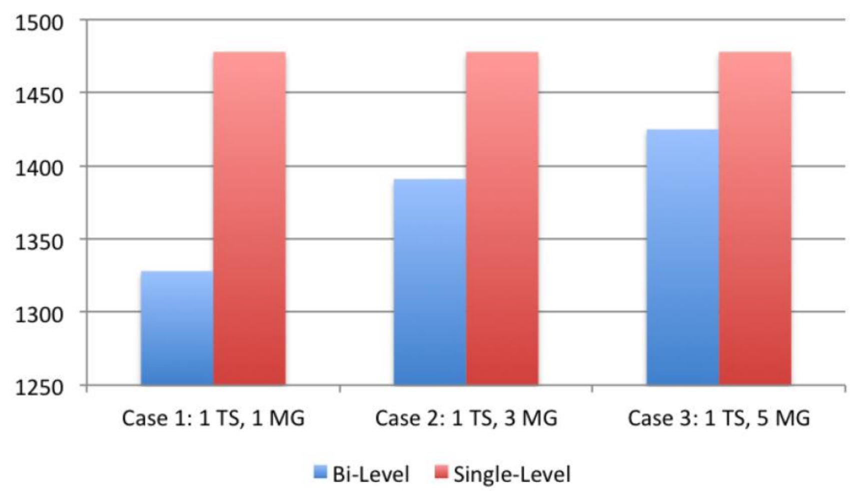

Figure 5.2 Comparison of Average Distribution System Cost between Bi-Level and Single-Level Optimization in System with 1, 3 &5 MicroGrids

Results show that microgrid cost increases as the number of microgrids in the system increases; such cost increases being balanced by transmission system cost decreases. The costs are seen to shift because the transmission system has more supply choices under the bi-level scheme with increased access to demand response resources and microgrid energy export. Access to more supply options lowers the corresponding costs in the transmission system under the co-operative framework. However, with the microgrid contributions to transmission system balancing needs being better represented, the associated microgrid costs from supplying demand response and energy exports are seen to rise.

Under the single-level framework, there are no interactions between the high- and low-voltage networks, so the microgrid costs do not change as the number of microgrids in the system increases. Figure 5.6 shows the changing use of DG and DR within the microgrids as the number of connected microgrids increases from one to three to five. This chart shows the average DER dispatch, demonstrating that proportionally more DER is used by the system as the number of microgrids, and associated DER capacity, increases.

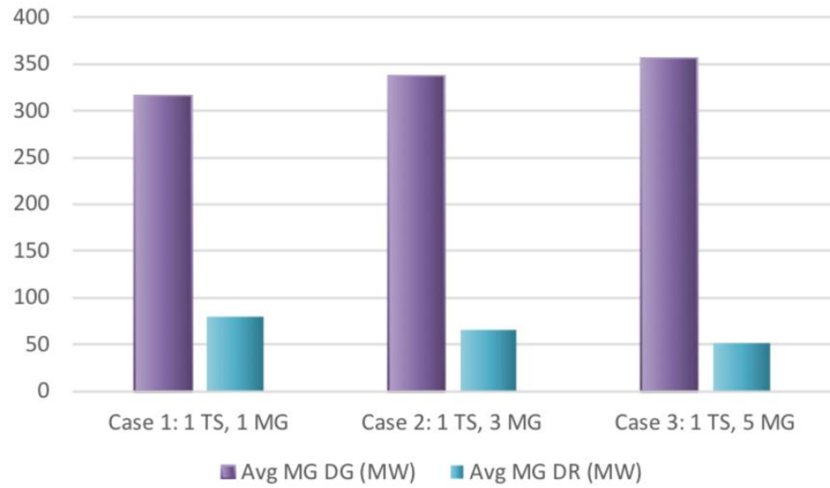

Figure 5.3 Average Microgrid DG and DR Dispatch with 1, 3 & 5 MicroGrids

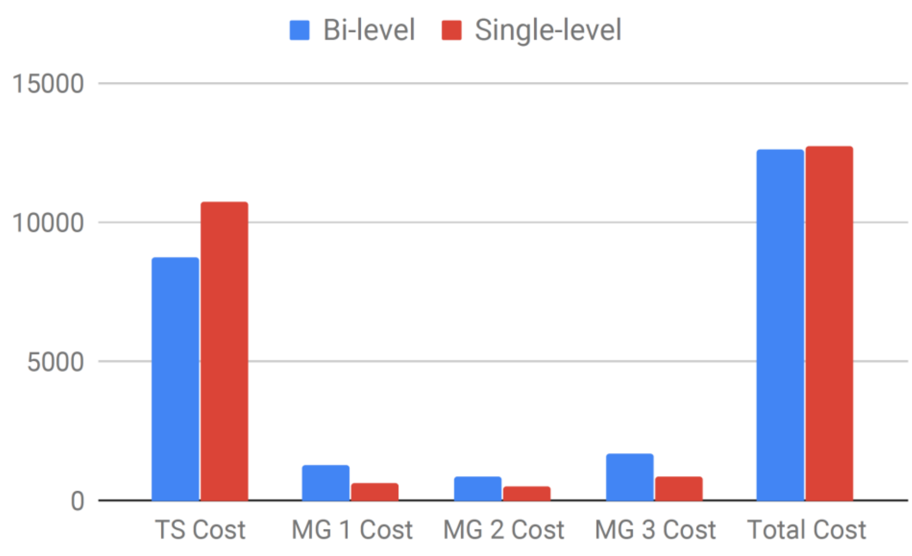

Figure 5.4 Transmission System & Microgrid Costs: Comparison between Bi-Level and Single-Level Optimization

Figure 5.4 compares costs in the high and low voltage systems under the bi-level framework versus the fixed LMP single-level scheme. Under this single-level optimization, the transmission system determines the nodal LMPs without using generation, demand response or price information from the microgrids. This transmission system LMP is used as the deterministic price for energy transactions between the microgrid and the transmission system. In this case, three microgrids are positioned at bus 5 (MG1 with base configuration), bus 10 (MG2 with 0.8 capacity of the base configuration) and bus 15 (MG3 with 1.2 capacity of the base configuration).

With deterministic LMP, the microgrid cost is lower in the traditional single-level optimization framework than in the bi-level framework. Microgrid costs are inappropriately attributed to the transmission system in the single-level optimization framework since detailed microgrid data and information are not taken into consideration in the determination of the pricing in this traditional framework. With the bi-level optimization, the transmission system cost is lower as the price is optimized for the interconnected system, assigning costs to the distribution system as appropriate. Under the bi-level framework, the maximum possible wind penetration, while maintaining system stability, is higher than under the single-level approach due to flexibility in pricing (with the bi-level framework). The total system operation cost under the bi-level framework is also lower.

Figures 5.5 and 5.6 show the high voltage transmission system cost with traditional, radial and passive distribution systems, again comparing results from single-level and bi-level optimization frameworks. The three distribution systems are positioned at the same buses and have the same configurations as the baseline microgrid, but now without distributed generation or energy storage. The traditional, single-level framework incurs higher average costs for the distribution systems as the number of connected distribution systems increases, due to higher generator costs from higher generation dispatch. The transmission system cost decreases accordingly.

Under the bi-level framework, the distribution system cost is lower than that under the single level counterpart as the distribution system participation is explicitly considered in the lower level objective function. These results demonstrate that the distribution system cost under the single level framework is under-evaluated; a result which will become increasingly inadequate as the distribution systems become more dynamic and multi-functional in the future power system. In addition, the decreasing average distribution system cost under the bi-level framework means that representing the distribution system as individual optimization entities yields additional benefits to each distribution system as more distribution systems participate in this optimization framework due to the mutual arbitrage among the optimization entities. The transmission system cost increases with more distribution systems participating in this bi-level framework as the transmission system has decreased advantage over the distribution system operations, as is appropriate.

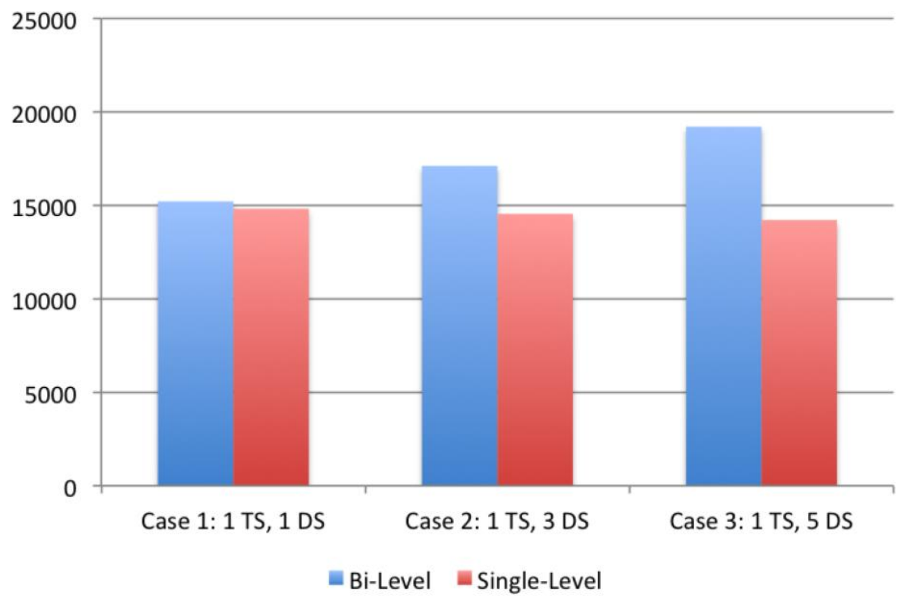

Figure 5.5 Comparison of Transmission System Cost between Bi-Level and Single-Level Optimization as Modeled with 1, 3 & 5 Passive Distribution Systems

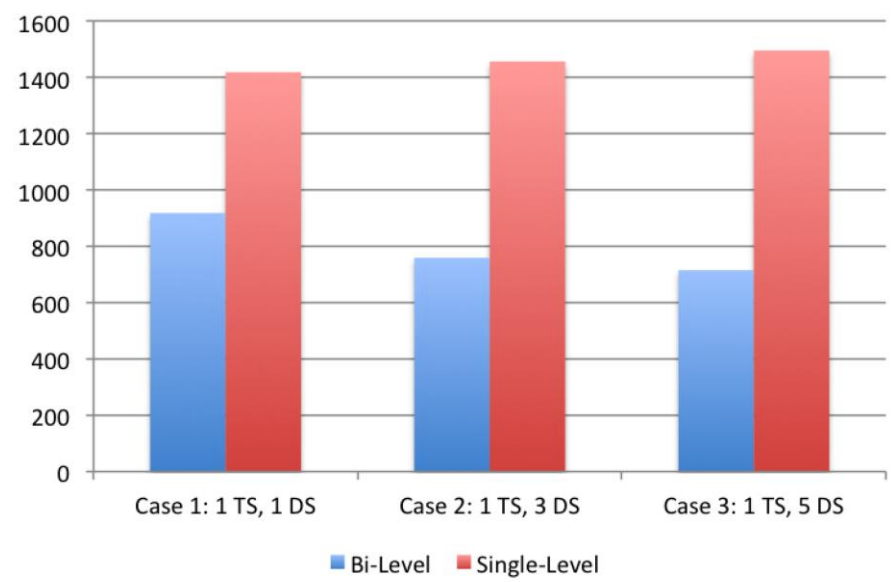

Figure 5.6 Comparison of Average Distribution System Cost between Bi-Level and Single-Level Optimization in System with 1, 3 &5 Passive Distribution Systems

6. Summary

This report proposes the use of a bi-level optimization algorithm to replace the traditional single-level optimization currently used for the analysis of power system costs and generator dispatch. Though the existing single-level framework adequately determines system performance at low levels of DER and microgrid penetration, as the use of new technologies and active devices becomes more widespread, the traditional single-level framework will become inadequate.

Bi-level optimization, for modeling and analyzing the combined operations of the transmission and distribution systems, is emerging as a framework that is likely to give results superior to those provided by the traditional single-level optimization framework. The bi-level formulation provides more accurate allocation of costs between the systems, improved overall system efficiency and better use of resources for mitigating uncertainty in generation from intermittent renewables. The initial analysis discussed above demonstrates the advantages that co-optimization offers in leveraging DER to benefit both transmission ***and*** distribution in the management of uncertainty from renewables.

The final set of results discussed above explored multiple distribution systems connected to the transmission system and showed that they can successfully compete to provide demand response to the transmission system. When the distribution systems each have a different resource mix, the traditional single level optimization cannot differentiate between the distribution systems, and so cannot facilitate an analysis of competition between the distribution systems. With the bi-level optimization, which incorporates the network model and power flow for the distribution systems, the opportunity for, and analysis of, competition between the distribution systems becomes possible.

Thus we find that co-optimization may support competition and cooperation between transmission and distribution. The benefits from the demand response availability in distribution are captured better in the bi-level framework. In addition, the bi-level framework developed here allows for competition among distribution systems in providing demand response to the transmission level. Traditional single level optimization cannot leverage differences in the interconnected distribution systems, and so cannot accommodate competition among them.

The case study in section 5 applies the bi-level optimization framework developed here to demonstrate its use with the IEEE 30 bus test system and an increasing number of active microgrids. The system simulations presented in this paper demonstrate that as DER use increases a bi-level optimization framework more accurately determines power system operating costs than does the traditional single-level optimization algorithm. Further detailed simulations could demonstrate additional challenges introduced by increasingly active low voltage systems, and explore the demonstrate benefitsof more detailed modeling of system interaction via bi-level optimization.

However, several open questions remain:

- The simulations analyzed here include a small number of distribution systems. Additional study is needed to understand h ow many distributions systems can reasonably be incorporated.

- The formulation developed here fixes the generator dispatch in the first stage, allowing for demand response to be utilized only in the second stage of the optimization. Further study will consider demand response and storage units in first-stage planning.
- The analysis of transmission congestion has not yet been included in the simulations for the bi-level optimization. In further analysis, congestion will likely have an impact in differentiating distribution systems, and so further increasing the benefits of co-optimization.

These open issues define the next areas to explore within the bi-level optimization:

- Results obtained from the bi-level optimization could differ if demand response were to be committed in the first stage of the analysis.
- Congestion in the transmission system emphasizes the importance of including distribution system details in the co-optimization, since the differences among the distribution systems, and subsequent access to these differing resources, will be highlighted by congestion between regions of the transmission system.

In conclusion, co-optimization may facilitate more effective use of resources in transmission and distribution.

References

[1] Jonathan F Bard and James E Falk. An explicit solution to the multi- level programming problem. Computers & Operations Research, 9(1):77– 100, 1982.

[2] Wayne F Bialas and Mark H Karwan. Two-level linear programming. Management science, 30(8):1004–1020, 1984.

[3] A. Bhardwaj, V. K. Kamboj, V. K. Shukla, B. Singh, and P. Khurana, "Unit commitment in electrical power system-a literature review," in Power Engineering and Optimization Conference (PEDCO) Melaka, Malaysia, 2012 Ieee International. IEEE, 2012, pp. 275–280.

[4] E. Hossain, E. Kabalci, R. Bayindir, and R. Perez, "Microgrid testbeds around the world: State of art," Energy Conversion and Management, vol. 86, pp. 132–153, 2014.

[5] C. Chen, S. Duan, T. Cai, B. Liu, and G. Hu, "Smart energy management system for optimal microgrid economic operation," IET renewable power generation, vol. 5, no. 3, pp. 258–267, 2011.

[6] A. Sinha, P. Malo, and K. Deb, "A review on bilevel optimization: from classical to evolutionary approaches and applications," IEEE Transactions on Evolutionary Computation, 2017.

[7] G. L. R. W. Energy, "Eastern wind integration and transmission study," Technical Report, National Renewable Energy Laboratory (NREL), 2010.

[8] C. Anderson and R. Zimmerman, "Wind output forecasts and scenario analysis for stochastic multiperiod optimal power flow," PSERC Webinar, pp. 1–38, 2011.

[9] C. Chen, S. Duan, T. Cai, B. Liu, and G. Hu, "Smart energy management system for optimal microgrid economic operation," IET renewable power generation, vol. 5, no. 3, pp. 258–267, 2011.

[10] J. F. Bard and J. E. Falk, "An explicit solution to the multi-level programming problem," Computers & Operations Research, vol. 9, no. 1, pp. 77–100, 1982.

[11] C. D. Kolstad and L. S. Lasdon, "Derivative evaluation and computational experience with large bilevel mathematical programs," Journal of optimization theory and applications, vol. 65, no. 3, pp. 485–499, 1990.

[12] D. J. White and G. Anandalingam, "A penalty function approach for solving bi-level linear programs," Journal of Global Optimization, vol. 3, no. 4, pp. 397–419, 1993.

[13] B. Colson, P. Marcotte, and G. Savard, "A trust-region method for nonlinear bilevel programming: algorithm and computational experience," Computational Optimization and Applications, vol. 30, no. 3, pp. 211–227, 2005.

[14] R. Mathieu, L. Pittard, and G. Anandalingam, "Genetic algorithm based approach to bi-level linear programming," RAIRO-Operations Research, vol. 28, no. 1, pp. 1–21, 1994.

[15] X. Li, P. Tian, and X. Min, "A hierarchical particle swarm optimization for solving bilevel programming problems," in International Conference on Artificial Intelligence and Soft Computing. Springer, 2006, pp. 1169–1178.

[16] X. Zhu, Q. Yu, and X. Wang, "A hybrid differential evolution algorithm for solving nonlinear bilevel programming with linear constraints," in Cognitive Informatics, 2006. ICCI 2006. 5th IEEE International Conference on, vol. 1. IEEE, 2006, pp. 126–131.

[17] G. G. Wang and S. Shan, "Review of metamodeling techniques in support of engineering design optimization," Journal of Mechanical design, vol. 129, no. 4, pp. 370–380, 2007.

[18] A. Sinha, P. Malo, and K. Deb, "A review on bilevel optimization: from classical to

evolutionary approaches and applications," IEEE Transactions on Evolutionary Computation, vol. 22, no. 2, pp. 276–295, 2018.
[19] W. F. Bialas and M. H. Karwan, "Two-level linear programming," Management science, vol. 30, no. 8, pp. 1004–1020, 1984.
[20] W. L. Winston, M. Venkataramanan, and J. B. Goldberg, Introduction to mathematical programming. Thomson/Brooks/Cole Duxbury; Pacific Grove, CA, 2003, vol. 1.
[21] E. W. E. Association, Wind energy-the facts: a guide to the technology, economics and future of wind power. Routledge, 2012.
[22] J. J. Ye, "Constraint qualifications and kkt conditions for bilevel programming problems," Mathematics of Operations Research, vol. 31, no. 4, pp. 811–824, 2006.
[23] S. Dempe and A. B. Zemkoho, "The bilevel programming problem: reformulations, constraint qualifications and optimality conditions," Mathematical Programming, vol. 138, no. 1-2, pp. 447–473, 2013.
[24] T. Ding, R. Bo, W. Gu, and H. Sun, "Big-m based miqp method for economic dispatch with disjoint prohibited zones," IEEE Transactions on power systems, vol. 29, no. 2, pp. 976–977, 2013.
[25] W. S. Dorn, "Duality in quadratic programming," Quarterly of Applied Mathematics, vol. 18, no. 2, pp. 155–162, 1960.
[26] Zimmerman, R.D. and Murillo-Sanchez, C. E. (2020). "Matpower User Manual Version 7.1". https://matpower.org/docs/MATPOWER-manual.pdf. pp. 121-126